Stellingen behorende bij het proefschrift

Hydrogen absorption in iron and steel during gas tungsten arc welding
Jaap Hooijmans
december 1994

1 De aanname van Chew and Willgoss dat in het lasbad grote verschillen optreden in waterstofconcentratie, is niet in overeenstemming met de werkelijkheid.
B. Chew and R.A. Willgoss, Proc. of Conf. on "Weld pool chemistry and metallurgy", (1980) 155-165.

2 Het feit dat de Wet van Sieverts ook geldt voor waterstofopname tijdens het booglassen, betekent niet dat onder deze omstandigheden evenwicht bestaat.
Dit proefschrift

3 De uitspraken die Terasaki et al. doen over de diffusie van waterstof in ijzer zijn niet zinvol, omdat geen rekening gehouden wordt met de chemische samenstelling van het gebruikte materiaal.
T. Terasaki, G.T. Hall and R.J. Pargeter, Trans. Jap. Weld. Soc. 22 (1991) 52-56.

4 De oplossing van lange-termijn problemen wordt belemmerd door de korte-termijn politiek van het democratische systeem.

5 Het op grote schaal inenten van kinderen in de derde wereld vergroot het probleem van de overbevolking.

6 Het belonen van studierendement, als beleidsinstrument voor de financiering van universiteiten, leidt tot verlaging van het studieniveau.

7 Het toenemende gebruik van Engelse woorden waar een goede Nederlandse vertaling voor bestaat, getuigt van een geringschatting van de Nederlandse taal.

8 De grootste bedreiging van de menselijke samenleving is het succes van de mens als soort.

9 Vogels spreken ons aan omdat ze, net als de mens, gebruik maken van auditieve en visuele communicatie.

Hydrogen absorption in iron and steel

during gas tungsten arc welding

Hydrogen absorption in iron and steel during gas tungsten arc welding

proefschrift

ter verkrijging van de graad van doctor
aan de Technische Universiteit Delft,
op gezag van de Rector Magnificus Prof. ir. K.F. Wakker,
in het openbaar te verdedigen ten overstaan van een commissie
aangewezen door het College van Dekanen,
op dinsdag 10 januari 1995 te 16.00 uur

door

Jacobus Wilhelmus HOOIJMANS

materiaalkundig ingenieur,
geboren te 's Gravenhage.

Dit proefschrift is goedgekeurd door de promotor

Prof. dr. G. den Ouden

Published and distributed by:

Delft University Press
Stevinweg 1
2628 CN Delft
The Netherlands

Telephone +31 15 783254
Fax +31 15 781661

CIP-DATA KONINKLIJKE BIBLIOTHEEK, DEN HAAG

Hooijmans, J.W.

Hydrogen absorption in iron and steel during gas tungsten arc welding / J.W. Hooijmans. - Delft : Delft University Press. - Ill.
Thesis Delft University of Technology. - With ref. - With summary in Dutch.
ISBN 90-407-1071-6
NUGI
Subject headings: hydrogen / welding / absorption

Printed in The Netherlands

Contents

Symbols

A	interface area between arc and liquid metal	m^2
A_m	weld metal transverse cross section area	m^2
B	interface area between liquid metal and the surrounding gas phase	m^2
c	concentration	wt.%
c_s	equilibrium concentration	wt.%
c_0	original hydrogen concentration in the material	wt.%
D	diffusion coefficient	m^2/s
D_0	diffusion constant	m^2/s
e	electron charge	$1.60 \cdot 10^{-19}$ C
E	electrical field strength	V/m
E_d	dissociation energy	eV
E_i	ionization energy	eV
f_1	heat transfer efficiency, the heat transferred to the workpiece per unit time divided by the power of the heat source	
f_2	melting efficiency, the heat used to form the weld divided by the power of the heat source	
H	enthalpy	J/mole
H_i	heat input	J/m
I	arc current	A
j	current density	A/m^2
J	flux, defined as the number of atoms of one element crossing unit area per unit time	$mole/m^2s$
k	Boltzmann constant	$1.38 \cdot 10^{-23}$ J/K
K	solubility coefficient	$Pa^{-1/2}$
K_0	solubility constant	$Pa^{-1/2}$
l	arc length	m
l_e	electron mean free path	m
m	mass	g
n_e	electron density	m^{-3}
p	pressure	Pa
p_{H2}	partial pressure of the hydrogen gas	Pa

q	heat required to elavate a given volume of metal from room temperature to its melting point and subsequently convert this volume from the solid state to the liquid state	J/m^3
Q	activation energy for diffusion	J/mole
r	radius of the arc	m
R	gas constant	8.31 J/mole K
R_m	melting rate	kg/s
s	surface area of the weld cross section	m^2
S	entropy	J/mole K
t	time	s
T	absolute temperature	K
v	travel speed of the heat source	m/s
V	arc voltage	V
W	weight of the liquid metal	g
x	distance	m
α	absorption coefficient (amount of hydrogen entering the liquid metal per unit area per unit time)	g/sm^2
α_d	degree of dissociation	%
α_i	degree of ionization	%
ß	desorption coefficient (a proportionality factor depending on the temperature of the liquid metal)	g/sm^2
η	constant representing the part of the hydrogen which is frozen in during solidification	
κ	thermal conductivity coefficient	W/mK
μ	chemical potential	J/mole
ρ	density of the material	g/m^3
σ	electrical conductivity	$\Omega^{-1}m^{-1}$

CHAPTER 1

Introduction

1.1 Arc welding

Over the years a number of methods have been developed for the durable joining of materials. Welding, soldering and adhesive bonding are well known examples, which are widely used in the metallurgical industry. Especially welding is extensively used in a wide range of industrial applications. The joints formed by the welding process can be used at high temperatures and in aggressive atmospheres.

Arc welding is a joining process in which two metal parts are bonded through fusion. The two metal parts to be joined melt as a result of the heat, which is developed by the electric arc burning between an electrode and the metal parts. During solidification of the molten material a joint is formed. The strength of the joint depends on the composition and the structure of the weld metal, the latter being strongly dependent on the thermal cycle of the welding process.
The more widely used arc welding processes are shielded metal arc welding (SMAW), gas tungsten arc welding (GTAW), plasma arc welding (PAW), gas metal arc welding (GMAW), electroslag welding (ESW) and submerged arc welding (SAW).

Gas tungsten arc (GTA) welding is an arc welding process in which arc heat is produced by an arc burning between a tungsten based non-consumable electrode and a metal workpiece. The process is normally carried out autogenously, i.e. without the addition of filler material.
During the GTA welding process the molten metal and the electrode are protected from the surrounding atmosphere by means of a shielding gas [1.1]. This shielding gas provides also the required arc characteristics. It is used to prevent any unwanted gas to come into contact with the molten metal and to protect the electrode from oxidation. Contact of the atmosphere with the liquid metal could lead to unsatisfactory welds. Problems which can occur are the absorption of hydrogen and nitrogen and the oxidation of the liquid metal or of alloying elements in the liquid metal.

Normally an inert gas is used as shielding gas. The advantage of this kind of gas is that there is no interaction between the gas and the liquid metal. Widely used are argon and helium or a mixture of both [1.2]. Helium is more expensive than argon, but has the advantage that it produces a higher heat input in the weld.
Sometimes small quantities of other gases are used as an addition to argon or helium [1.3]. The most important additions to the shielding gas are oxygen and carbon dioxide. Both gases are added to stabilize the arc and to obtain better penetration. In GMAW of mild steel carbon dioxide is added to achieve a better transfer of metal droplets from the electrode to the weld pool.

1.2 Hydrogen in arc welding

The history of arc welding shows that hydrogen is an element which easily promotes the formation of weld defects, especially in the case of welding iron and steel. The most important hydrogen related weld defect is hydrogen-induced cracking. Another source of concern is the formation of pores in the weld during the welding process.

Hydrogen cracking
Hydrogen-induced cracking has received a tremendous amount of attention as a topic for research and many papers have been written on this subject. In spite of this attention, there is still no generally accepted theory for the cracking mechanism [1.4]. In the past decennia different theories have been developed to explain the mechanism of hydrogen cracking [1.5,1.6]. However, there is strong evidence that hydrogen cracking is not caused by one mechanism only, but that it is a complex process in which different mechanisms are operating simultaneously [1.7].

In the welding industry hydrogen cracking plays an extremely important role [1.8-1.10]. In fact, its occurrence poses manufacturing problems which are a source of great concern. For example, a large part of the cost needed for repair is related to hydrogen-induced cracking. A significant number of these costly failures has originated at small pre-existing cracks in the heat-affected zone (HAZ) of the parent steel adjacent to the weld. However, hydrogen cracking may also occur in the weld metal. The fracture of pressure vessels during hydraulic testing and the collapse of structural steelwork in service have both provided instances of failures in which hydrogen cracking was involved [1.11].

Hydrogen cracking will often occur some time after welding has been completed and, although extensive, may be difficult to detect. Thus a heavy responsibility is placed on the fabricator to match the welding procedure with the material for each application in order that cracking does not occur. The incidence of failures suggests that this has not always been successful.

In addition to the presence of hydrogen there are three other factors which are essential for the initiation of hydrogen-induced cracking. These factors are: a susceptible microstructure, implying the presence of hard constituents such as martensite or bainite, the presence of residual stresses, and a relatively low temperature (<200°C) [1.13-1.15]. When these conditions are fulfilled simultaneously cracking of the welded structure is a possibility.

There is a number of locations in the HAZ where the cracks can be found. Depending on the location a distinction can be made between root cracks, toe cracks, underbead cracks and transverse cracks (Fig. 1.1) [1.16]. In recent years, the development of leaner alloyed constructional steels led to the situation that more and more hydrogen-induced cracking is found in the weld metal, rather than in the heat-affected zone [1.17].

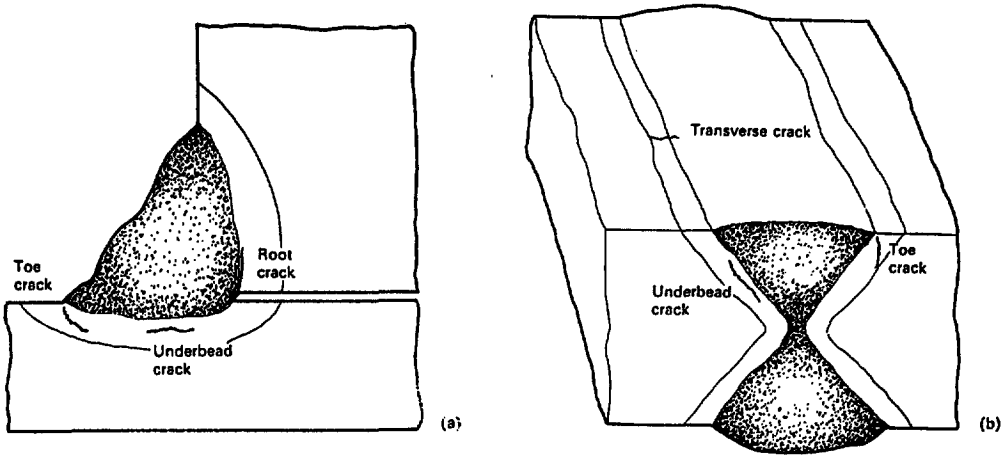

Fig. 1.1 Hydrogen-induced cracks in HAZs of (a) a fillet weld and (b) a butt weld [1.11].

Pore formation

Pore formation during arc welding can be due to two different mechanisms. The first mechanism is a direct consequence of the fact that under the arc more hydrogen can be absorbed than corresponds to the solubility in equilibrium with 1 bar molecular hydrogen gas. The second mechanism of pore formation is related to the difference in solubility of hydrogen in the liquid and in the solid phase of the metal. When the liquid solidifies the surplus of hydrogen will be concentrated just ahead of the solidification front. Because of the increasing amount of hydrogen the solubility will be locally exceeded resulting in the nucleation and growth of bubbles. When the bubbles are caught up by the solidification front, this will result in porosity in the weld.

In the case of welding aluminium hydrogen pore formation is a well known phenomenon [1.18-1.21]. Experimental work has shown that pore formation also occurs during the welding of steel [1.22-1.24].

Under certain conditions methane can be formed from the hydrogen and the carbon present in the material. This will result in a combined effect of pore formation due to the production of methane and changes in the composition of the weld metal due to the disappearance of carbon [1.25].

In spite of the fact that hydrogen plays an extremely important role during arc welding of iron and steel, limited information is available concerning the hydrogen absorption process. A number of investigations dealt with the question in what way hydrogen can be prevented from entering the weld [1.26-1.29], but most of this work is rather practical in nature and does not yield insight in the absorption process.

1.3 Scope of this thesis

This thesis deals with the process of hydrogen absorption during arc welding of iron and steel. Fundamental insight in this process is of vital importance as the hydrogen absorbed by the weld metal can result in serious problems, as described in the foregoing. Understanding of the absorption mechanism will make it possible to indicate in which ways hydrogen absorption can be reduced.

This thesis has the following structure.
In Chapter 2 the theoretical background of the behaviour of hydrogen during arc welding will be given. This includes the hydrogen behaviour in the welding arc and the absorption of hydrogen in the weld pool. Because of the lack of data concerning the behaviour of hydrogen during welding, a number of data will be presented which originate from non-arc equilibrium measurements. This applies especially to the solubility and diffusion data of hydrogen in iron and steel. The main sources of hydrogen during welding will be described, and the negative effects of hydrogen in iron and steel will be discussed. In the final part of this chapter the different methods for determining the hydrogen concentration in the weld will be presented.
In Chapter 3 the influence of hydrogen on the arc is analyzed using photographs of the arc and using the current-voltage characteristics with different shielding gas compositions. Also the influence of hydrogen on the weld pool shape is presented. Finally, the combination of the change in arc shape and weld pool shape will be discussed.
In Chapter 4 the results of the hydrogen absorption obtained under stationary arc conditions are given. Due to the fact that under these conditions no melting and solidification occurs a stable situation can be reached during the experiments. By means of a numerical method the initial hydrogen concentration in the liquid metal is calculated. This results in the proposal of a model for the absorption of hydrogen during welding under stationary arc conditions. The chapter ends with the application of the model under different experimental conditions.
In Chapter 5 the results are presented of absorption experiments carried out under arc welding conditions. Again the different welding parameters are varied and attempts are made to calculate the initial hydrogen concentration in the weld pool. The model obtained in Chapter 4 for welding under stationary arc conditions is extended to welding under travelling arc conditions and is used to explain the test results obtained under different experimental arc conditions.

References

1.1 T. Okada, H. Yamamoto and S. Harada, "Observation of the shielding gas flow pattern during arcing by the use of a laser light source", in Proceedings of International Conference on Arc Physics and Weld Pool Behaviour, London, The Welding Institute (1979), 203-213.

1.2 K. Schöbel, "Schutzgasschweißen mit Helium und Argon/Helium-Gemischen", Der Praktiker 29 (1977), 20-22.

1.3 D. Hilton, "Shielding gases for gas metal arc welding", Welding & Metal Fabrication 58 (1990), 333-334.

1.4 S.A. Gedeon and T.W. Eagar, "Assessing hydrogen-assisted cracking fracture modes in high-strength steel weldments", Welding Journal (Welding Research Supplement) 69 (1990), 213s-220s.

1.5 R.A. Oriani, "Hydrogen - the versatile embrittler", Corrosion 43 (1987), 390-397.

1.6 J.P. Hirth, "Effects of hydrogen on the properties of iron and steel", Metallurgical Transactions 11A (1980), 861-890.

1.7 S.P. Lynch, "Mechanism of hydrogen-assisted cracking", Metals Forum 2 (1979), 189-200.

1.8 P.C. van der Willigen, "Einfluß von Wasserstoff auf die Eigenschaften der Schweiße", Schweißen und Schneiden 9 (1957), 517-521.

1.9 J. Ruge, "Wasserstoffversprödung beim Schweißen höherfester Stählen", Schweißtechnik 27 (1977), 181-184.

1.10 J. Hewitt and J.D. Murray, "Effect of sulphur on the production and fabrication of carbon-manganese steel forgings", British Welding Journal 15 (1968), 151-158.

1.11 N. Bailey, F.R. Coe and T.G. Gouch, Welding steels without hydrogen cracking, Cambridge, Abbington (1993).

1.12 T. Terasaki, R. Karppi and K. Satoh, "Relationship between critical stress of HAZ cracking and residual diffusible hydrogen content", Transactions of the Japan Welding Society 10 (1979), 53-57.

1.13 G. Gnirß, "Wasserstoff und seine Wirkung beim Schweißen", TÜ 17 (1976), 367-377.

1.14 D. Hardie and J.J.F. Butler, "Effect of hydrogen charging on fracture behaviour of 304L stainless steel", Materials Science and Technology 6 (1990), 441-446.

1.15 T. Boniszewski and F. Watkinson, "Effect of weld microstructures on hydrogen-induced cracking in transformable steels: part I", Metals and Materials 7 (1973), 90-96.

1.16 F. Schat, "Koudscheuren in lasverbindingen", Utrecht (1981).

1.17 J. Vuik, "An update on the state-of-the-art of weld metal hydrogen cracking", Welding in the World 31 (1993), 308-321.

1.18 T. Shinoda and I. Masumoto, "Effects of chlorine additions on the occurrence of porosity in aluminium MIG welds", Welding International 12 (1989), 1034-1039.

1.19 D.G. Howden, "Porosity formation in aluminium weldments", Welding Journal 50 (1971), 112-114.

1.20 H. Thier, "Ursachen der Porenbildung beim Schutzgasschweißen von Aluminium und Aluminiumlegierungen", Schweißen und Schneiden 25 (1973), 491-494.

1.21 G.D. Nikiforov and A.G. Makhortova, "The conditions for pore formation when welding aluminium and its alloys", Welding Production 7 (1961), 9-16.

1.22 M. Uda, "A new process for preparation of ultrafine metal particles", Transactions of National Research Institute for Metals 24 (1982), 218-225.

1.23 M. Uda, T. Dan and S. Ohno, "Effect of hydrogen on blowhole formation in pure iron during solidification", IIW Doc. II-817-77 (1977).

1.24 R.E. Trevisan, D.D. Schwemmer and D.L. Olson, in Welding: Theory and Practice, D.L. Olson, R. Dixon and A.L. Liby (eds.), Amsterdam, Elsevier (1990), 79-145.

1.25 C.D. Lundin and K.K. Kahn, "Examination of creep rupture samples tested in hydrogen at elevated temperatures", Welding Research Council Progress Reports 45 (1990), 33-40.

1.26 D.S. Dunn, C.A. Nathalie and D.L. Olson, "Sol-gel fluxes for flux cored welding consumables", Journal of Materials for Energy Systems 8 (1986), 176-184.

1.27 D. McKeown, "Hydrogen and its control in weld metal", Metal Construction 7 (1985), 655-661.

1.28 B. Chew, "Hydrogen control of basic coated MMA welding electrodes - the relationship between coating moisture and weld hydrogen", Metal Construction 14 (1982), 373-377.

1.29 B. Chew, "Moisture loss and regain by some basic flux covered electrodes", Welding Journal (Welding Research Supplement) 55 (1976), 127s-134s.

CHAPTER 2

Theoretical background

2.1 Introduction

In this chapter the role of hydrogen in arc welding will be discussed in more detail.
First, the behaviour of hydrogen in iron and steel under equilibrium conditions will be presented, including the influence of welding on this behaviour. Emphasis is put on diffusion and solubility.
After describing the arc welding process in general, and especially the arc itself, the influence of hydrogen on the arc and vice versa will be reviewed.
Subsequently, attention will be given to the influence of hydrogen on the weld geometry.
Also the effects of hydrogen on the behaviour of the material, such as pore formation and cold cracking will be discussed.
Finally some remarks will be made about the analysis of the hydrogen concentration in welds.

2.2 Hydrogen in iron and steel

Values of the diffusion coefficient and the solubility of hydrogen in iron and steel are difficult to obtain experimentally. In literature the values of these parameters, often obtained under different conditions, are subject to some discussion. In the following sections the diffusion coefficient and the solubility, including the influence of other elements present in steel on these parameters, will be discussed.

2.2.1 *Diffusion*

Diffusion is the material transport taking place as a result of the existence of a concentration gradient of a specific element in a material. This is formulated by Fick's First Law, which in one-dimensional form can be written as [2.1]:

$$J = -D\frac{dc}{dx} \tag{2.1}$$

in which J = flux, defined as the number of atoms of an element crossing unit area per unit time,
c = concentration,
dc/dx = concentration gradient in direction x,
D = diffusion coefficient.

This equation shows that material transport will occur as long as a concentration gradient exists, which implies that if there is no concentration gradient the material transport due to diffusion will be zero.
If a steady state does not exist, that is, if the concentration at some point is changing with time, Eq. (2.1) should be used in combination with a mass balance equation. This leads to Fick's Second Law of diffusion, which describes the change in concentration in an infinitely small element where the flux on one side is different from the flux on the other side [2.1]:

$$\frac{\partial c}{\partial t} = D\frac{\partial^2 c}{\partial x^2} \tag{2.2}$$

in which c = concentration,
t = time,
D = diffusion coefficient,
x = distance.

The diffusion coefficient is dependent on the temperature according to the Arrhenius equation:

$$D = D_0 \exp\left(\frac{-Q}{RT}\right) \tag{2.3}$$

in which D = diffusion coefficient,
D_0 = diffusion constant,
Q = activation energy for diffusion,
R = gas constant,
T = absolute temperature.

A considerable amount of experimental work has been carried out on the diffusion of hydrogen in iron. Alefeld and Völkl [2.2] gathered the results of forty-six studies concerning the diffusion of hydrogen in alpha-iron. The values obtained are depicted in Fig. 2.1. The figure shows the occurrence of quite unsatisfactory scatter, especially at low temperatures. At 500 K the scatter is about one order of magnitude and decreases slightly with increasing temperature. Different explanations have been given for the observed scatter in the obtained results. These explanations are based on phenomena such as surface effects, trapping of hydrogen at lattice imperfections like impurities, dislocations, precipitates, grain boundaries, etcetera, the formation of immobile di-interstitials and the formation of molecular hydrogen in micro- or macropores.
About the value of the diffusion coefficient in gamma-iron less information is available, but the scatter in the results is considerably smaller.
The values of the diffusion data used in this thesis are given in Table 2.1. The used diffusion coefficient is given as a function of temperature in Fig. 2.2. For each of the phases of iron (liquid, delta, gamma and alpha) a value is used which is about the average of the values obtained in the various investigations. For temperatures below 400 K the values of D_0 and Q deviate considerably from those used for higher temperatures. This is due to the presence of imperfections in the material affecting the diffusion at low temperatures.
It is interesting to note that due to the small size of the hydrogen atom the activation energy for diffusion in iron is very low. As a result the hydrogen will diffuse extremely fast through the material even at temperatures below 750 K.

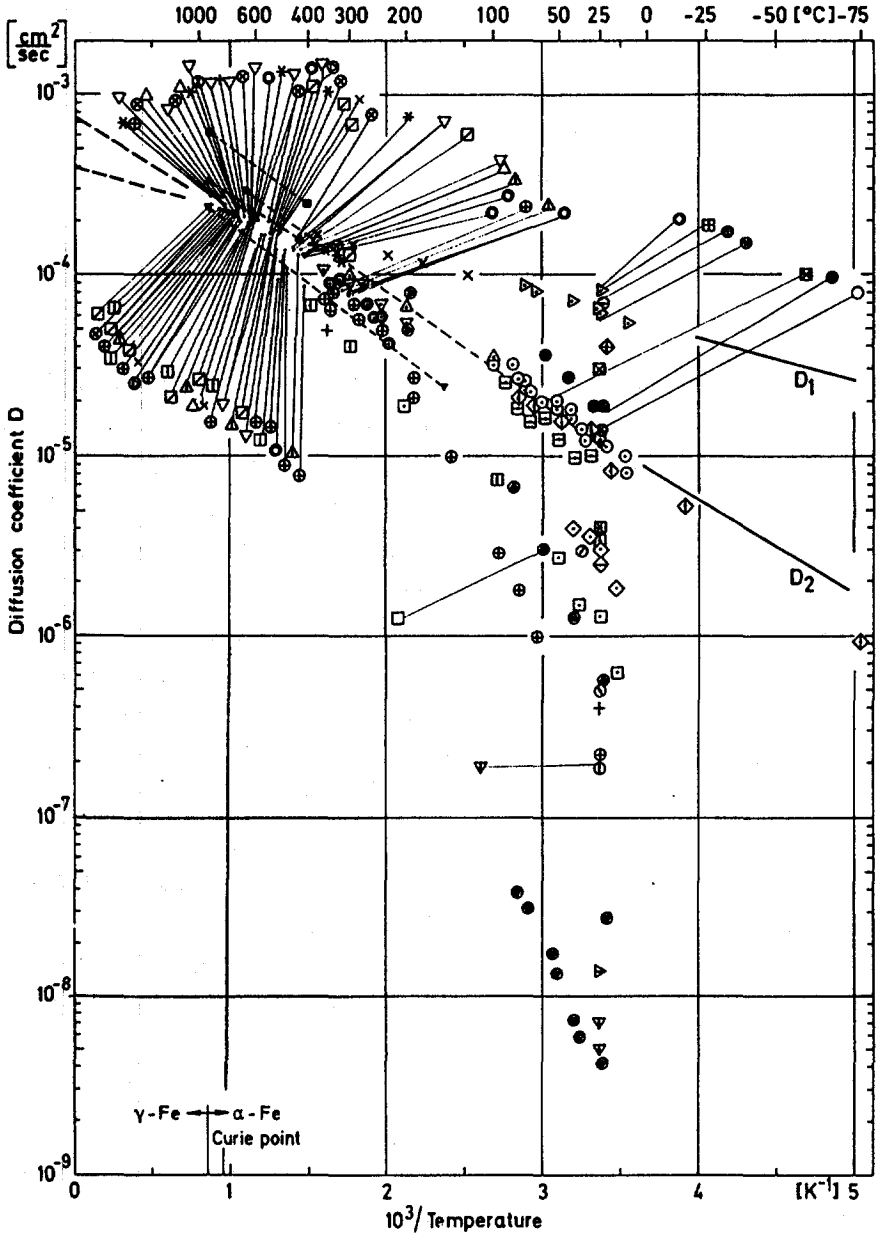

Fig. 2.1 Hydrogen diffusion coefficient in α-iron as a function of temperature, the results of 64 studies [2.2].

Table 2.1 Diffusion data for hydrogen in different phases of iron.

phase	temperature region (K)	D_0 (cm^2/s)	Q (J/mole)	Refs.
alpha-iron	273-473	1.20×10^{-1}	32719	2.5
alpha-iron	473-1185	1.40×10^{-3}	13296	2.5
gamma-iron	1185-1667	2.90×10^{-3}	32085	2.3
delta-iron	1667-1811	1.40×10^{-3}	13296	2.5
liquid iron	1811-1950	4.37×10^{-3}	17127	2.4

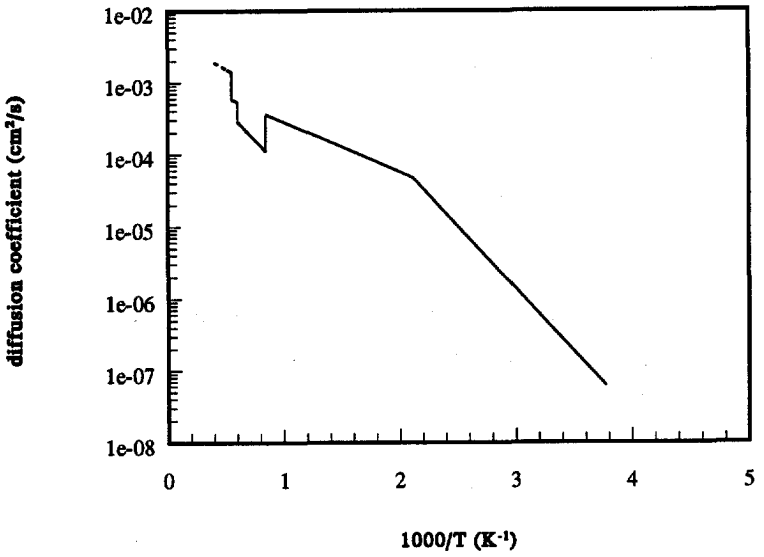

Fig. 2.2 Diffusion coefficient of hydrogen in iron as a function of temperature.

2.2.2 *Trapping*

A hydrogen atom present in a material can become attached to discontinuities in the microstructure, such as grain boundaries, dislocations, voids and alloying atoms [2.6]. These discontinuities are called "trap sites" or "traps".
As generally recognized, the concentration of hydrogen in trap site X, where near saturation occurs at low temperatures, must be expressed in terms of Fermi-Dirac statistics. For a single trap site the appropriate reaction is:

$$\underline{H} + X \rightleftharpoons H_x \tag{2.4}$$

in which $\underline{H}$ = hydrogen atom dissolved in the material,
X = trap site,
H_x = hydrogen atom attached to a trap.

For this reaction the equilibrium distribution can be expressed by the equation:

$$\frac{c_b}{(1-c_b)} = c \cdot \exp\left(\frac{H_b}{kT}\right) \tag{2.5}$$

in which c_b = concentration of hydrogen atoms bonded to a trap,
c = hydrogen concentration in the bulk material,
H_b = bonding enthalpy,
k = Boltzmann constant,
T = absolute temperature.

It must be mentioned that this equation does not apply for all traps and under all conditions [2.6]. For a more realistic description more complex equations must be used. However, Eq. (2.5) will help to illustrate the role of traps.
In Eq. (2.5) the relation between the concentration of hydrogen atoms bonded to a trap and the bulk concentration is given. The equation shows that the amount of hydrogen bonded to a trap increases when the binding enthalpy of the trap increases, when the concentration in the bulk material increases and when the temperature decreases.
The strength of a trap, characterized by the bonding enthalpy, is dependent on the type of

trap. For a number of different traps the bonding enthalpy is given in Table 2.2., together with the critical temperature T_c. Above this temperature the amount of bonded hydrogen decreases rapidly.
It should be realized that the amount of hydrogen bonded by traps is not only dependent on the type of trap, but also on the density and the distribution of the traps.

Table 2.2 Data for trapping of hydrogen in iron [2.6].

Trap	H_B (kJ/mole)	T_{crit} [1] (K)
H - perfect lattice	0	-
H - C	3.3	28
H - H	4.2	35
H - N	≥12.5	105
H - Ti	26.1	219
H - ½H_2, vapour phase or in void	28.6	-
H - dislocation core (screw)	20-30	≈210
H - dislocation core (mixed)	58.6	493
H - grain boundary	≈58.6	493
H - AlN interface	65	546
H - free surface [2]	70.7	594
H - Fe_3C interface	≥84	706
H - TiC interface	94.6	795
H - free surface [2]	95.5	803

[1] Calculated for bulk concentration $c_0 = 6.13 \times 10^{-7}$ at.%.

[2] Differences caused by surface roughness.

2.2.3 Solubility

Hydrogen has a relatively small solubility in iron and is easily trapped at defect sites. Because of this, there is little direct evidence about the nature of the sites occupied in the dissolved state. Impurity interstitials in a body centred cubic (BCC) lattice are generally assumed to occupy either octahedral or tetrahedral sites. Although the hydrogen site in iron has not yet been determined directly, evidence of studies of hydrogen in other BCC metals favours the tetrahedral site [2.7]. Both sites are small with respect to the size of the hydrogen atom and as a result the lattice in the vicinity will be locally strained.

The solubility of hydrogen in a material is determined by its chemical potential. This is expressed by the equation [2.7]:

$$\mu(c,T) = \Delta H - T\Delta S + RT \cdot \ln(c) \tag{2.6}$$

in which μ = chemical potential,
c = concentration,
T = absolute temperature,
ΔH = change in enthalpy,
ΔS = change in entropy,
R = gas constant.

The concentration is defined as the number of atoms per interstitial site. Generally speaking, the entropy term is negligibly small in relation to the enthalpy term. As a result Eq. (2.6) can be rewritten as:

$$c = K \cdot \exp\left(\frac{\mu}{RT}\right) \tag{2.7}$$

in which c = concentration,
K = solubility coefficient,
μ = chemical potential,
R = gas constant,
T = absolute temperature.

The solubility coefficient, which characterizes the solubility of hydrogen in a material, is defined as:

$$K = K_0 \cdot \exp\left(\frac{-\Delta H}{RT}\right) \tag{2.8}$$

in which K = solubility coefficient,
K_0 = solubility constant,
ΔH = change in enthalpy,
R = gas constant,
T = absolute temperature.

The solubility of hydrogen in a material is dependent on the lattice type and on the microstructure. In spite of the small dimensions of the hydrogen atom, the solubility is low at room temperature in ferritic materials (BCC) [2.8]. Because of the relatively large size of the octaeder sites in the face centred cubic (FCC) lattice, hydrogen has a relatively good solubility in austenitic materials.

A problem which can occur when measuring the solubility of hydrogen in materials is the influence of traps (see section 2.2.2). At room temperature there is a number of possible traps for hydrogen in the iron lattice as shown in Table 2.2. Often the solubility of hydrogen at room temperature is determined by extrapolation of values obtained at higher temperatures, where there are no or less trap sites present. Due to the presence of traps the actual solubility is higher than the value obtained by extrapolation.
In Fig. 2.3 the hydrogen solubility in pure iron is plotted as a function of temperature. To circumvent the problems concerning the solubility at low temperatures due to the presence of traps the figure shows only the solubility above 600°C [2.9].

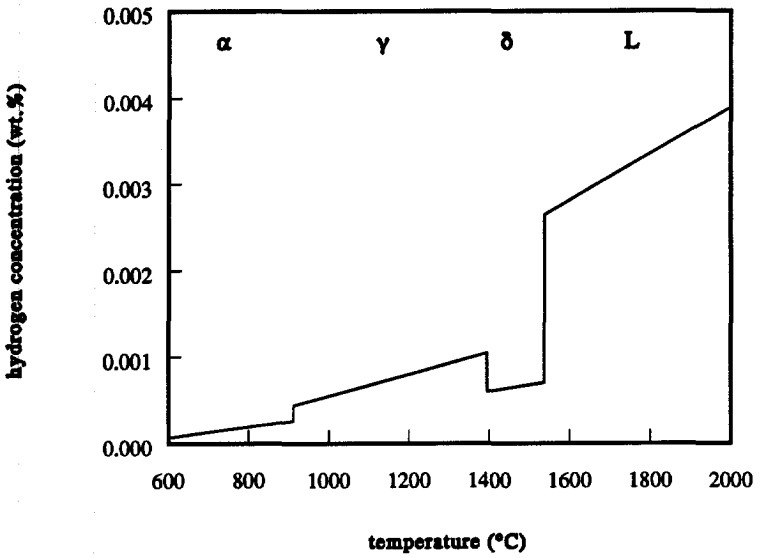

Fig. 2.3 The solubility of hydrogen in pure iron in equilibrium with 1 bar H_2 as a function of temperature [2.9].

2.2.4 Sieverts' Law

It is evident that the solubility of a gas in a material, as defined in the previous section, is dependent on the external partial pressure of the gas.
The relation between the solubility and the partial pressure in the case of a di-atomic gas is given by Sieverts' Law [2.10-2.12]. In the case of hydrogen Sieverts' Law can be written as:

$$[H] = K\sqrt{p_{H_2}} \tag{2.9}$$

in which [H] = hydrogen concentration in the metal,
K = solubility coefficient,
p_{H2} = hydrogen partial pressure.

Sieverts' Law predicts a direct proportional relation between the hydrogen concentration in the molten metal and the square root of the hydrogen partial pressure. This relation has been experimentally confirmed by many investigators (e.g. [2.13]).

The solubility coefficient K can be written as a function of temperature. This leads for hydrogen in molten iron to the equation [2.13]:

$$K = \frac{[H]}{\sqrt{p_{H_2}}} = 0.0001 \cdot \exp\left(\frac{-4388}{T} + 5.55\right) \qquad (2.10)$$

in which K = solubility coefficient,
[H] = hydrogen concentration in the metal,
p_{H2} = hydrogen partial pressure,
T = absolute temperature.

In Fig. 2.4 the hydrogen solubility in pure iron is plotted as a function of the hydrogen percentage in the gas at 1600°C according to Eq. (2.10).

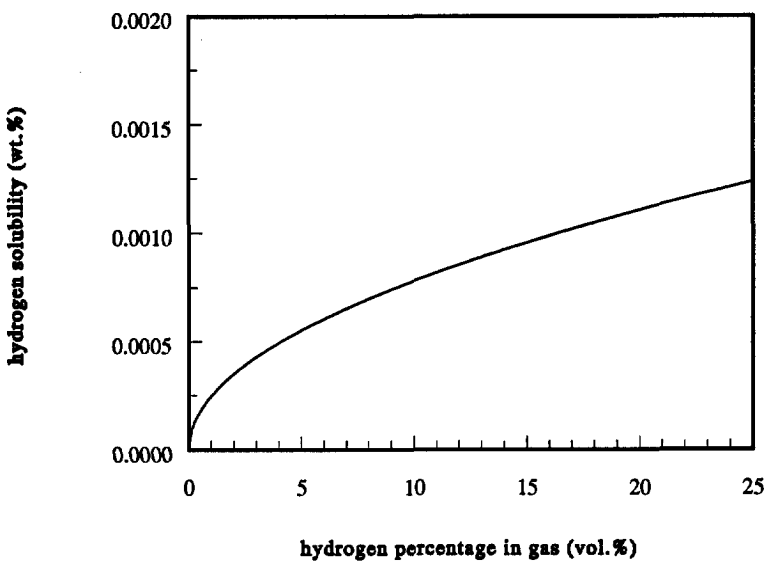

Fig. 2.4 Equilibrium hydrogen solubility in pure iron as a function of hydrogen percentage in the gas at a temperature of 1600°C.

Under equilibrium conditions Eq. (2.9) is always valid, but this is not necessarily the case for arc welding, due to the fact that the temperature of the arc plasma is much higher than the temperature of the weld metal and dissociation of molecular hydrogen may take place.
Under these conditions Eq. (2.9) takes the form:

$$[H] = 2\alpha_d C_1 p_{H_2} + C_2\sqrt{(1-\alpha_d)p_{H_2}} \qquad (2.11)$$

in which [H] = hydrogen concentration in the metal,
α_d = fraction of the hydrogen which is dissociated,
C_1, C_2 = constants,
p_{H2} = hydrogen partial pressure.

2.2.5 Influence of alloying elements and impurities

Elements present in iron alloys can be divided into two categories. The first group consists of alloying elements. These elements are added intentionally to the metal for improving the properties of the material. The other group of elements comprises the impurities, which are left behind after purification of the material.
All elements have a specific influence on the solubility of hydrogen in iron. This can be an increase (as in the case of Ti, Ta, V, Cr and Mn [2.9]) or a decrease of the solubility (as in the case of Cu, Co, Sn, Al, Si, B, C, P and S [2.9]). In Fig. 2.5 the influence of a number of elements on the solubility of hydrogen in iron at 1600°C is given.
Little is known about the influence of those elements which form chemical compounds with hydrogen in the liquid phase, or during solidification. For example, it is known that rare-earth metals form stable hydrates in the liquid phase [2.14]. Titanium seems to form hydrates during solidification and in this way is assumed to prevent hydrogen cracking [2.15].

The presence of alloying elements and impurities also affects the diffusion behaviour of hydrogen in iron. This occurs essentially in two ways: by trapping the hydrogen atoms and by straining the iron lattice.
As an example the influence of chromium on the diffusion coefficient of hydrogen in iron can be mentioned. Bockris et al. [2.16] studied the diffusion of hydrogen in various iron-chromium alloys. They found a distinct change in diffusion coefficient with increasing chromium content. When increasing the chromium content to 10 at.% the diffusion coefficient at room temperature decreases about three decades, whereas a further increase in the chromium content to 25 at.% results in a much smaller decrease of the diffusion coefficient.

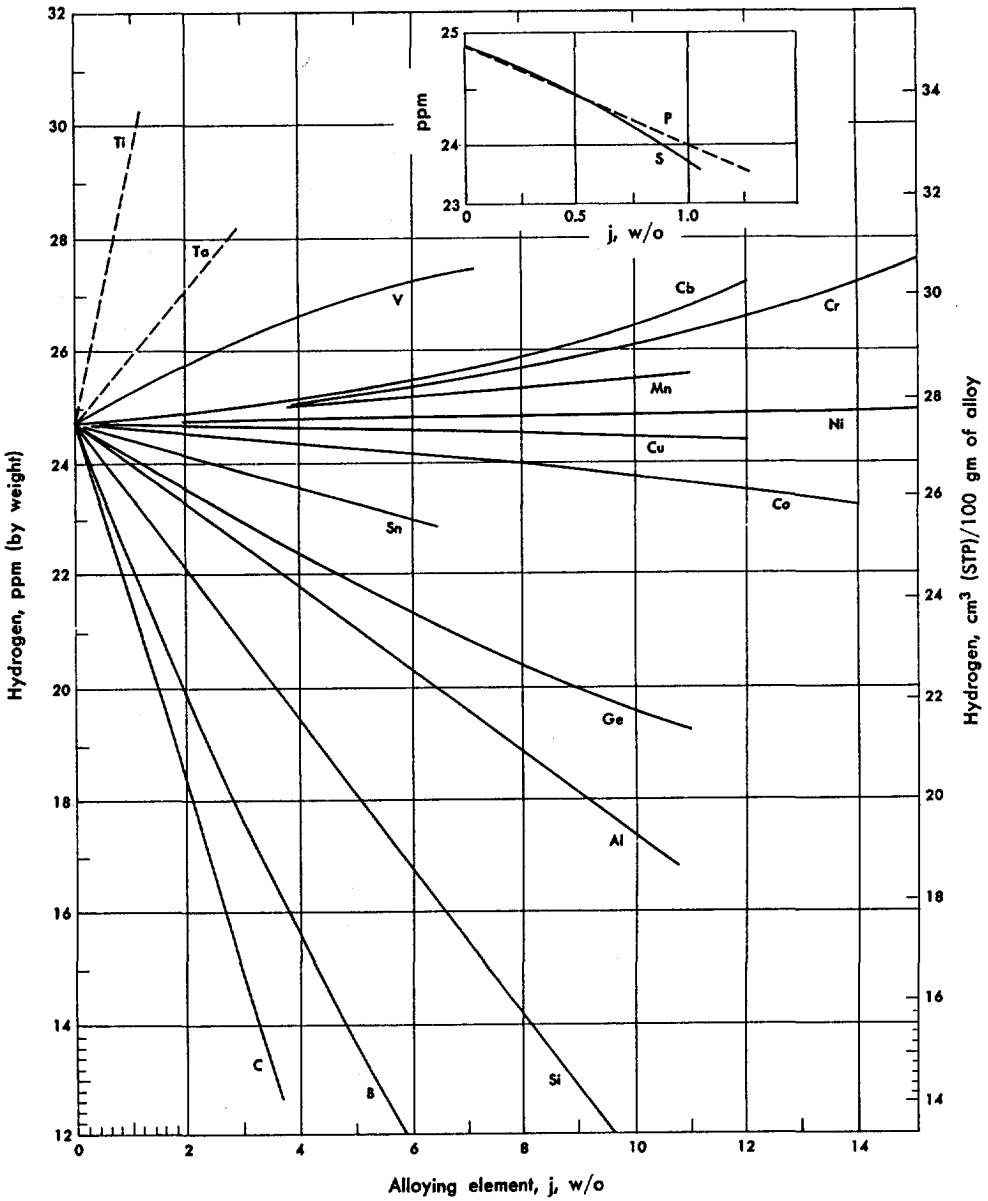

Fig. 2.5 Hydrogen solubility in iron in equilibrium with 1 bar hydrogen gas as a function of the concentration of a number of elements at 1600°C [2.9].

2.3 The welding arc

2.3.1 General description

The electric arc is an electric discharge in a partially ionized gas (plasma). Electric arcs can be distinguished from other types of gas discharges by their relatively high current (10 to 1000 A) and relatively low voltage (10 to 40 V). In the low current region, a lower current limit exists because the plasma temperature decreases with decreasing arc current, ultimately resulting in an insufficient degree of ionization. To maintain a sufficient degree of ionization, arc voltage must increase and the glow discharge regime is entered. Generally speaking, there is no upper limit for the arc current, although arc stability may suffer as the arc plasma tends to become turbulent at high arc current [2.17].

The electric arc is used on a broad scale for lighting purposes (arc lamps), for melting (steel production) and for welding (arc welding).
In the case of arc welding the arc burns between a cylindrical (consumable or non-consumable) electrode and the workpiece to be welded. The distance between the electrode and the workpiece ranges from 1 to 10 mm and under these conditions the arc is bell-shaped. Due to the heat produced by the arc a weld pool is formed in the workpiece, which upon solidification turns into the required weld. To prevent contact between the liquid metal and the surrounding atmosphere a shielding gas is used, in most cases argon or helium. The situation is schematically presented in Fig. 2.6.
The most readily obtainable parameters governing arc behaviour are arc current and arc voltage. The arc current-arc voltage characteristic depends on arc length and on shielding gas composition, and also on the chemical composition of the anode and the cathode.
When the arc length is increased, the arc voltage also increases. This increase is approximately proportional to arc length, suggesting that the field strength in the arc column is independent of the arc length. The surface condition of the anode and the cathode also plays a significant role in the physics of the arc, changes in the thermodynamic state of these surfaces can substantially affect arc voltage. This can be the case when GTA welding in a hydrogen containing atmosphere. The presence of hydrogen results in a decrease of oxygen in the surface layer of the electrode. This oxygen, mostly bonded to thorium or zirconium, is added to the tungsten electrode to favour the electron emission.

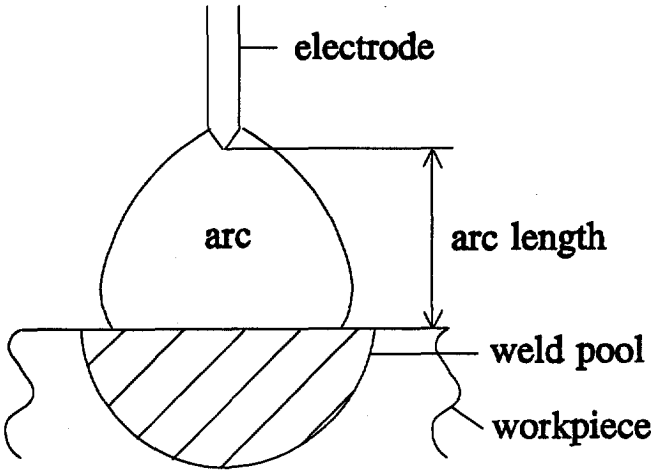

Fig. 2.6 Schematic presentation of the arc.

The welding arc can be divided in three regions: the anode fall region, the cathode fall region and the arc column. The anode fall region and the cathode fall region are the boundary regions between the arc column and the anode and cathode, respectively. They are extremely thin, in the order of the electron mean free path. The electric field strength in these regions can be as high as 10^7 V/m. Due to the high field strength and the modest collision frequencies, the electron temperature and the heavy particle temperature differ significantly.

The arc column is a region, in which well established plasma physics theories can be applied. The plasma in the arc column is considered to be in Local Thermodynamic Equilibrium (LTE). This means that the energetic coupling between electrons and heavy particles is relatively strong and electrons and heavy particles are in mutual equilibrium (i.e. have the same temperature). However, total equilibrium does not exist, since the electrons and heavy particles are not in equilibrium with the photons, which can escape from the plasma. The field strength in the arc column is relatively low (~10^3 V/m) and the temperature of the arc column is high (5000-25000 K, see Fig. 2.7).

In the fall region above the weld metal the temperature is much lower than the temperature in the arc column. It will be close to the temperature of the metal, i.e. 2500 to 3000 K.

About the precise temperature of the weld pool surface no exact data are available. However, Block-Bolten and Eagar [2.18] state that the temperature does not exceed 2800 K in the case of steel.

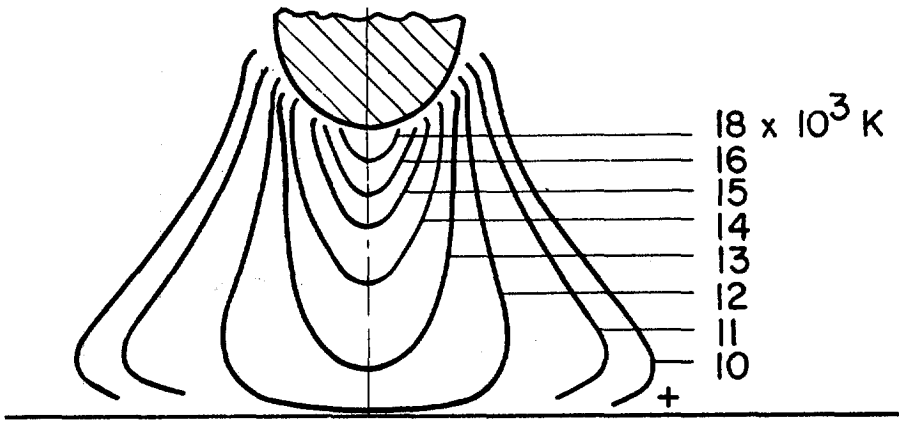

Fig. 2.7 Isothermal map of an argon-tungsten arc [2.19].

2.3.2 Physical properties

A very important arc parameter is the electrical conductivity σ. It determines the current density and plays a decisive role in the heat balance of the arc. The electrical conductivity can be expressed as:

$$\sigma = \frac{j}{E} = \frac{e^2 n_e l_e}{\sqrt{8 m_e kT/\pi}} \qquad (2.12)$$

in which σ = electrical conductivity,
j = current density,
E = electrical field strength,
e = electron charge,
n_e = electron density,
l_e = electron mean free path,
m_e = electron mass,
k = Boltzmann constant,
T = absolute temperature.

The electron density and the mean free path of the electron are only dependent on temperature. This means that also the electrical conductivity is only a function of the temperature.
In addition to electrons, ions also contribute to the charge transport in the arc. However, as the mass of electrons is much smaller than that of ions, the charge transport is realized primarily by electrons. A good estimate of the ratio of the current carried by electrons and that carried by ions is given by the equation:

$$\frac{j_e}{j_i} \approx \sqrt{\frac{m_i}{m_e}} \qquad (2.13)$$

in which j_e = electron current density,
j_i = ion current density,
m_e = electron mass,
m_i = ion mass.

For argon, the ion contribution amounts to about 0.4% of the total current, for hydrogen this fraction is about 2.3%. Thus, it can be concluded that the electron current density is much more important than the ion current density.

To maintain an arc over longer periods of time a sufficiently large degree of ionization of the plasma is required. The degree of ionization depends strongly on the temperature and can be written in the form (Eggert-Saha equation [2.19]):

$$\frac{\alpha_i^2}{1-\alpha_i^2} = C_1 \frac{T^{5/2}}{p} \cdot \exp\left(\frac{-E_i}{kT}\right) \tag{2.14}$$

in which α_i = degree of ionization,
C_1 = constant,
T = absolute temperature
p = pressure,
E_i = ionization energy,
k = Boltzmann constant.

An important parameter in Eq. (2.14) is the ionization energy. Values of the ionization energy for a number of atoms and molecules are presented in Table 2.3.

Table 2.3 Ionization energy of some atoms and molecules [2.20].

element	E_i (eV)	element	E_i (eV)
He	24.59	O_2	12.06
Ar	15.76	C	11.26
H	13.60	P	10.49
H_2	15.43	S	10.36
N	14.53	Fe	7.87
N_2	15.58	Ti	6.82
O	13.62	W	7.98

During ignition of the arc the only elements which can be ionized are the elements present in the shielding gas. During the welding process metallic elements, which vaporize from the weld pool and enter the arc will play a dominant part in the electrical conductivity of the plasma due to their relatively low ionization energy.

When di-atomic gases are present in the shielding gas dissociation can also play a role, due to the high temperature of the arc. The degree of dissociation is a function of the temperature and can be expressed by the equation [2.19]:

$$\frac{4\alpha_d^2}{1-\alpha_d^2} = C_2 \frac{T^{5/2}}{p} \cdot \exp\left(\frac{-E_d}{kT}\right) \qquad (2.15)$$

in which α_d = degree of dissociation,
C_2 = constant,
T = absolute temperature,
p = pressure,
E_d = dissociation energy,
k = Boltzmann constant.

An important parameter in Eq. (2.15) is the dissociation energy. Values of the dissociation energy of hydrogen, nitrogen and oxygen are listed in Table 2.4. In the case of hydrogen, which has a relatively small dissociation energy, 50% will be dissociated at a temperature of 4000 K and more than 95% will be dissociated at a temperature of 6000 K.

Table 2.4 Dissociation energy of some di-atomic gases [2.20].

gas	E_d (eV)
H_2	4.48
N_2	9.76
O_2	5.08

The composition of a hydrogen arc as a function of temperature is given in Fig. 2.8. The figure shows that the hydrogen starts to dissociate above a temperature of about 2000 K, whereas ionization of the hydrogen atoms starts to occur at considerably higher temperatures (above 8000 K). Ionization of molecular hydrogen is of no importance in the temperature range of the welding arc.

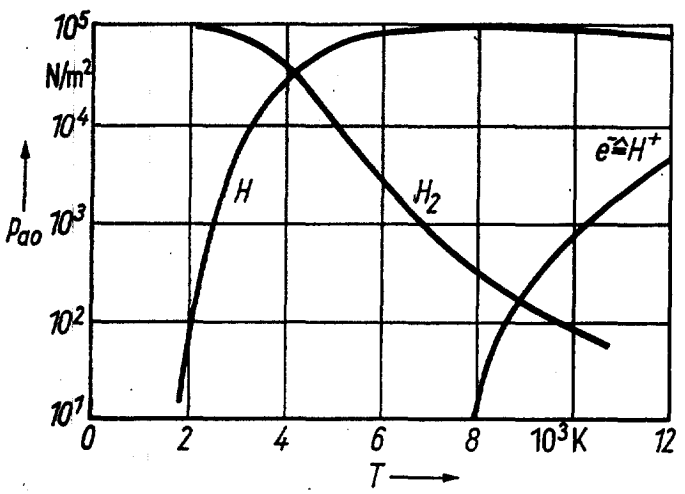

Fig. 2.8 Hydrogen arc composition as a function of temperature (total pressure 1 bar = 10^5 N/m²) [2.21].

During welding an important part of the energy of the plasma is transferred by means of thermal conduction. The thermal conductivity is defined as:

$$\Delta Q = \kappa \frac{dT}{dx} \tag{2.16}$$

in which ΔQ = heat flowing through unit surface area per unit time,
κ = thermal conductivity coefficient,
dT/dx = temperature gradient in direction x.

The total thermal conductivity is the sum of a number of different contributions, which can be expressed as:

$$\kappa = \kappa_g + \kappa_e + \kappa_i + \kappa_d \tag{2.17}$$

in which κ = total thermal conductivity coefficient,

κ_g = thermal conductivity coefficient due to the collisions of heavy particles,

κ_e = thermal conductivity coefficient due to the collisions between electrons and heavy particles,

κ_i = thermal conductivity coefficient due to the diffusion of ionized atoms and electrons,

κ_d = thermal conductivity coefficient due to the diffusion of dissociated molecules.

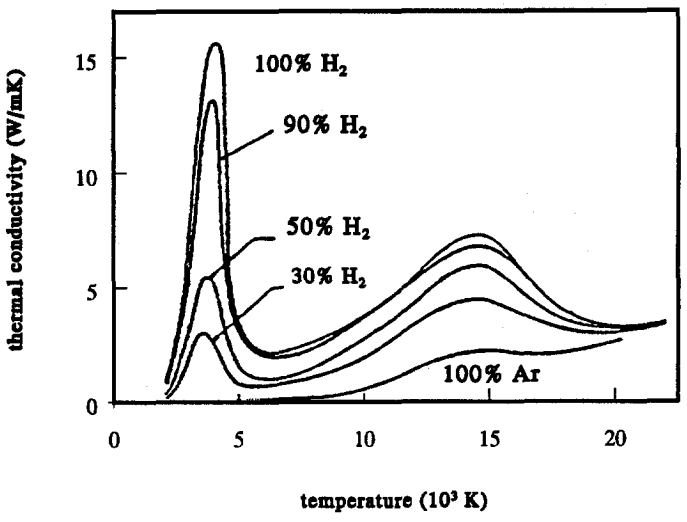

Fig. 2.9 Thermal conductivity of some argon-hydrogen mixtures as a function of the temperature (pressure 1 bar) [2.22].

In Fig. 2.9 the total thermal conductivity is given as a function of the temperature for some argon-hydrogen mixtures. The figure shows that the thermal conductivity of hydrogen is very high compared to that of argon and has a prominent peak (due to dissociation) at approximately 4000 K and a somewhat less pronounced peak (due to ionisation) at approximately 14000 K.

2.4 Weld bead formation

During the welding process a weld is formed by melting and subsequent solidification of metal. The quality of the weld produced depends primarily on its mechanical properties. However, also the geometry of the weld plays a role of importance. This geometry is determined by two factors: the heat input and the heat flow in the weld pool.

2.4.1 Heat input

The heat input is the quantity of energy introduced in the weld per unit length and can be expressed by the equation [2.19]:

$$H_i = \frac{f_1 VI}{v} \tag{2.18}$$

in which H_i = heat input,
f_1 = heat transfer efficiency, the heat transferred to the workpiece per unit time divided by the power of the heat source,
V = arc voltage,
I = arc current,
v = travel speed of the heat source.

Only part of the energy introduced in the material is used for the actual formation of the weld. This is expressed by the melting efficiency f_2. This parameter is defined as the minimum amount of energy required for heating (from room temperature to the melting point) and melting the metal divided by the heat generated by the heat source. This can be written as [2.19]:

$$f_2 = \frac{qA_m v}{VI} \tag{2.19}$$

in which f_2 = melting efficiency,
q = heat required to elevate a given volume of metal from room temperature to its melting point and subsequently convert this volume from the solid state to the liquid state,
A_m = weld metal transverse cross section area,
v = travel speed of the heat source,
V = arc voltage,
I = arc current.

The melting efficiency depends both on the process used and the material being welded. It also depends on factors such as joint configuration and plate thickness.

2.4.2 Flow in the weld pool

The geometry of the weld pool is for an important part determined by heat conduction in the material, i.e. the heat flow from the heat source (arc) through the weld pool to the surrounding metal. In the simple case of a point-like heat source under three-dimensional heat flow conditions (thick plate) the shape of the weld pool (transverse cross-section) will be semi-circular (see Fig. 2.10a). In the more realistic situation of a radially extended heat source (for instance with Gaussian radial energy distribution) the weld pool will assume a more flattened shape, the width being more than twice the penetration depth (see Fig. 2.10b).

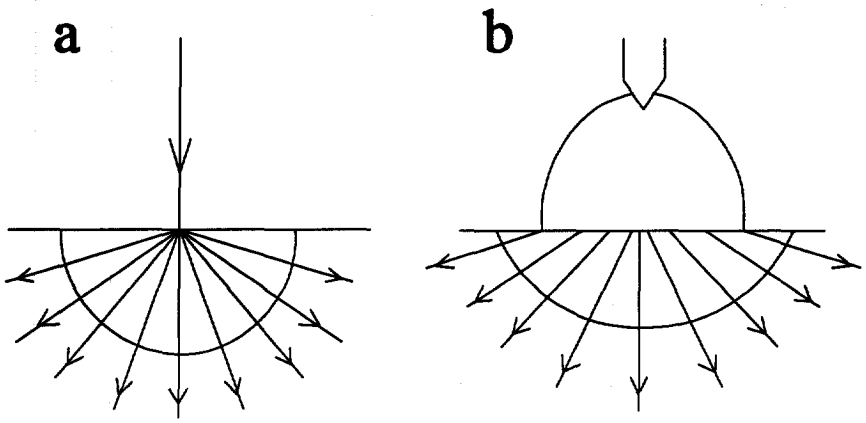

Fig. 2.10 Transverse cross section of the weld pool for a) a point-like heat source and b) an extended heat source (arc).

In addition to heat conduction, flow of the liquid weld metal (fluid flow) will also play an important role in determining the weld pool shape. In fact, it can lead to significant deviations from the weld pool shape(s) mentioned above.

Several forces may generate flow of the liquid metal in the weld pool. These forces include drag due to gas flow, electromagnetic forces (Lorentz forces), surface tension forces (Marangoni forces) and arc jet forces [2.23].
In most cases the fluid flow in the weld pool is dominated by Marangoni forces, which are caused by the gradient of the surface tension acting on the weld pool surface [2.24]. The surface temperature drops from a maximum at the arc root to the melting point at the weld pool boundary. In pure liquid metal the surface tension increases as the temperature drops, resulting in a force acting away from the centre and outward to the weld pool boundary. Surface active elements in molten metal segregate preferentially in the vicinity of the surface of the solvent liquid metal and lower the magnitude of the surface tension. Small concentrations of surface active additions generally change the temperature dependence of the surface tension of the solvent metal or alloy so that, for a limited range of temperatures above the melting point, the surface tension increases with increasing temperature. Such a surface tension gradient will lead to flow in the opposite direction, radially inward. In Fig. 2.11 the surface tension of a molten iron alloy with and without surface active elements is presented as a function of the temperature. The two

conditions depicted generate weld pool flows as shown in Fig. 2.12 [2.25]. When the flow of the metal in the vicinity of the surface is outward, the weld pool is wide and shallow, when the flow is inward the weld pool is small and deep.

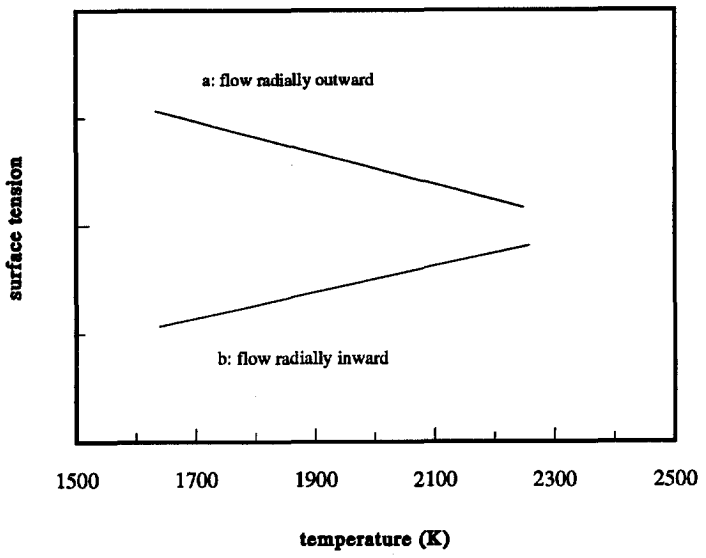

Fig. 2.11 Surface tension as a function of temperature of an iron alloy, a) without surface active elements and b) with surface active elements.

Positive temperature coefficients of the surface tension are particularly apparent in binary iron systems containing Group VI metalloids (O, S, Se, Te), which exhibit very high surface activity in this solvent. Hydrogen on the other hand is not significantly surface active in iron [2.26]. If the presence of hydrogen has an influence on the concentration of free surface active elements, then hydrogen will also have an (indirect) influence on the weld pool flow [2.24].

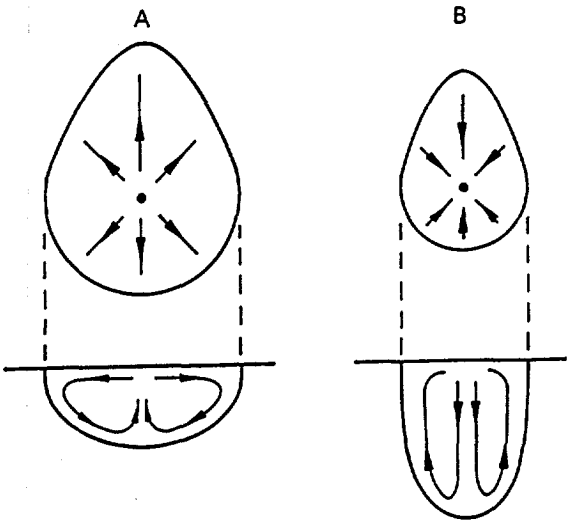

Fig. 2.12 Surface tension induced fluid flow in a weld pool: a) without surface active elements and b) with surface active elements [2.25].

2.5 Sources of hydrogen during welding

As mentioned earlier, hydrogen plays an important role in arc welding, mostly in a negative sense. In fact, it can be the main cause of serious manufacturing problems of welded structures.

Hydrogen can originate from the following sources:

Welding consumables. In general, most investigators believe that under practical welding conditions the main origin of hydrogen is to be found in water in the welding consumables [2.27-2.29]. Water can be present in the welding consumables in different forms:

1) Free moisture present as water molecules absorbed by most powdery materials when exposed in humid air. This water is readily expelled by drying at around 100°C.

2) Moisture absorbed from the air, especially by the dried silicate networks and the alkaline oxide residues of some organic extrusion aids after baking. This moisture too is readily dislodged at a temperature of 100°C.

3) Moisture retained by the silicate binders during initial drying. Heating up to 400°C is needed to remove this.

4) Crystallization moisture and colloidally absorbed moisture, which may be present in many of the minerals, e.g. feldspars, clays, micas etcetera, used in consumable manufacturing. This moisture will disappear by heating above 300°C.

In addition structural hydroxyl groups can be present in some organic substances, e.g. alginates and cellulose. Most of these groups decompose and release hydrogen at around 200-300°C. There are also some inorganic compounds, e.g. clays, in which structural hydroxyl groups are present. Some of these do not completely release their hydrogen until heating above 900°C.

The surrounding atmosphere. The atmospheric humidity can also be an important source of hydrogen. By using a shielding gas the arc and the liquid metal can be excluded from the surrounding atmosphere. In this respect one should be aware of the fact that the shielding gas might contain very small amounts of water as impurity.

Metal surface. The most important hydrogen sources on the metal surface are: moisture, grease, organic compounds, paint and atmospheric dust. They can be easily removed by cleaning the surface of the metal.

Oxides on the surface of the material. It is probable that the oxide layer is hygroscopic and hence contains water. Oxides may not only exist of Me_xO_y, but may also contain hydroxides, $Me_x(OH)_y$. Butkova et al. [2.30] and Murphy et al. [2.31] state that the hydrated oxide layer is the most important source of hydrogen when welding aluminium. In the case of steel it is possible to remove the oxide layer from the surface.

2.6 Negative effects of hydrogen on iron and steel

The mechanical properties of iron and steel are in general negatively affected by the presence of hydrogen. The hydrogen degradation of iron and steel can be the result of different mechanisms [2.32]. In the case of arc welding of steel two phenomena are of particular importance: pore formation and hydrogen-induced cracking.

2.6.1 Pore formation

When the concentration of a gas dissolved in molten metal exceeds the solubility, bubble formation may occur. This is a phenomenon which can easily take place during arc welding. It can manifest itself in two different situations: in the weld pool and during solidification of the weld at the solidification front.

In the first case the amount of gas absorbed during the arc welding process exceeds the solubility in the heated metal, resulting in the nucleation and growth of bubbles. In the second case bubbles are produced at the solidification front due to the fact that the solubility of the gas in the solid metal is much lower than that in the molten metal. The jump in solubility at the solidification temperature results in a surplus of the gas ahead of the solidification front. The gas concentration ahead of the solidification front rises and eventually exceeds the solubility of the gas at that

temperature, resulting in the nucleation and growth of bubbles.
Bubble formation leads to porosity when the bubbles are caught up by the moving solidification front [2.33]. In the case of arc welding of steel pore formation by hydrogen has been observed in different situations [2.34-2.36].

2.6.2 Hydrogen-induced cracking

Hydrogen-induced cracking is also known as cold cracking or delayed cracking. It occurs in steels during fabrication and in service and is thus not confined to welding. However, when it occurs as a result of welding, the cracks are sited either in the heat affected zone (HAZ) of the parent material or in the weld metal itself.

Hydrogen-induced cracking in the HAZ is only possible when the conditions outlined below occur simultaneously.

- Hydrogen dissolved in the material. When hydrogen is present in the arc it can be absorbed by the weld pool and transferred to the HAZ by diffusion.
- Tensile stresses act on the weld. These arrive inevitably from thermal contractions during cooling and may be supplemented by other stresses developed as a result of rigidity in the parts to be joined.
- A susceptible HAZ microstructure is present. In the HAZ microstructures like bainite and martensite can be formed by rapid cooling. These microstructures are more susceptible to hydrogen embrittlement than other microstructures of the HAZ. Hydrogen cracks, when present, are invariably initiated in these microstructures.
- A low temperature is reached. The greatest risk of cracking occurs when temperatures near ambient are reached and cracking may thus take place several hours after welding has been completed. Cracking is unlikely to occur in structural steels above about 150°C, and in any steel above about 250°C.

Cracks in the HAZ are usually sited either at the weld toe, the weld root, or in an underbead position. Hydrogen cracks may be intergranular, transgranular, or a mixture with respect to the transformed microstructure in which they lie. They may vary in length from a few microns to several millimetres. In Fig. 2.13 an example of a crack in a multipass fillet weld in the HAZ in C-Mn steel is given [2.37].
Under certain circumstances hydrogen cracking can also occur in the weld metal. As the alloy contents of both parent plate and weld metal are increased, cracking in the weld metal rather than in the HAZ may become the principal problem. The same conditions which lead to HAZ cracking apply to weld metal, namely hydrogen, stress, susceptible microstructures and low temperature.

If the cracks originate at the weld root they are often longitudinal to the weld. If they are buried or are located at the surface, they may be transverse to the weld. Under the microscope they are usually recognized as being predominantly transgranular.

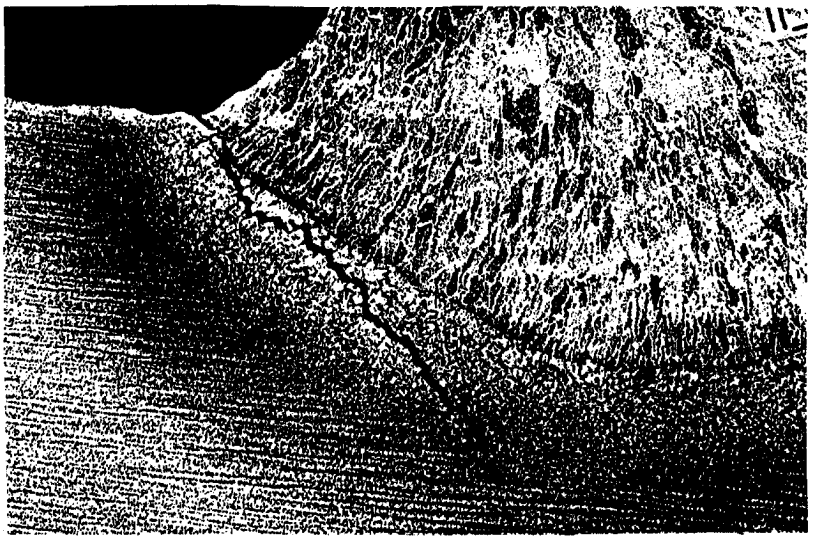

Fig. 2.13 Hydrogen-induced crack at the toe of a multipass fillet weld in the HAZ in C-Mn steel (x20) [2.37].

The interactions between the four factors responsible for hydrogen cracking are of great concern. Although a number of theories explaining the crack initiation exists, the initiation is still relatively unclear [2.6,2.38]. Today it is generally accepted that the entire process is caused by a combination of different mechanisms.

To prevent hydrogen cracking, the risk caused by the four factors mentioned above must be minimized.
The hydrogen absorbed by the weld metal, which is dealt with in this study, will be distributed as a result of diffusion over the HAZ and the parent metal. The amount of hydrogen in these regions depends on several factors such as the original amount absorbed, the size of the weld and the cooling conditions. In general, the more hydrogen present in the metal, the greater the risk of cracking.

2.7 Hydrogen analysis

The problems encountered when analyzing the hydrogen concentration in ferritic weld metal are a direct consequence of the high diffusion rate of hydrogen in iron and steel. Even at room temperature the diffusion rate of hydrogen is still considerable and as a result hydrogen can easily escape from the material.
At room temperature hydrogen can be present in iron alloys in two forms. In the first place hydrogen can be present as atoms trapped at special sites in the lattice. This is the so called residual hydrogen (see section 2.2.2), which becomes mobile at high temperatures. In the second place hydrogen can be present as so called diffusible hydrogen. During and directly after welding the main part of this hydrogen disappears through diffusion to the surrounding atmosphere. A small part of the diffusible hydrogen remains behind in the metal and it is this hydrogen which forms the main cause of hydrogen-induced cracking.

In the following a brief description is given of the most important methods developed to determine the hydrogen present in welds.

Mercury method.
A number of methods has been developed for the analysis of diffusible hydrogen in weld metal. Most of these methods are based on the principle of rapid cooling of the weld and collecting the hydrogen by storing part of the weld for a long period of time under a fluid [2.39].
The most important of these methods are extensively described in British Standard 6693 (1986) [2.40], DIN 8572 (1981) [2.41] and International Institute of Welding Doc.II-1155-91 (1991) [2.42].
The method developed by the International Institute of Welding (II-1155-91) is used in the experiments described in Chapter 5 of this thesis. The method includes a strict procedure for welding. Welding must take place on a certain base material of specific dimensions with prescribed welding parameters. After welding the sample is stored in alcohol or acetone saturated with solid carbon dioxide. For determination of the diffusible hydrogen the sample is placed under mercury in an eudiometer for 72 hours, after which the amount of evolved hydrogen gas is measured. Because of the toxicity of mercury, safety precautions should be taken. Because of this the method cannot be used in all situations. When the use of mercury is not tolerated there is the possibility to use glycerol under reduced pressure, which gives roughly the same results.

Chromatographic method.

Another method used for determining diffusible hydrogen is the chromatographic method [2.39,2.43,2.44]. After welding the sample is stored under liquid nitrogen. To determine the hydrogen content, the sample is placed in the chromatograph in which it is heated to the desired temperature. The hydrogen which leaves the sample is carried away by a carrier gas to a measuring cell. Determination of hydrogen may be performed by measurement of the thermal conductivity of the gas mixture, by pressure measurements after separation of the hydrogen by physical methods, or by pressure measurements after oxidation and separation of the water formed. It is generally accepted that all these methods give reliable results in an appropriate way, and the choice of the method is thus a matter of convenience [2.45]. The chromatographic method is used in the experiments described in Chapter 4 of this thesis.

Analysis of residual hydrogen.

The advantage of the chromatographic method is that besides the diffusible hydrogen also the residual hydrogen can be measured. When the temperature of the sample is raised to a sufficiently high level the traps present in the metal are no longer active and all the hydrogen can diffuse through the metal. Also melting of the metal makes it possible to measure both the diffusible and the residual hydrogen.

References

2.1 P.G. Shewmon, Diffusion in solids, New York, McGraw-Hill (1963), 1-19.

2.2 G. Alefeld and J. Völkl, in Diffusion in solids - recent developments, A.S. Nowick and J.J. Burton (eds.), New York, Academic Press (1975), 231-302.

2.3 H. Schenck and K.W. Lange, "Diffusion in iron", Diffusion Data 1 (1967), 17-19.

2.4 P.J. Depuydt and N.A.D. Parlee, "Diffusion of hydrogen in liquid alloys", Diffusion Data 4 (1970), 83.

2.5 E.W. Johnson and M.L. Hill, "The diffusivity of hydrogen in alpha iron", Transactions of the Metallurgical Society AIME 218 (1960), 1104-1112.

2.6 J.P. Hirth, "Effects of hydrogen on the properties of iron and steel", Metallurgical Transactions 11A (1980), 861-890.

2.7 M.P. Puls, in Hydrogen degradation of ferrous alloys, R.A. Oriani, J.P. Hirth and M. Smialowski (eds.), Park Ridge, Noyes (1985), 114-130.

2.8 D. Warren, "Hydrogen effects on steel", Materials Performance 26 (1987), 38-48.

2.9 J.F. Elliott, M. Gleiser and V. Ramakrishna, "Thermochemistry for Steelmaking, volume II", Addison-Wesley, Reading, Massachusetts (1963).

2.10 A. Sieverts and W. Krumbhaar, "Über die Löslichkeit von Gasen in Metallen und Legierungen", Berichte der deutschen chemischen Gesellschaft 43 (1910), 893-900.

2.11 A. Sieverts, "Die Löslichkeit von Wasserstoff in Kupfer, Eisen und Nickel", Zeitschrift für Physikalische Chemie 77 (1911), 591-613.

2.12 A. Sieverts, G. Zapf and H. Moritz, "Die Löslichkeit von Wasserstoff, Deuterium und Stickstoff in Eisen", Zeitschrift für Physikalische Chemie A-138 (1938-1939), 19-37.

2.13 S.A. Gedeon and T.W. Eagar, "Thermochemical analysis of hydrogen absorption in welding", Welding Journal (Welding Research Supplement) 79 (1990), 264s-271s.

2.14 P. Wehr and J. Ruge, "Wasserstoffverteilung in Schweißverbindungen aus TiAl6V4", Schweißen und Schneiden 28 (1976), 411-414.

2.15 V.A. Nechaev and M.M. Timofeev, "Effect of rare-earth metals and an air flow on the absorption of hydrogen in consumable electrode welding", Welding Production 23 (1976), 8-10.

2.16 J.O.M. Bockris, M.A. Genshaw and M. Fullenwider, "The electro-permeation of hydrogen into metals", Electrochemical Acta 15 (1970), 47-60.

2.17 The physics of welding, J.F. Lancaster (ed.), Oxford, Pergamon (1986).

2.18 A. Block-Bolten and T.W. Eagar, "Metal Vaporization from weld pools", Metallurgical Transactions 15B (1984), 461-469.

2.19 Welding Handbook, 7th edition, volume 1, "Fundamentals of welding", Miami, Florida, American Welding Society (1976).

2.20 Handbook of Chemistry and Physics, 67th edition, Boca Raton, Florida, CRC (1987).

2.21 M. Shellhase, "Der Schweißlichtbogen - ein technologisches Werkzeug", Deutscher Verlag für Schweißtechnik, Düsseldorf (1985).

2.22 H. Li, Hydrogen behavior in arc welding, Ph.D.Thesis, Toronto, Canada (1990).

2.23 K. Easterling, Introduction to the physical metallurgy of welding, Oxford, Butterworth-Heinemann (1992).

2.24 C.R. Heiple and J.R. Roper, in Welding: Theory and Practice, D.L. Olson, R. Dixon and A.L. Liby (eds.), Amsterdam, Elsevier (1990).

2.25 G. den Ouden, Lastechnologie, Delft, Delftse Uitgevers Maatschappij, (1990).

2.26 B.J. Keene, "Review of data for the surface tension of iron and its binary alloys", International Materials Review 33 (1988), 1-37.

2.27 D. McKeown, "Hydrogen and its control in weld metal", Metal Construction 17 (1985), 655-661.

2.28 B. Chew, "Hydrogen control of basic coated MMA welding electrodes - the relationship between coating moisture and weld hydrogen", Metal Construction 14 (1982), 373-377.

2.29 Y. Hirai, T. Hiro and J. Tsuboi, "Behavior of hydrogen in arc welding (report 2) - sources of hydrogen in a shielded metal arc welding -", Transactions of the Japan Welding Society 5 (1974), 111-116.

2.30 E.I. Butkova, O.D. Smiyan, D.M. Kaleko and N.Y. Reznichenko, "Distribution of hydrogen and oxygen in the weld metal in percussion capacitor discharge welding of studs of AMg6 alloy", Welding International 3 (1989), 374-378.

2.31 J.L. Murphy, R.A. Huber and W.E. Lever, "Joint preparation for electron beam welding thin aluminum alloy 5083", Welding Journal (Welding Research Supplement) 69 (1990), 125s-132s.

2.32 J.P. Hirth and H.H. Johnson, "Hydrogen problems in energy related technology", Corrosion 32 (1976), 3-13.

2.33 R.A. Woods, "Porosity and hydrogen absorption in aluminum welds", Welding Journal (Welding Research Supplement) 53 (1974), 97s-108s.

2.34 D.R. White and W.G. Chionis, in Hydrogen embrittlement: Prevention and Control, L. Raymond (ed.), Philadelphia, ASTM (1988), 287-298.

2.35 I.I. Pirch, A.A. Erokhin and A.I. Pugin, "Relationships governing the absorption of hydrogen by liquid metals in arc heating", Welding Production 27 (1980), 8-11.

2.36 N. Jenkins and F.R. Coe, "Extraction and analysis of gases from pores in weld metal", Metal Construction and British Welding Journal 2 (1970), 27-31.

2.37 N. Bailey, F.R. Coe and T.G. Gouch, Welding steels without hydrogen cracking, Cambridge, Abington (1993).

2.38 R.A. Oriani, "Hydrogen - The versatile embrittler", Corrosion 43 (1987), 390-397.

2.39 I.K. Pokhodnya, A.P. Pal'tsevich and I.R. Yavdoshin, "Effects of the methods by which specimens of weld metal are taken on determining the amount of diffusible hydrogen in them", Automatic Welding 39 (1986), 26-30.

2.40 BS 6693, "Diffusible Hydrogen", (1986).

2.41 DIN 8572, "Determination of diffusible hydrogen in weld metal", (1981).

2.42 IIW Doc. No II-1155-91, "Measurement of hydrogen in ferritic arc weld metal", (1991).

2.43 W. Schwarz, "Verfahren zur Bestimmung des Wasserstoffgehaltes von Schweißgut", Berg- und Hüttenmannische Monatshefte 115 (1970), 151-155.

2.44 I.K. Pokhdonya and A.P. Pal'tsevich, "The chromatographic method of determining the amount of diffusible hydrogen in welds", Automatic Welding 33 (1980), 37-39.

2.45 "Determination of total hydrogen contents in weld metal", Welding in the World 2 (1964), 12-21.

CHAPTER 3

Influence of hydrogen on arc and weld pool geometry

3.1 Introduction

The influence of hydrogen on the mechanical properties of iron and steel is well known and was the subject of many studies [see, for instance, 3.1]. Generally speaking, this influence is of a detrimental nature (hydrogen cracking, pore formation) and it is for this reason that many attempts have been made in the past and are being made at present to prevent the absorption of hydrogen, especially during welding.
In this chapter attention is given to the influence of hydrogen on the physical properties of the arc and on the weld pool geometry during GTA welding. This influence is of basic importance for understanding the hydrogen absorption by the weld metal, which is dealt with in Chapters 4 and 5.
The first part of this chapter deals with the change in optical appearance of the arc with addition of hydrogen to the shielding gas on the basis of direct observations and photography, and with the change in arc properties, such as temperature, temperature distribution, voltage-current relations, etcetera. In the second part the influence of hydrogen on the weld pool geometry is discussed, with emphasis on melting efficiency and flow of the liquid weld metal. Finally, attention is given to hydrogen porosity and to the conditions under which pore formation takes place.

3.2 Experimental conditions

3.2.1 Materials

For the experiments three materials were used: pure iron (Armco), mild steel (Fe 360) and austenitic stainless steel (AISI 321). The chemical compositions of these materials are given in Table 3.1. Bead on plate welds were produced on 10 mm thick plates under partial penetration conditions. Before welding the plates were mechanically ground. In this

way the oxide layer was removed. After this, the plates were chemically degreased to eliminate any unwanted dirt.

Table 3.1 The chemical compositions (wt.%) of the materials used.

element	pure iron Armco	mild steel Fe 360	stainless steel AISI 321
Cr	0.0179	0.015	21.1
Ni	0.013	0.02	14.3
Mo	0.005	-	2.31
C	0.026	0.47	0.029
P	0.0047	0.019	0.034
S	0.005	0.031	0.013
Si	0.0379	0.23	0.923
Al	0.0398	-	0.0855
Ti	0.00107	-	0.00071
Mn	0.031	0.67	1.60
O	0.002	1.01	0.016
N	0.001	0.004	0.002
H	0.000009	0.000022	0.000064

3.2.2 Equipment

The experiments were carried out with GTA welding equipment under travelling arc conditions. The experimental setup is schematically given in Fig. 3.1. Above the workpiece to be welded a thoria-doped tungsten electrode, having a diameter of 3.2 mm, is placed. This electrode can be moved in vertical direction to make it possible to weld with different arc lengths. During welding the workpiece moves in a horizontal direction with respect to

the electrode.

The shielding gas was forced to flow along the electrode through a normal gas cup (8 mm diameter), thus shielding electrode, arc and weld pool from the influence of the surrounding air. The arc welding experiments were performed with mixtures of argon (purity 99.998%) and hydrogen (purity 99.998%). These mixtures were obtained by mixing the two gases in a chamber consisting of a number of parallel plates in which small holes were drilled. The two gases to be used were brought into the chamber and, because of the turbulent flow in the chamber, were completely mixed. The concentration of hydrogen in the shielding gas was varied between 0 and 25 vol.%.

The flow rate of the component gases was adjusted and measured using flow controllers. The flow rate of the gas mixture was adjusted to 10 l/minute. Each flow controller has an accuracy of about 1%.

Arc welding was carried out using a GTA welding torch with a DC welding power source (ESAB DTA300). This welding power source is provided with high frequency ignition facilities, with which the arc was ignited. Arc voltage and arc current were measured continuously with the use of a shunt and a welding monitor. Both were registered by means of an x-t recorder.

During the experiments the influence of different process parameters on the behaviour of arc and weld pool was studied. This was done by varying each of these process parameters while the others were kept at the standard values listed in Table 3.2.

Table 3.2 Standard arc welding conditions.

arc current	100 A
arc voltage	11.0 V
arc length	3 mm
polarity	electrode negative
electrode diameter	3.2 mm
electrode top angle	60°
shielding gas composition	argon-hydrogen
shielding gas flow rate	10 l/minute
travel speed	3 mm/s

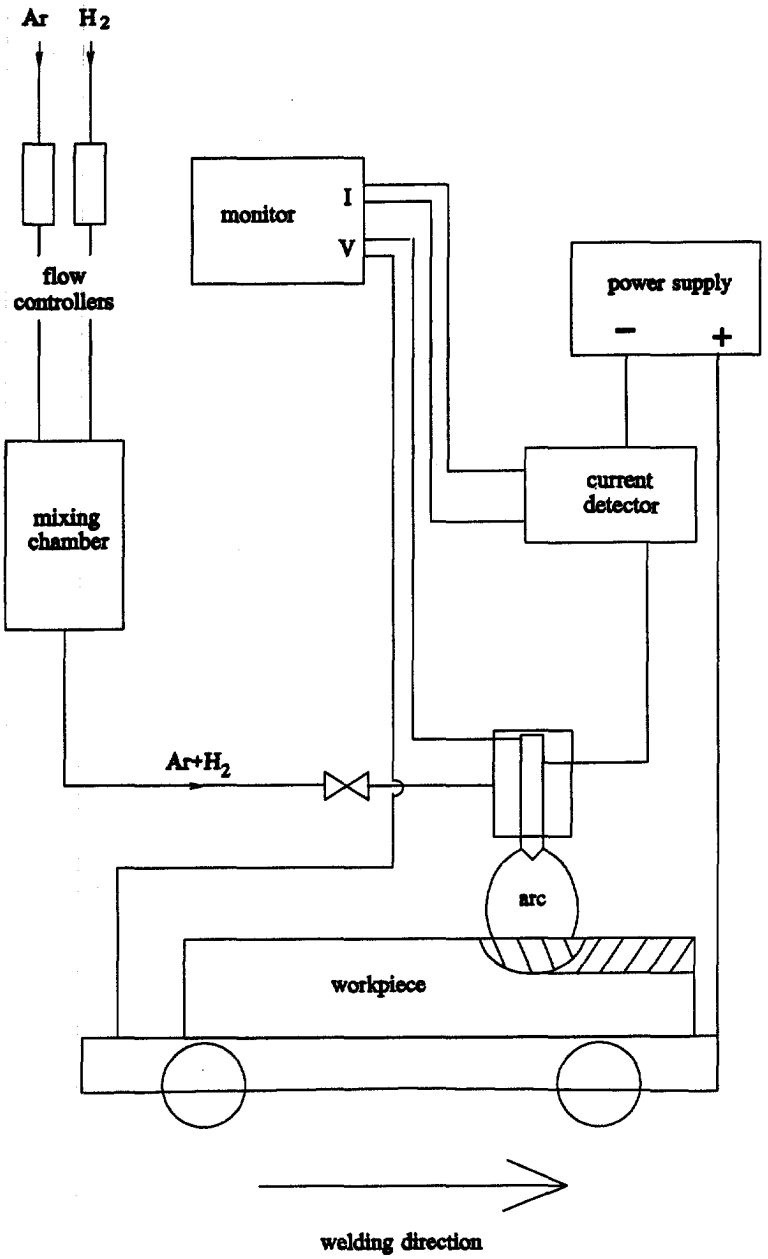

Fig. 3.1 Schematic presentation of the experimental setup used in the experiments.

3.2.3 Analysis of arc and weld pool

To evaluate the influence of the shielding gas composition on the visible shape of the arc photographs of the arc were made with a Nikon camera during welding using argon shielding gas containing 0 to 25 vol.% hydrogen and pure iron and stainless steel as workpiece. Eight optical grey filters were used to reduce the intensity of the arc radiation.

The influence of the shielding gas composition on the weld pool geometry was determined by carrying out welding experiments with three materials (pure iron, mild steel and stainless steel). The welds obtained were transversely sectioned at various locations. After grinding and polishing the cross sections up till 3 μm, they were etched with Kalling (5 g $CuCl_2$ in 100 ml ethyl alcohol and 100 ml hydrochloric acid). Kalling, which etches the grain boundaries, is used because of its capability to reveal the weld pool shape.
The width, depth and cross section area of the weld were measured with the use of a Leica CBA 8000 image analyzing computer. For each experimental situation two welds were made and both were used for the measurement.
Optical microscopy was performed to obtain images of the weld shape, using a Leitz Neophot 2 metallographic microscope at a magnification of 10 times.

3.3 Influence of hydrogen on the arc

In this section the influence of hydrogen addition to the shielding gas on the arc will be discussed. First, attention will be given to the influence on the arc appearance (visible shape and colour). After that, the influence of the addition of hydrogen to the shielding gas on some physical properties of the arc will be presented.

3.3.1 Optical arc appearance

To analyze the change in arc appearance due to the addition of hydrogen to the argon shielding gas, photographs of the arc were made. These photographs were made during welding under the standard welding conditions listed in Table 3.2. The welds were made with pure iron and stainless steel as workpiece material.

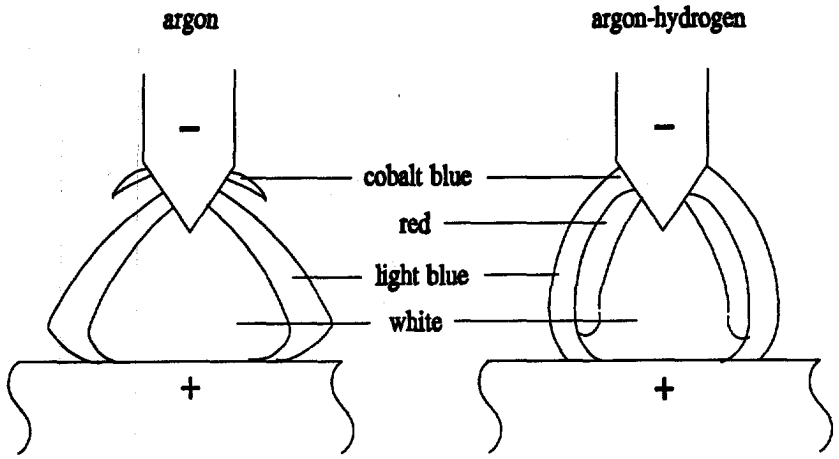

Fig. 3.2 Schematic presentation of the visible part of an argon and an argon-hydrogen arc.

In Fig. 3.2 a schematic presentation of an argon arc and an argon-hydrogen arc as observed is given. The argon arc is bell-shaped and exists of a white centre, where the arc is optically thick, surrounded by a blue fringe, where the arc becomes optically thin. A faint cobalt blue corona is present around the arc. It was shown by Ton [3.2] that the blue colour in the optically thin outside region of the arc is due to blue transitions in the argon spectrum.
With addition of hydrogen to the shielding gas the appearance of the arc changes gradually from bell-shaped to spherical. Furthermore, the optically thick central part contracts to a channel-like core and a red zone develops between this core and the blue outer region of the arc. The red colour of this zone is due to the red spectral transition of hydrogen [3.3].

The observed effects can be ascribed to changes in the temperature and the temperature distribution, which take place due to the hydrogen addition to the shielding gas. These changes in the temperature and the temperature distribution are a direct consequence of the difference in thermal conductivity between argon and hydrogen.

The temperature distribution of the arc is determined by the energy balance which states that under stationary conditions the energy produced in a certain volume per unit time is equal to the energy lost per unit time:

$$E_{el} = E_{cond} + E_{rad} + E_{conv} \tag{3.1}$$

in which E_{el} = electrical energy produced in a unit volume of the arc per unit time,
E_{cond} = energy lost from a unit volume per unit time by heat conduction,
E_{rad} = energy lost from a unit volume per unit time by radiation,
E_{conv} = energy lost from a unit volume per unit time by convection.

All terms of Eq. (3.1) are functions of temperature. However, when expressed as a function of temperature Eq. (3.1) takes a very complex form and cannot be solved analytically. A reasonable approach of the temperature distribution of the arc can be obtained by using the Elenbaas-Heller equation [3.4], which is a simplified energy balance in which the radiation term and the convection term are neglected with respect to the heat conduction term. The Elenbaas-Heller equation can be written as:

$$\sigma E^2 = \frac{-1}{r}\frac{d}{dr}\left(r\kappa\frac{dT}{dr}\right) \tag{3.2}$$

in which σ = electrical conductivity,
E = electrical field strength,
r = radius of the arc,
κ = thermal conductivity,
T = absolute temperature.

This equation can be solved and yields the temperature distribution of the arc with the heat conduction as parameter.
In Fig. 3.3 the radial temperature distribution in normalised form (i.e. the maximum temperature of all three arcs is taken to be equal) is presented of an argon arc, an argon-hydrogen arc and a hydrogen arc.
The temperature distribution of the pure argon arc has a Gaussian shape. The shoulder in the temperature distribution of the argon-hydrogen arc and the hydrogen arc is due to the dissociation peak in the heat conduction of hydrogen (see section 2.3.2).

At a certain temperature a plasma starts to emit visible light. This temperature (the threshold temperature T_{th}) is marked in Fig. 3.3 by a horizontal line. The figure shows that addition of hydrogen to argon shielding gas results in contraction of the visible arc, which is consistent with the observations made.

An other important aspect of the role which hydrogen plays in the arc is its influence on the contact area between the arc and the liquid metal in the weld pool. This contact area is an important parameter for the absorption of hydrogen by the liquid weld metal, as will be shown in Chapters 4 and 5. In Fig. 3.4 the contact area between the arc and the liquid metal is plotted as a function of the hydrogen percentage in the shielding gas. The figure clearly shows that the contact area increases with increasing hydrogen partial pressure.

The results described above were obtained by welding with pure iron as workpiece. Similar results were obtained in welding experiments using stainless steel as workpiece.

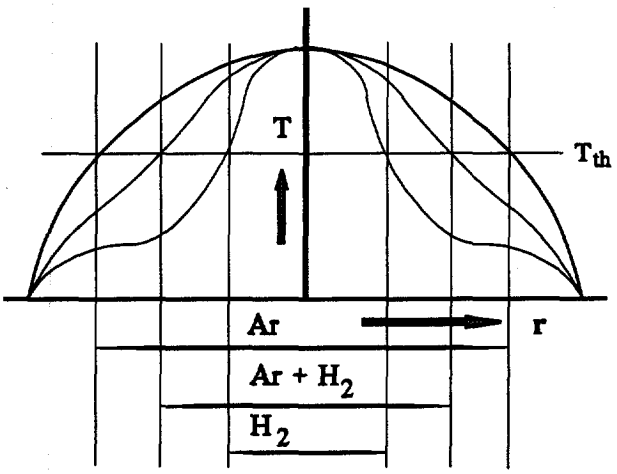

Fig. 3.3 Effect of the temperature distribution on the visible shape of the arc.

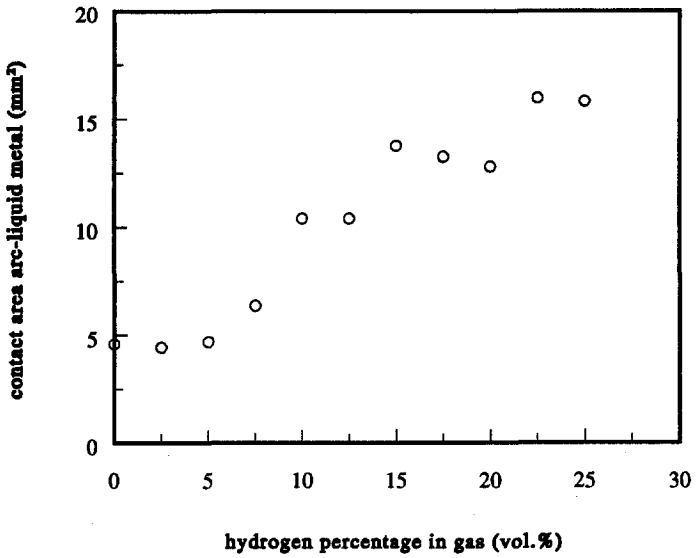

Fig. 3.4 Contact area between the arc and the liquid iron in the weld pool as a function of the hydrogen percentage in the argon shielding gas.

3.3.2 Arc characteristics

To study the influence of hydrogen on the electrical characteristics of the arc the arc voltage was recorded during each experiment. In Fig. 3.5 the arc voltage is plotted as a function of the arc current for a pure argon arc, while the other process parameters were kept constant at their standard values, see Table 3.2. In the figure also the data for an argon-15 vol.% hydrogen arc are given. The measured curves have both the typical features of an arc voltage-arc current characteristic as described in section 2.3.1. In the low arc current region (below about 75 A) the arc voltage decreases with increasing arc current, in the higher arc current region the arc voltage increases slightly with increasing arc current. Although the shape of both curves is similar, the arc voltage of the argon-hydrogen arc is considerably larger than that of the argon arc.

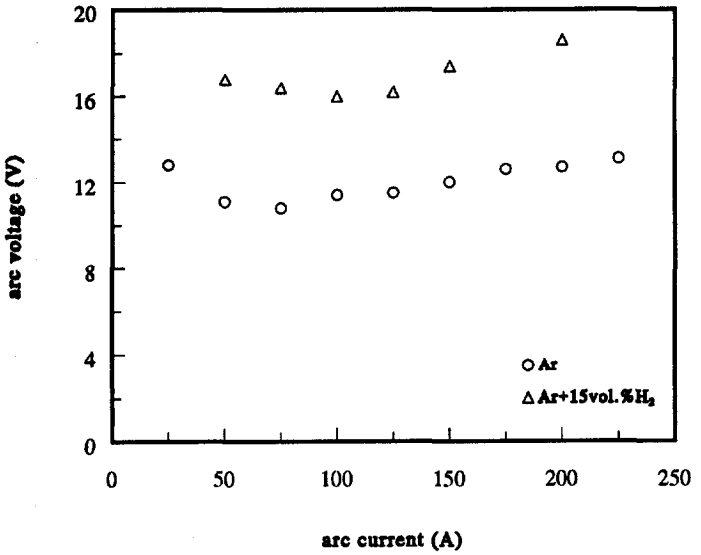

Fig. 3.5 Arc voltage as a function of arc current for a pure argon arc and an argon-15 vol.% hydrogen arc.

Differences in arc voltage due to changes in shielding gas composition can be attributed to differences in the first ionization potential of the gas. However, no significant difference exists between the first ionization potential of argon and the effective first ionization potential of hydrogen (see section 2.3.2). In addition, it should be kept in mind that the ionization of hydrogen and argon is overshadowed by the ionization of the metal vapour present in the arc.

The observed difference in arc voltage as observed in the present case between the argon-hydrogen arc and the pure argon arc is believed to be due to the large difference in heat conduction of both shielding gases. Since more energy disappears per unit time by heat conduction in the case of the argon-hydrogen arc than in the case of the pure argon arc, more energy is required to maintain a specific arc current (see the energy balance, Eq. (3.1)). This extra energy can only be supplied by an increase in arc voltage.

As was mentioned in section 2.3.1 the welding arc can be divided in three regions: the cathode fall, the anode fall and the arc column. Each of these three regions is characterized by its own specific properties.
It is evident that the sum of the voltage drops over the three regions is equal to the total arc voltage:

$$V_t = V_c + V_a + V_p = V_c + V_a + E \cdot l \tag{3.3}$$

in which V_t = total arc voltage,
V_c = cathode voltage drop,
V_a = anode voltage drop,
V_p = voltage drop over the arc column,
E = electric field strength,
l = arc length.

It was shown in the foregoing that addition of hydrogen to the shielding gas has a distinct effect on the total arc voltage. In order to determine in what way and to what degree hydrogen affects the values of V_c, V_a and V_p (E) separately, experiments were carried out in which the arc voltage was measured as a function of arc length for different values of the hydrogen concentration in the shielding gas.
The results of these measurements are presented in Fig. 3.6. The figure shows that in each case the arc voltage increases linearly with increasing arc length, which is in agreement with Eq. (3.3). Extrapolation to zero arc length results in the sum of the cathode voltage drop and the anode voltage drop (see Eq. (3.3)). For the five different hydrogen percentages in the shielding gas this extrapolation yields almost the same value for the arc voltage at zero arc length (about 9 V). Thus it can be concluded that the hydrogen does not significantly influence the sum of the anode voltage drop and the cathode voltage drop.
The electrical field strength of the arc column can be obtained from the slope of the arc voltage-arc length plot. In Fig. 3.6 it can be seen that the electrical field strength of the arc column increases with increasing hydrogen percentage in the shielding gas. Apparently, a higher electrical field strength is needed to compensate for energy losses due to the higher thermal conductivity of the arc column as a result of the increasing amount of hydrogen in the shielding gas.

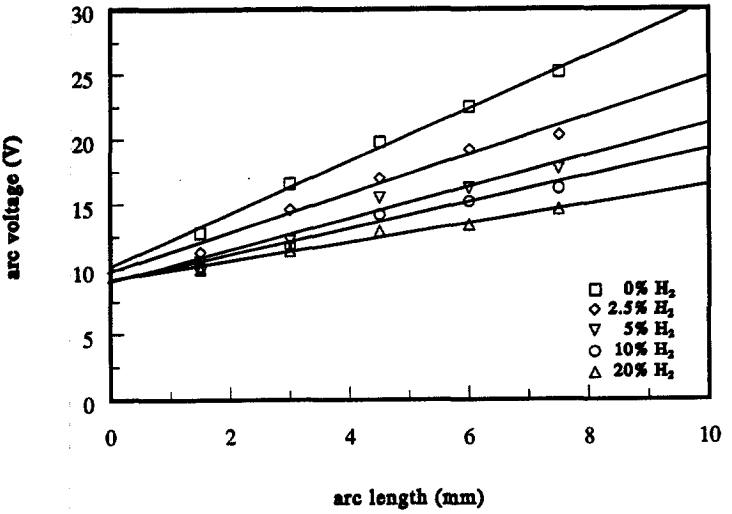

Fig. 3.6 Arc voltage as a function of arc length for five different values of the hydrogen percentage in the shielding gas.

The addition of hydrogen to the shielding gas has a distinct influence on the electrical characteristics of the welding arc. This was demonstrated in the foregoing by measurement of the arc voltage as a function of arc current and arc length for different shielding gases (see Fig. 3.5 and Fig. 3.6). Arc voltage measurements were also carried out as a function of hydrogen content in the shielding gas at constant arc current (100 A). This was done for three different materials: pure iron, mild steel and stainless steel.
In Fig. 3.7 the arc voltage for the three different materials is plotted as a function of the hydrogen partial pressure. The figure shows that for each material the arc voltage increases about linearly with increasing hydrogen percentage in the shielding gas.

For pure iron the arc voltage in a pure argon arc is measured to be about 11 V, whereas a hydrogen percentage in the shielding gas of 25 vol.% results in an arc voltage of about 21 V.
For mild steel the change in arc voltage with changing hydrogen percentage is virtually the same as that in the case of pure iron. No tests were performed with mild steel with more than 10 vol.% hydrogen, due to bubble formation starting to occur above 7.5 vol.% hydrogen.
In the case of stainless steel the arc voltage in a pure argon arc was about 10.5 V. With

25 vol.% hydrogen in the shielding gas the voltage was measured to be about 18 V. When welding stainless steel the arc voltage increases less rapidly with increasing hydrogen percentage in the shielding gas than when welding pure iron or mild steel. Apparently, the alloying elements present in the arc in the case of welding stainless steel due to the vaporisation of weld metal, reduce the electrical field strength of the arc column. Especially chromium, having a relatively low ionization energy, might play a role in this respect.

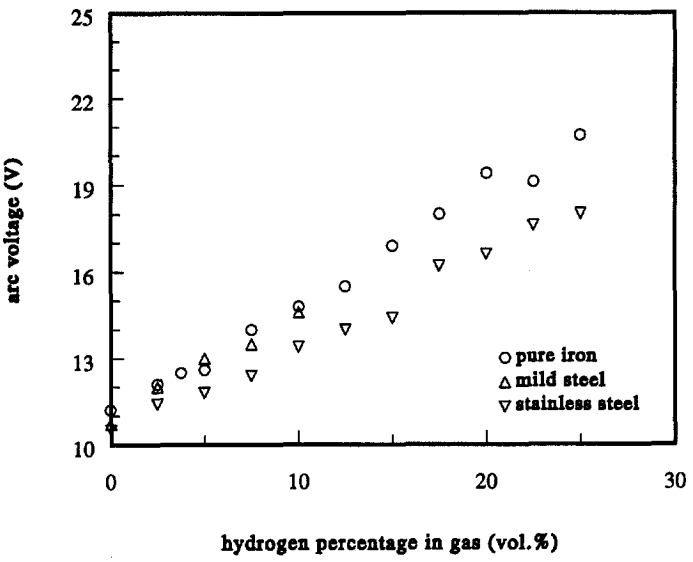

Fig. 3.7 Arc voltage as a function of the hydrogen percentage in the shielding gas, when welding pure iron, mild steel and stainless steel with a 100 A arc.

3.4 Influence of hydrogen on the weld pool geometry

The quality of a weld is determined by its mechanical properties and its geometry. The important dimensions of a weld are: cross sectional area, width and depth. The depth-to-width ratio is often used as a measure of the weld quality.
In the following sections the influence of the addition of hydrogen to the argon shielding gas on the geometry of the weld pool in pure iron, mild steel and stainless steel, is discussed on the basis of experiments carried out under various experimental conditions. Unless otherwise stated, the experimental conditions used are the standard conditions given in Table 3.2.

3.4.1 Influence of hydrogen on the weld pool geometry of pure iron

The first series of experiments was performed with pure iron as workpiece. The hydrogen content of the argon based shielding gas was varied from 0 to 25 vol.%. The results of these experiments are presented in Fig. 3.8 to Fig. 3.12.

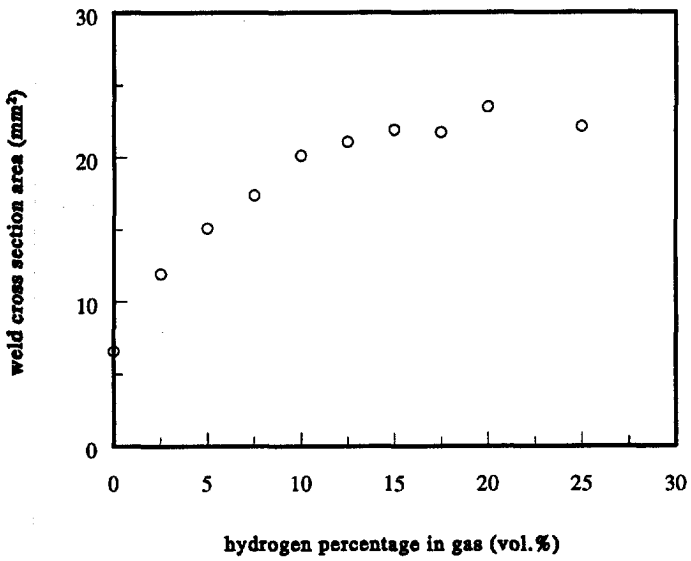

Fig. 3.8 Weld cross section area in pure iron as a function of the hydrogen percentage in the shielding gas.

In Fig. 3.8 the weld cross section area is plotted as a function of the hydrogen percentage in the shielding gas. The figure shows that the weld cross section area increases from about 6 to about 20 mm^2 when the hydrogen percentage in the shielding gas is increased from 0 up to 10 vol.%, whereas a further increase in the hydrogen percentage has only a small effect on the weld cross section area. The growth of the weld with increasing hydrogen in the shielding gas is due to the increase in heat transferred from the arc to the weld pool, which in turn is directly related to the increase in arc voltage with increasing hydrogen in the shielding gas (see Fig. 3.7).

An important parameter in arc welding is the melting efficiency. This parameter is defined as the fraction of the total arc energy required to heat and melt the metal (see section 2.4.1).
The melting efficiency can be obtained from the welding parameters and the weld pool dimensions with the help of the equation [3.4]:

$$f_2 = \frac{qA_m v}{VI} \tag{3.4}$$

in which f_2 = melting efficiency, the minimum amount of energy required for heating (from room temperature to the melting point) and melting the metal divided by the heat generated by the heat source,

q = heat required to elevate a given volume of metal from room temperature to its melting point and subsequently convert this volume from the solid state to the liquid state,

A_m = weld metal transverse cross section area,

v = travel speed of the heat source,

V = arc voltage,

I = arc current.

In Fig. 3.9 the melting efficiency is presented as a function of the hydrogen percentage in the shielding gas, taking for q the value 11 J/mm^3.
It appears that the melting efficiency increases with increasing hydrogen content from about 0.1 in pure argon to about 0.3 when adding 7.5 vol.% hydrogen. A further increase of the hydrogen content in the shielding gas does not result in a higher value of the melting efficiency.

The observed increase in melting efficiency is a direct consequence of the contraction of the arc column (see section 3.3.1) and the increase of the thermal conductivity of the shielding gas (see section 2.3.2) with addition of hydrogen. The fact that the melting efficiency reaches a saturation level is directly related to the increase in the contact area between the arc and the liquid weld metal above a certain hydrogen percentage (about 7.5 vol.%, see Fig. 3.4).

It is evident that the large increase in the melting efficiency with addition of hydrogen to the shielding gas is of considerable technological importance. Unfortunately, the application of the addition of hydrogen to the shielding gas is limited to the welding of metals (in particular austenitic stainless steel), which are not susceptible to pore formation and hydrogen induced cracking.

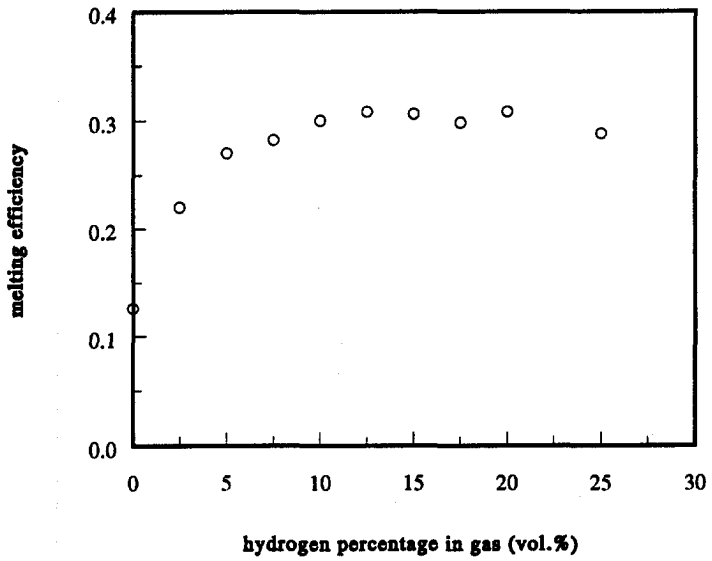

Fig. 3.9 Melting efficiency as a function of the hydrogen percentage in the argon shielding gas for pure iron.

In Fig. 3.10 the weld width is given as a function of the hydrogen percentage in the shielding gas. The weld width increases from about 5.5 mm when welding in pure argon up to about 10 mm when welding with 15 vol.% hydrogen in the shielding gas. When further increasing the hydrogen in the shielding gas the weld width remains virtually constant.
In Fig. 3.11 the weld depth is plotted as a function of the hydrogen percentage in the shielding gas. The figure shows that the weld depth increases with increasing hydrogen in the shielding gas up to about 7.5 vol.%, after which it becomes constant.
The data of Fig. 3.10 and Fig. 3.11 are combined in Fig. 3.12, which presents the depth-to-width ratio of the weld as a function of the hydrogen concentration in the shielding gas.

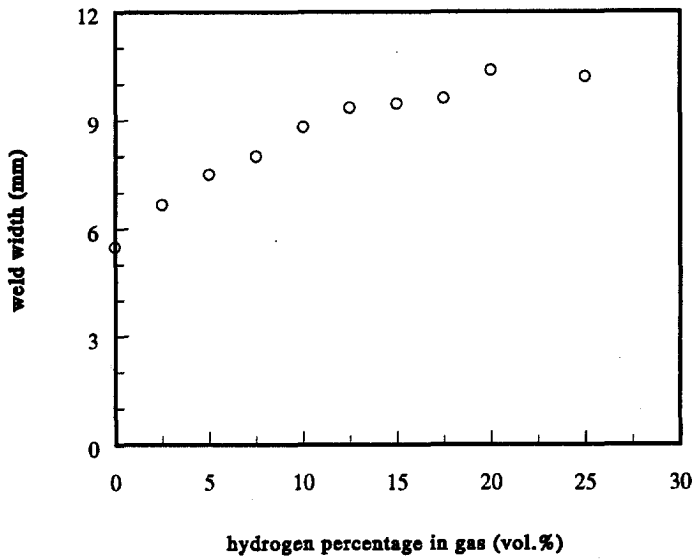

Fig. 3.10 Weld width in pure iron as a function of the hydrogen percentage in the shielding gas.

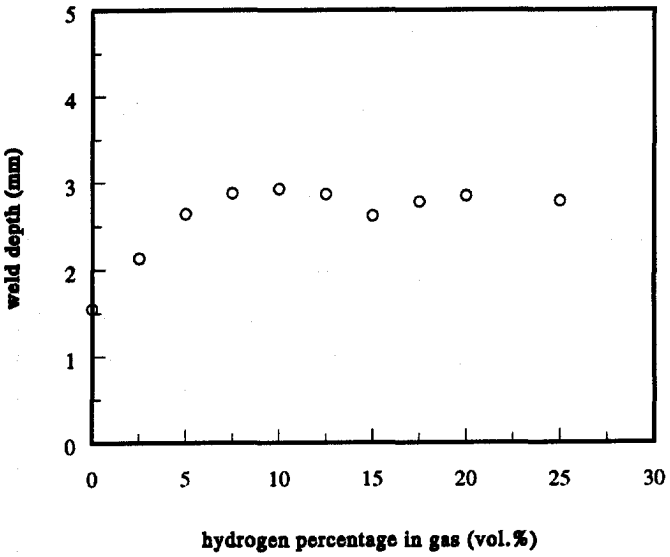

Fig. 3.11 Weld depth in pure iron as a function of the hydrogen percentage in the shielding gas.

As was shown in section 2.4.2, the shape of the weld is not only dependent on the heat conduction in the material, but also on the fluid flow in the weld pool, which in turn is dependent on the surface tension. The latter is determined by the chemical composition (the presence of surface active elements) and the temperature distribution in the weld pool. Two types of fluid flow can be distinguished in the weld pool [3.5]. A negative surface tension temperature coefficient will generate an outward flow and a positive surface tension temperature coefficient will generate an inward flow. The first type results in a shallow and wide weld, the second type leads to a deep and narrow weld. Hydrogen is reported to have no influence on the surface tension [3.6].
The results presented in Fig. 3.10 to Fig. 3.12 indicate that in the case of pure iron fluid flow in the weld pool does not play an important role and that the flow, if present, is radially outward in nature, which is consistent with expectations [3.6].

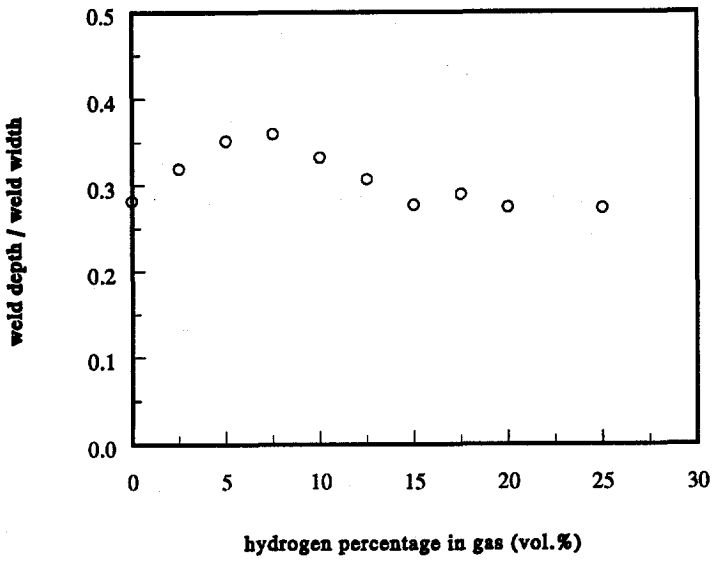

Fig. 3.12 Weld depth-to-width ratio in pure iron as a function of the hydrogen percentage in the shielding gas.

3.4.2 *Influence of hydrogen on the weld pool geometry of mild steel and stainless steel*

Experiments were also carried out with mild steel (Fe 360) and austenitic stainless steel (AISI 321) as workpiece. In the case of mild steel the hydrogen percentage of the shielding gas was varied up to 7.5 vol.%. Above this percentage pore formation started to occur in the weld, which made the measurement of the weld dimensions unreliable.
In the case of stainless steel the hydrogen percentage of the shielding gas was varied up to 15 vol.%, this percentage being the porosity limit for stainless steel.

The results obtained with mild steel were found to be similar to those obtained with stainless steel. In Fig. 3.13 to Fig. 3.16 the results obtained with stainless steel are presented.
The figures show that with increasing hydrogen content in the shielding gas:

- the weld cross section area increases,
- the weld width remains virtually constant and
- the weld depth increases.

As far as the effect of hydrogen on the weld cross section area is concerned, the results obtained with stainless steel (and with mild steel) are in agreement with those obtained with pure iron (compare Fig. 3.8 and Fig. 3.13). However, in the case of stainless steel (and mild steel), the extra heat transferred from the arc to the weld pool due to the addition of hydrogen to the shielding gas results primarily in an increase of the weld depth, whereas in the case of pure iron the extra heat results in an increase of both the weld width and the weld depth.

This difference in behaviour is attributed to the fact that in the case of stainless steel a strong radially inward flow occurs in the weld pool, which is due to the presence of surface active elements, notably oxygen and sulphur [3.5], in the surface layer of the weld pool.

The existence of radially inward flow in the case of stainless steel was confirmed by additional experiments in which aluminium oxide powder was deposited onto the surface of the weld pool during welding. Under the influence of the fluid flow this powder moved to the centre of the weld pool, where it was fixed during solidification of the weld. A similar effect was not observed in the case of pure iron.

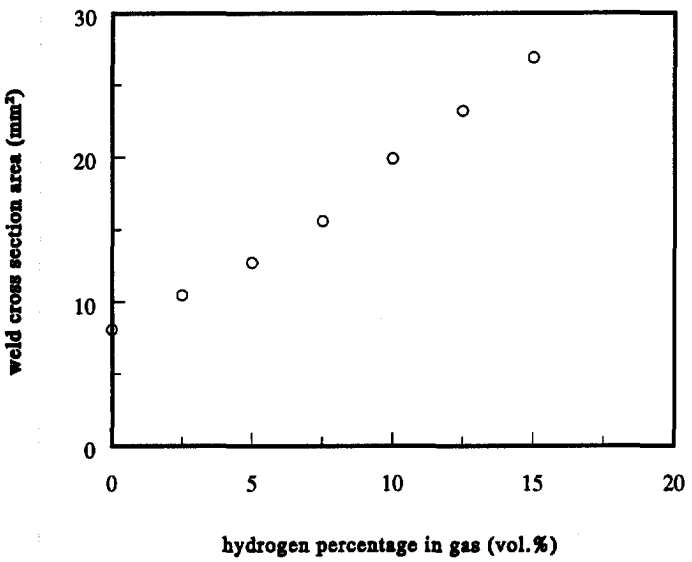

Fig. 3.13 Weld cross section area in stainless steel as a function of the hydrogen percentage in the shielding gas.

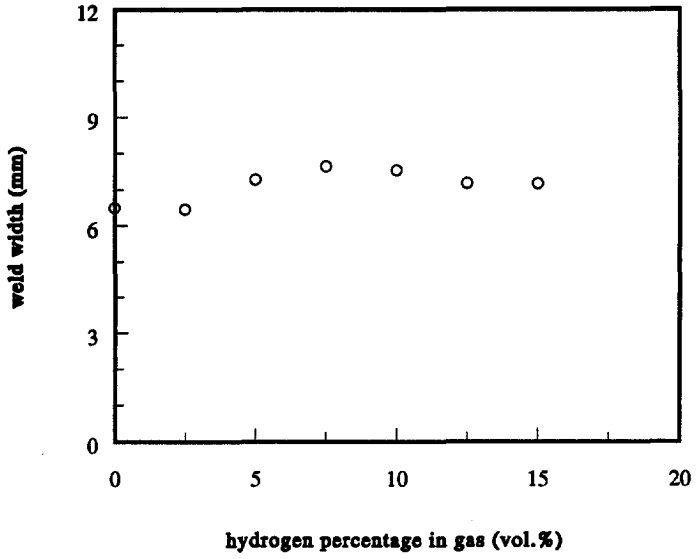

Fig. 3.14 Weld width in stainless steel as a function of the hydrogen percentage in the shielding gas.

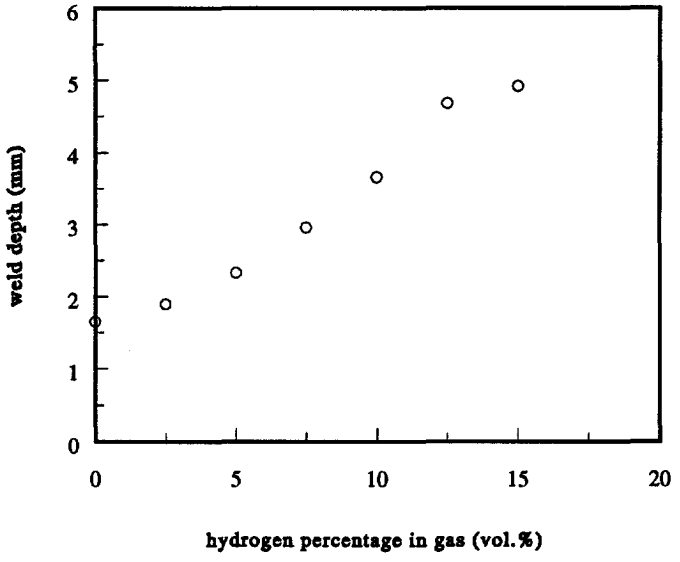

Fig. 3.15 Weld depth in stainless steel as a function of the hydrogen percentage in the shielding gas.

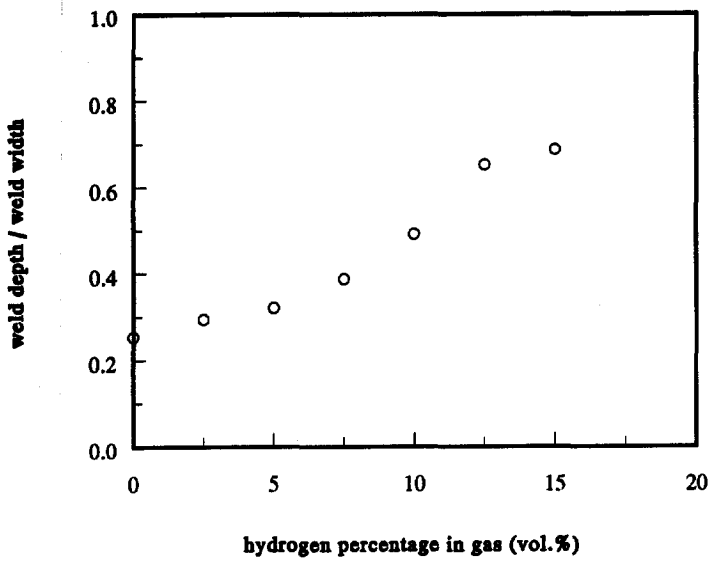

Fig. 3.16 Weld depth-to-width ratio in stainless steel as a function of the hydrogen percentage in the shielding gas.

3.4.3 Influence of hydrogen on pore formation

In the experiments with pure iron, no pore formation was found, even with hydrogen percentages in the shielding gas as high as 30 vol.%. However, in the experiments with mild steel and stainless steel, pore formation was observed under certain conditions. In the case of mild steel, porosity was found in the weld with a hydrogen percentage in the shielding gas of 7.5 vol.% or more, whereas in the case of stainless steel pore formation starts to occur at a hydrogen percentage of 15 vol.%. As an example Fig. 3.17 shows porosity in a stainless steel weld obtained by welding with an argon based shielding gas containing 20 vol.% hydrogen.

Pore formation due to hydrogen is possible when the actual hydrogen concentration in the liquid metal exceeds the solubility in equilibrium with 1 bar hydrogen gas.
This situation can easily occur at the solidification front, due to the smaller solubility of hydrogen in solid metal compared to that in the liquid metal. During solidification hydrogen will be expelled from the solid to the liquid and this will give rise to an increase of the hydrogen concentration of the liquid metal just ahead of the solidification front. When the hydrogen concentration rises above the solubility, hydrogen filled bubbles are

formed, assuming that nucleation sites are available. These bubbles will tend to rise to the surface due to gravitational forces [3.7, 3.8]. However, part of the bubbles may be caught up by the progressing solidification front, which results in pores in the solidified weld metal.

Pore formation in pure iron does not occur up to 30 vol.% hydrogen in the shielding gas, whereas pore formation in mild steel and austenitic stainless steel starts already at 7.5 vol.% and 15 vol.%, respectively. This observation can be explained by the fact that in the case of the steels nucleation sites are available in the form of alloying elements, oxides and inclusions, while in the case of pure iron these sites are absent. Also the presence of oxygen in mild steel and stainless steel facilitates pore formation, as oxygen lowers the surface tension of liquid metals and, hence, reduces the surface energy needed for the nucleation of bubbles. The lower tendency for pore formation of stainless steel in comparison to mild steel is attributed to the higher solubility of hydrogen in austenitic stainless steel, due to the presence of alloying elements [3.9].

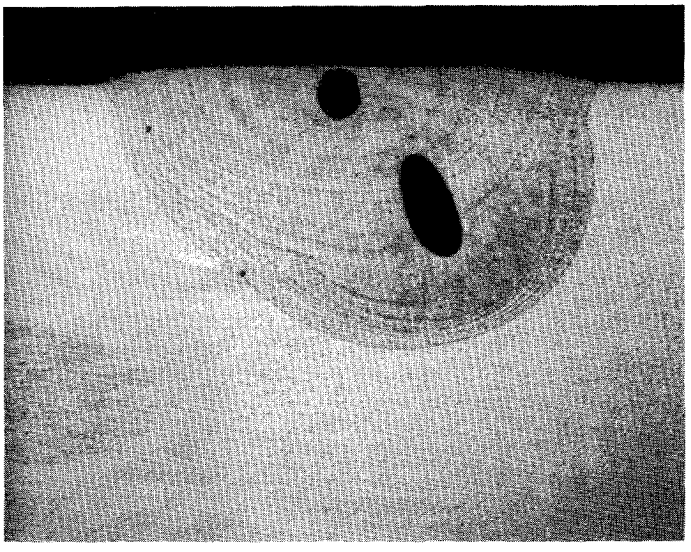

Fig. 3.17 Porosity in a stainless steel weld obtained with argon-20 vol.% hydrogen as shielding gas.

It is evident that the pore formation tendency (the hydrogen percentage in the shielding gas above which pore formation occurs) is dependent on the experimental conditions, in particular the solidification rate. In fact, it should be expected that an increase in the solidification rate (i.e. an increase in the travel speed) will facilitate pore formation.

3.5 Conclusions

This chapter deals with the influence of the addition of hydrogen to the argon shielding gas on the arc and the weld pool geometry. The results obtained lead to the following conclusions.

- The optical appearance of the arc changes slightly with hydrogen addition to the shielding gas, the most important change being contraction of the arc. This effect is directly related to the changes in the temperature and the temperature distribution in the arc, which are due to the higher thermal conductivity of hydrogen compared to that of argon. Furthermore, the contact area between the arc and the liquid metal increases with hydrogen percentage in the shielding gas, starting at about 7.5 vol.%.
- The arc voltage increases with increasing hydrogen partial pressure. This increase is attributed to a rise in electrical field strength, which is related to the higher thermal conductivity of hydrogen compared to that of argon.
- The addition of hydrogen to the shielding gas results in a larger heat input and in an increase of the melting efficiency.

  In the case of pure iron this leads to an increase of both the weld width and the weld depth.

  In the case of mild steel and stainless steel the extra heat input leads primarily to an increase of weld depth. This is a result of the fluid flow in the weld pool, which is directed inward.
- Above a critical hydrogen level in the shielding gas, pore formation starts to occure in the weld pool. This critical hydrogen level depends on material composition and welding conditions.

References

3.1 N. Baily, F.R. Coe, T.G. Gooch, P.H.M. Hart, N. Jenkins and R.J. Pargeter, Welding steels without hydrogen cracking, Cambridge, Abington (1993), 1-15.

3.2 H. Ton, "Physical properties of the plasma-MIG welding arc", Journal of Applied Physics 8 (1975), 922-933.

3.3 Club E.D.F. Arc Electrique, L'arc electrique et ses applications, Centre National de la Recherche Scientifique, Paris (1984).

3.4 Welding Handbook, 7th edition, volume 1: "Fundamentals of welding", Miami, Florida, American Welding Society (1976).

3.5 C.R. Heiple and J.R. Roper, in Welding: Theory and Practice, D.L. Olson, R. Dixon and A.L. Liby (eds.), Amsterdam, Elsevier (1990), 1-34,

3.6 B.J. Keene, "Review of data for the surface tension of iron and its binary alloys", International Material Reviews 33 (1988), 1-37.

3.7 D.R. White and W.G. Chionis, in Hydrogen embrittlement: Prevention and Control, L. Raymond (ed.), Philadelphia, ASTM (1988), 287-298.

3.8 I.I. Pirch, A.A. Erokhin and A.I. Pugin, "Relationships governing the absorption of hydrogen by liquid metals in arc heating", Welding Production 27 (1980), 8-11.

3.9 J.F. Elliott, M. Gleiser and V. Ramakrishna, "Thermochemistry for steelmaking, volume II", Reading, Massachusetts, Addison-Wesley (1963).

CHAPTER 4

Hydrogen absorption under stationary arc conditions

4.1 Introduction

The absorption of hydrogen by liquid weld metal during arc welding is a highly complex phenomenon, in which many factors play a role, such as hydrogen partial pressure in the shielding gas, arc current, arc length (arc voltage) and travel speed. Also the composition and the geometry of the workpiece influence the absorption process.
It is evident that the best approach of studying such a complex phenomenon is to simplify the experimental conditions as much as possible. This can be realized by carrying out experiments in which only one parameter is varied, whereas the others are kept constant. Another significant simplification can be achieved by ruling out the travel speed as parameter. This is the case when arc welding is carried out under stationary arc conditions.

This chapter deals with experiments in which small samples of iron and steel are welded with a gas tungsten arc (GTA) in a hydrogen containing argon based shielding gas under stationary (zero travel speed) conditions.
First a description is given of the materials and the equipment used and the experimental procedure followed. After this the results are presented of experiments in which each of the process parameters is varied, whereas the other parameters are kept constant. Then attention is given to the hydrogen leaving the sample during cooling to room temperature directly after welding. Attempts are made to determine the initial hydrogen concentration experimentally and by calculation.
On the basis of the results obtained a model is developed which can be used to explain the absorption phenomenon observed and to predict the hydrogen concentration in the sample when the experimental conditions are known. The model is applied to explain the results obtained in the experiments with varying process parameters.

4.2 Experimental conditions

4.2.1 Materials

Experiments were carried out with three materials: technical pure iron (Armco), mild steel (Fe 360) and austenitic stainless steel (AISI 321), with emphasis on pure iron. The materials were used in the form of small buttons having a weight of about 0.9 g. The chemical compositions of the materials are given in Table 4.1.

Table 4.1 The chemical compositions (wt.%) of the materials used.

element	pure iron Armco	mild steel Fe 360	stainless steel AISI 321
Cr	0.0179	0.07	21.1
Ni	< 0.015	< 0.015	14.3
Mo	< 0.015	< 0.015	2.31
C	0.026	0.025	0.029
P	< 0.04	-	< 0.04
S	0.005	-	0.013
Si	0.0379	0.4	0.923
Al	0.0398	-	0.0855
Ti	0.00107	-	0.00071
Mn	0.031	1.00	1.60
O	0.002	0.038	0.014
N	0.001	0.001	0.001
H	0.000006	0.000038	0.000102

The button shaped samples were obtained from bulk wire with a diameter of 2.5 mm. Rust on the surface was removed by grinding the wire, after which the wire was cleaned by means of anti-grease and acetone. Then the wire was cut into pieces of the desired weight, which were placed in acetone containing a water-binder to prevent oxidation.
Following this, the pieces were premelted in a pure argon atmosphere using a 100 A arc. In this way the samples obtained a button-like shape. This pre-treatment was necessary to achieve identical starting conditions for all samples in the experiments.

4.2.2 Equipment

All experiments were carried out using a GTA torch under stationary arc conditions, which means that the arc does not move with respect to the sample to be melted. In Fig. 4.1 the complete experimental setup, which was also used in previous experiments, is schematically shown [4.1,4.2]. Central part of the equipment is a stainless steel chamber (shown in more detail in Fig. 4.2) provided with a thoria-doped tungsten electrode, having a diameter of 3.2 mm. The electrode is located in a vertical position above a water-cooled copper table on which the sample to be melted could be placed. It was possible to seal the chamber, so that it could be evacuated and subsequently filled with the desired gas mixture.
The experiments were performed in mixtures of argon (purity 99.998%) and hydrogen (purity 99.998%). These mixtures were obtained by mixing the two gases in a chamber containing a number of parallel plates in which small holes were drilled. The two gases to be mixed were brought into the chamber and, because of the turbulent flow in the chamber, were completely mixed.
The flow rate of the two component gases was adjusted and measured using flow controllers. The flow rate of the gas mixture was adjusted to 10 l/minute. Each flow controller has an accuracy of about 1%.

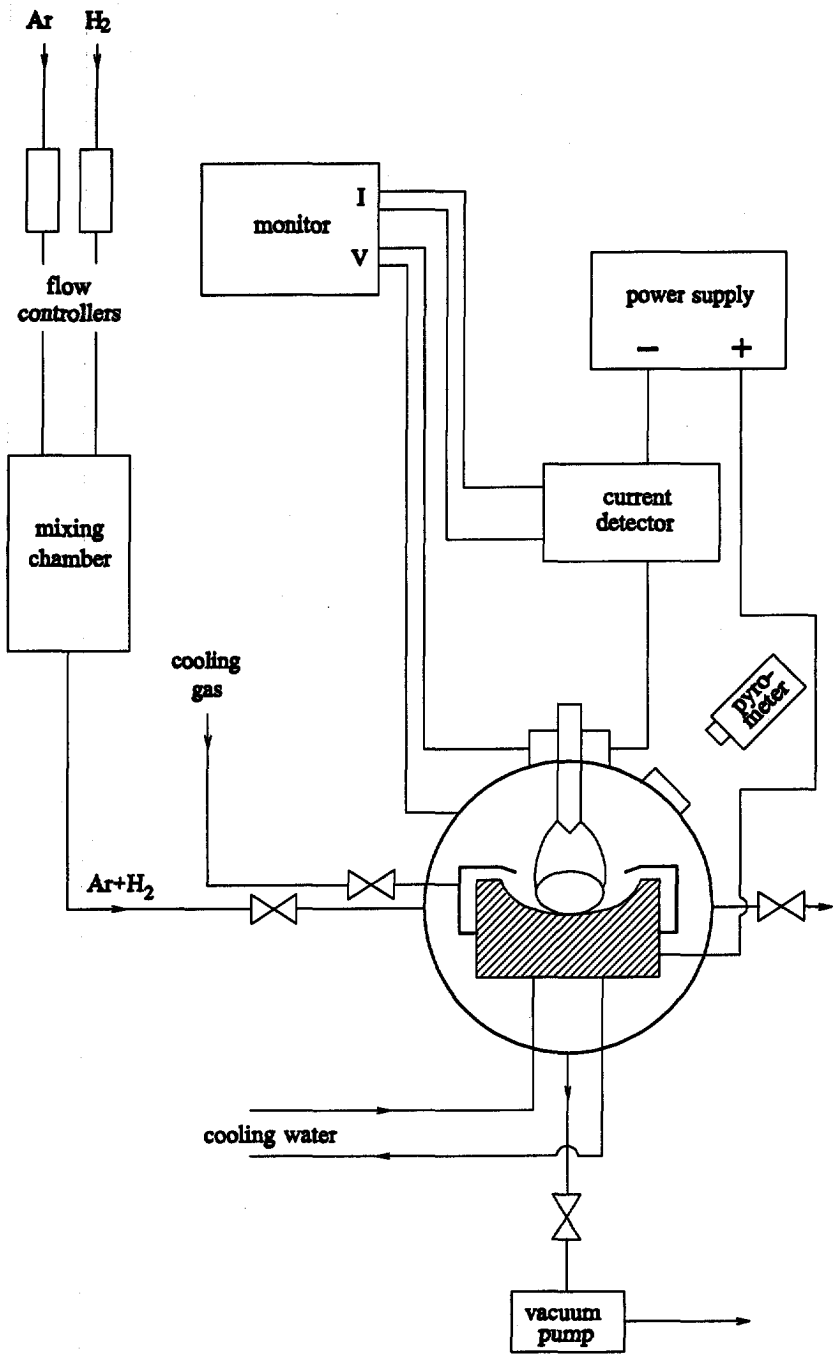

Fig. 4.1 Schematic presentation of the equipment used.

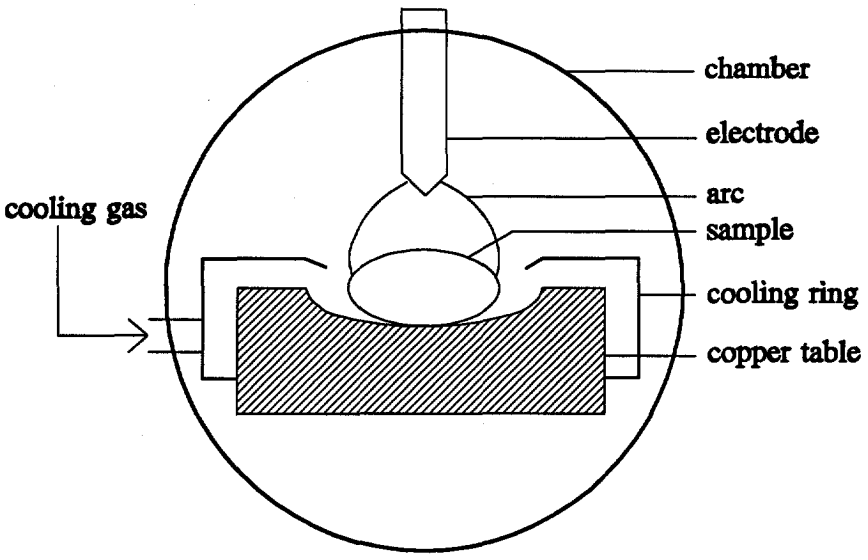

Fig. 4.2 Schematic presentation of the central part of the equipment used.

Arc melting was carried out using a DC welding power source (ESAB DTA300). This welding machine is provided with high frequency ignition facilities, with which the arc was ignited. Arc voltage and arc current were measured continuously using a shunt and a welding monitor. Both were registered by means of an x-t recorder.
After the arc welding period was completed the sample was rapidly cooled by a gas flow. This was realized by leading a gas through a metal ring which was placed around the button-like sample (see Fig. 4.2). In this way the gas flow was focused directly unto the sample, so it was evenly cooled from all sides. By changing the composition of the cooling gas the sample could be cooled down with different cooling rates.

The surface temperature of the sample was measured using an optical pyrometer (L.I.E. Automatic Precision Pyrometer). The obtained data were registered by means of an x-t recorder. The pyrometer could only be used when the arc was extinguished, because the radiation of the burning arc results in too much interfering. In Fig. 4.3 a typical temperature recording curve is given. The first part of the curve represents the situation during the time that the arc is still burning. After the arc is extinguished the temperature drops until the sample starts to solidify. The solidification is represented by a horizontal part in the curve. When the total sample is solidified the temperature decreases further until the lower detection limit of the pyrometer is reached.

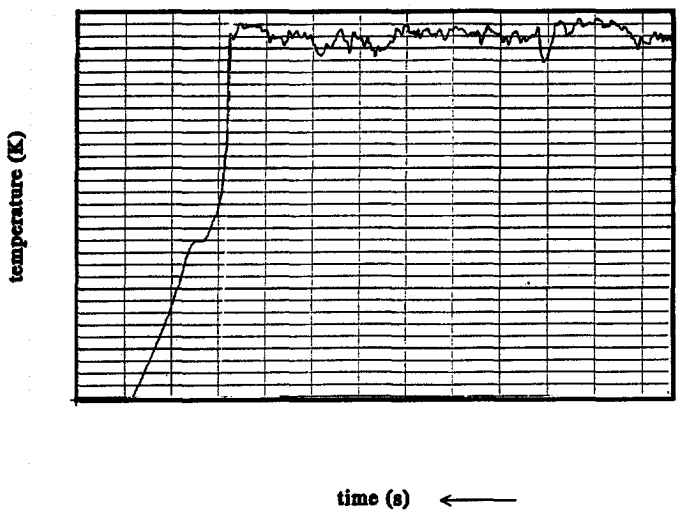

Fig. 4.3 Surface temperature of a sample as a function of time, recorded by means of optical pyrometry.

In the experiments carried out the influence of each of the different process parameters was determined separately. This was done by varying each process parameter, while the others were kept constant.

The standard conditions used are listed in Table 4.2. These conditions are chosen as close as possible to the conditions which are normally used in GTA welding.

Helium was chosen as cooling gas, as with this gas a fast cooling rate could be obtained.

Table 4.2 Standard conditions for welding under stationary arc conditions.

arc current	100 A
arc voltage	12 V
arc length	3 mm
polarity	electrode negative
sample weight	0.9 g
electrode diameter	3.2 mm
electrode top angle	60°
shielding gas composition	95% argon- 5% hydrogen
shielding gas flow rate	10 l/minute
cooling gas	helium

4.2.3 Experimental procedure

The following procedure was followed for each experiment.
First the chamber was opened, and the inside was cleaned thoroughly, so that all unwanted dirt from the previous experiment was removed from the wall of the chamber, the copper electrode table and the tungsten electrode. Then the premelted button-shaped sample was taken out of the acetone, in which it was kept. After the acetone was evaporated the sample was placed on the copper table. The chamber was then sealed off.
In order to remove unwanted gases, the chamber was evacuated three times and filled again with the desired gas mixture. When this procedure was followed little difference was found in the hydrogen concentration in the samples, obtained during experiments carried out under identical conditions.
After the chamber was filled for the third time with the desired gas mixture, the valve connecting the chamber with the ambient air opened, so that the gas mixture could flow through the chamber. Due to the overpressure at the moment the outside valve opened, no air could enter the chamber. Immediately after opening the outside valve the arc was ignited with the use of the high frequency facilities. In most cases the arc started burning instantly and the entire sample was molten within half a second. The arc time was set beforehand and did not include the time needed for ignition of the arc and melting of the

sample.
After extinguishing the arc, the valve to the cooling gas opened and the cooling gas was forced to flow towards and around the sample. After the sample was cooled down to about room temperature the chamber was opened. The sample was taken out of the chamber and immediately placed into a container filled with liquid nitrogen, in which it was kept until it was analyzed. The time between the moment of opening the chamber and the moment the sample was placed into the liquid nitrogen was approximately 5 seconds.

4.2.4 Analysis

The hydrogen content of the samples was measured using a gas chromatograph (Ströhlein equipment of the type H-MAT 251).
In all cases the same procedure for analyzing the samples was followed. After the samples were taken out of the liquid nitrogen in which they were stored, they were placed in acetone and warmed up to room temperature, which took about 5 seconds. Acetone was used because when warming the samples in air the surface was rapidly covered with ice, which can not easily be removed. The acetone was removed from the surface of the sample in a gas flow of cold air. The sample was then placed in the gas chromatograph, which took another 10 to 15 seconds. The entire procedure from the moment of taking the sample out of the liquid nitrogen up to the start of the actual analysis was thus performed in less than 20 seconds.

As mentioned in section 2.2.2 hydrogen can be present in a metal in two forms:
- as residual hydrogen, which is trapped in the metal and can not move below a certain temperature;
- as diffusible hydrogen, which can diffuse freely through the metal.

There are three possible ways to measure hydrogen concentrations in metal samples using the gas chromatograph:
a: Measurement of the total hydrogen concentration.
For the determination of the total hydrogen concentration the sample is completely molten. In this way all hydrogen is released from the sample and the hydrogen leaving the sample is carried away with an argon gas flow to the measuring cell.

b: Measurement of the diffusible hydrogen concentration.
For the determination of the diffusible hydrogen the sample is heated at a temperature of 350°C. At this temperature diffusible hydrogen leaves the sample in a relatively short time (a few minutes), while residual hydrogen remains behind in the sample. The diffusible hydrogen is again carried away with an argon gas flow to the measuring cell.

c: Measurement of the residual hydrogen concentration.
The determination of the residual part of the hydrogen can take place when the diffusible part has left the sample. The residual hydrogen concentration is determined in the same way as the total hydrogen concentration. The sample is completely molten and hydrogen leaving the sample is carried away with an argon gas flow to the measuring cell.

Unless otherwise stated, the hydrogen concentration values mentioned in this chapter are values of the total hydrogen concentration (i.e. diffusible hydrogen plus residual hydrogen). Each value is the average of at least five measurements, carried out under identical process conditions.

4.3 Hydrogen absorption measurements

In this section the results of the hydrogen absorption measurements are presented. First attention is given to the influence of the arc time on the absorption. Then the influence of the most important process parameters (hydrogen partial pressure, arc current, arc length, arc voltage and sample weight) on the absorption are dealt with. Finally, the results of measurements on two types of steel are discussed.

4.3.1 Time dependence of the hydrogen absorption

It is evident that hydrogen absorption is a time dependent process. In order to obtain information about this process, experiments were carried out with different arc times, ranging from 2 to 180 seconds, the other welding parameters being kept at the standard values given in Table 4.2. This was done for four different argon-hydrogen mixtures as shielding gas (2.5, 5, 10 and 20 vol.% hydrogen). The arc time was taken to be the time between the moment of ignition of the arc and the moment of extinction of the arc.
The results of the experiments are presented in Fig. 4.4 to Fig. 4.7. In these figures the

hydrogen concentration in the sample is plotted as a function of the arc time. For all four hydrogen percentages the amount of absorbed hydrogen increases rapidly in the beginning, tends to increase more slowly after a few seconds and finally reaches a saturation level. The fact that a saturation level (equilibrium concentration) is reached implies that the amount of hydrogen entering the metal per unit time equals the amount of hydrogen leaving the metal per unit time.

The absorption curves in the case of the four hydrogen partial pressures have approximately the same shape. Furthermore, the equilibrium hydrogen concentration is directly related to the hydrogen partial pressure: the higher the hydrogen partial pressure the higher the equilibrium hydrogen concentration in the sample. This is expected because a higher hydrogen partial pressure results in an increase in hydrogen present at the surface of the sample, and consequently a larger amount of hydrogen will be absorbed.

Under the present experimental conditions the measured hydrogen saturation value corresponding with 2.5 vol.% hydrogen in the shielding gas (Fig. 4.4) is about 0.00032 wt.%, which is reached within 10 seconds after ignition of the arc. The saturation hydrogen concentration corresponding with 5 and 10 vol.% hydrogen in the shielding gas is about 0.00048 and 0.00064 wt.%, respectively (Fig. 4.5 and Fig. 4.6). For these gas compositions the saturation level is reached after about 10 to 20 seconds. When 20 vol.% hydrogen is present in the shielding gas (Fig. 4.7) the equilibrium value is 0.00080 wt.%, which is reached after about 30 seconds. These findings are consistent with the results obtained by Tsuboi et al. [4.3].

The relation between the saturation hydrogen concentration in the sample and the hydrogen percentage in the shielding gas will be further dealt with in section 4.3.2.

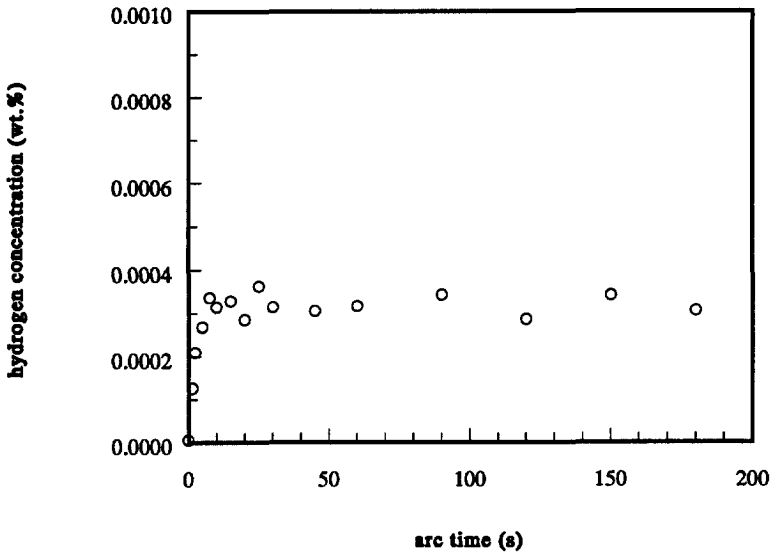

Fig. 4.4 Hydrogen concentration in the sample as a function of arc time for argon shielding gas mixed with 2.5 vol.% hydrogen.

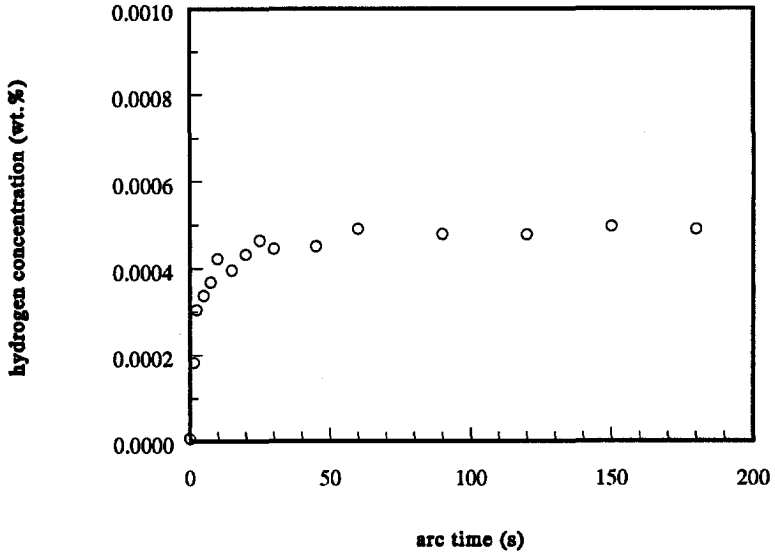

Fig. 4.5 Hydrogen concentration in the sample as a function of arc time for argon shielding gas mixed with 5 vol.% hydrogen.

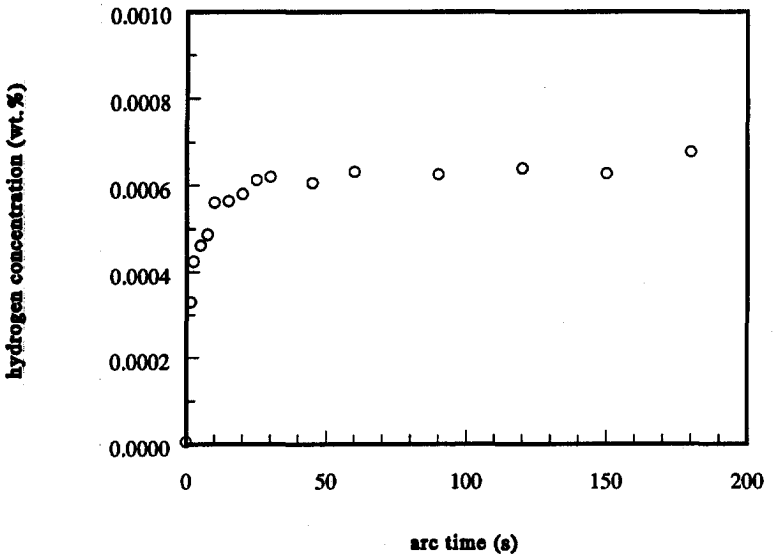

Fig. 4.6 Hydrogen concentration in the sample as a function of arc time for argon shielding gas mixed with 10 vol.% hydrogen.

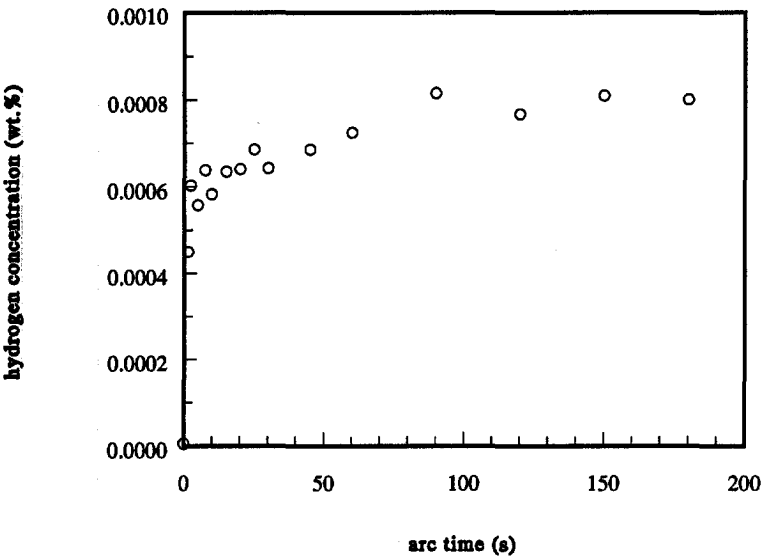

Fig. 4.7 Hydrogen concentration in the sample as a function of arc time for argon shielding gas mixed with 20 vol.% hydrogen.

4.3.2 Influence of hydrogen percentage in the shielding gas on hydrogen absorption

It was shown in the previous section that the amount of hydrogen absorbed in the sample increases with arc time and that after a sufficiently long arc time a saturation value is reached. It was also shown that this saturation level increases with increasing hydrogen percentage in the shielding gas. In order to study the influence of the hydrogen percentage in the shielding gas on the saturation level of the absorbed hydrogen in more detail, a series of experiments was carried out with different hydrogen contents (0-40 vol.%) in the shielding gas. The results of these experiments are presented in Fig. 4.8.

The figure shows that the hydrogen saturation concentration in the sample increases with addition of hydrogen to the shielding gas. The rate of increase is relatively large for small values of the hydrogen percentage in the shielding gas, but decreases for larger values of the hydrogen percentage in the shielding gas. With 40 vol.% hydrogen in the shielding gas the hydrogen concentration in the sample is found to be about 0.0009 wt.%.

An identical increase of the hydrogen concentration with increasing hydrogen content in the shielding gas was observed by Salter [4.4].

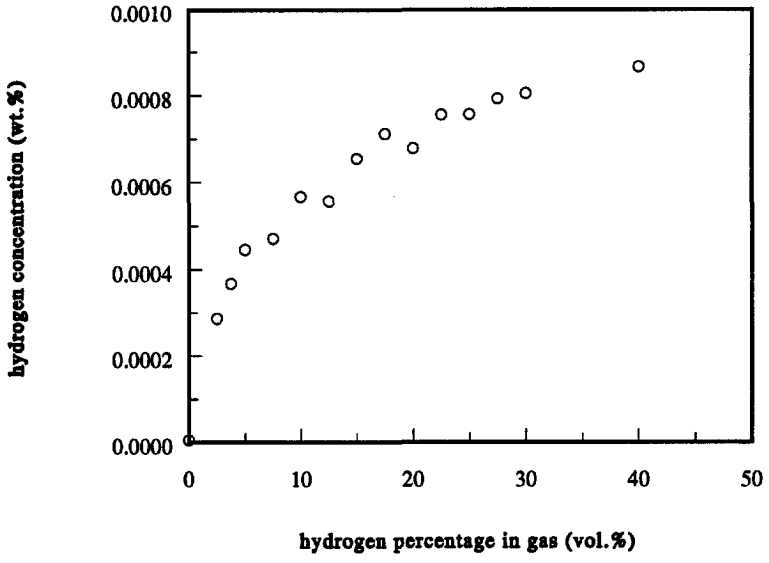

Fig. 4.8 Hydrogen concentration (saturation value) in the sample as a function of the hydrogen percentage in the shielding gas.

On theoretical basis it should be expected that with increasing hydrogen content in the shielding gas the hydrogen concentration in the sample will eventually reach a maximal value. This will occur when the actual hydrogen concentration equals the solubility of hydrogen in iron in equilibrium with hydrogen gas of 1 bar pressure, which at 1600°C has a value of 0.0026 wt.% [4.5]. Since a significant part of the hydrogen absorbed by the sample is lost during solidification and cooling of the sample (see section 4.4), it is not clear whether such a maximum is already reached in the present experiments. The fact that no pore formation was observed during the experiments suggests that this is not the case.

4.3.3 Influence of arc current on hydrogen absorption

In order to determine the influence of arc current on the hydrogen absorption, experiments were also carried out for different values of the arc current between 10 and 300 A. The other process parameters were kept at the standard values listed in Table 4.2. The results are given in Fig. 4.9, in which the hydrogen saturation concentration in the sample is plotted as a function of the arc current.

The figure shows that the hydrogen concentration in the sample increases with increasing arc current and levels off to a value of about 0.0006 wt.% above an arc current of about 100 A. A similar relationship for the hydrogen concentration with arc current was reported by Salter [4.4].

The increase in the hydrogen concentration in the sample with increasing arc current can be explained in terms of two phenomena: the increase in the arc shape and the increase in temperature of both the arc and the metal with increasing arc current. This will be further dealt with in section 4.7.2.

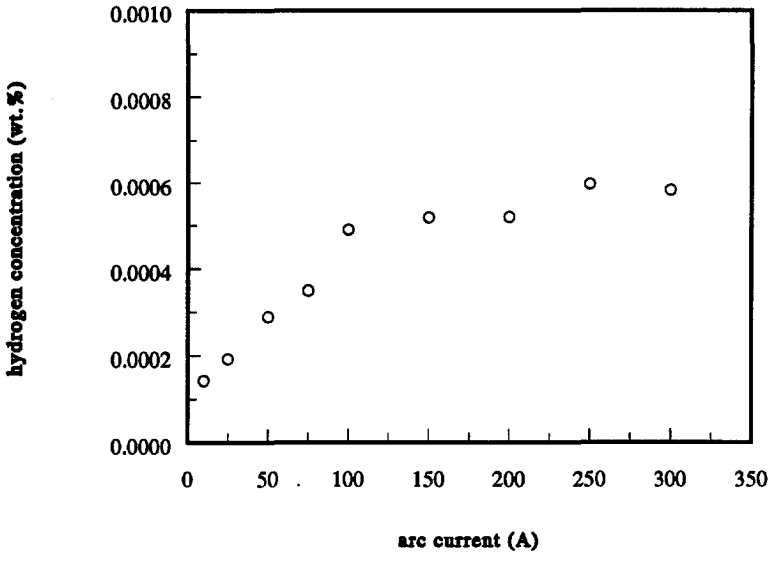

Fig. 4.9 Hydrogen concentration (saturation value) in the sample as a function of arc current.

4.3.4 Influence of arc length (arc voltage) on hydrogen absorption

The influence of the arc length on the hydrogen absorption, as obtained from a series of experiments with varying arc length values, is demonstrated in Fig. 4.10. In this figure the hydrogen concentration in the sample is plotted as a function of the arc length, for arc length values in the range of 1.5 to 7.5 mm.
The figure shows that the influence of the arc length on the hydrogen concentration in the sample is relatively small. The hydrogen concentration in the sample decreases from about 0.0005 wt.% at 1.5 mm to about 0.0004 wt.% at 7.5 mm arc length. Similar results were obtained by Salter [4.4].

As shown in section 2.3.1 the arc length is directly related to the arc voltage. This means that the data plotted in Fig. 4.10 can be translated in a hydrogen concentration versus arc voltage plot. The result of such a translation is given in Fig. 4.11.
The observed decrease in the hydrogen concentration in the sample with increasing arc length (arc voltage) is directly related to the changing properties of the arc with increasing arc length, as will be explained in section 4.7.3.

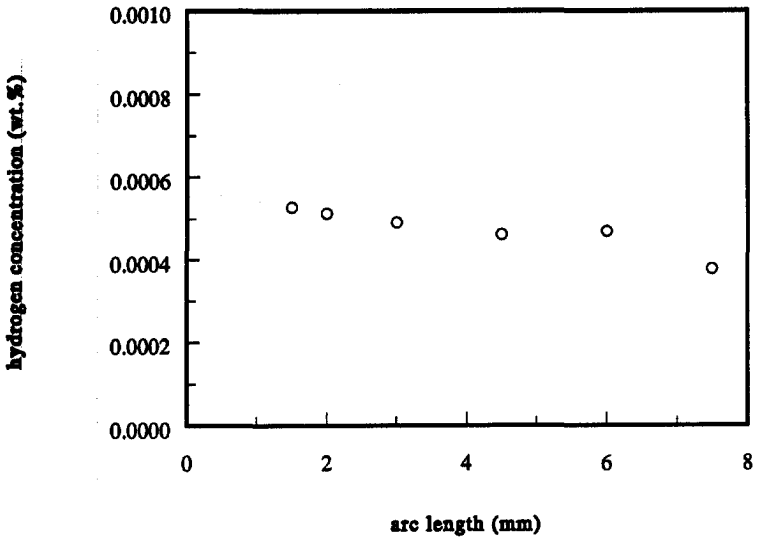

Fig. 4.10 Hydrogen concentration (saturation value) in the sample as a function of arc length.

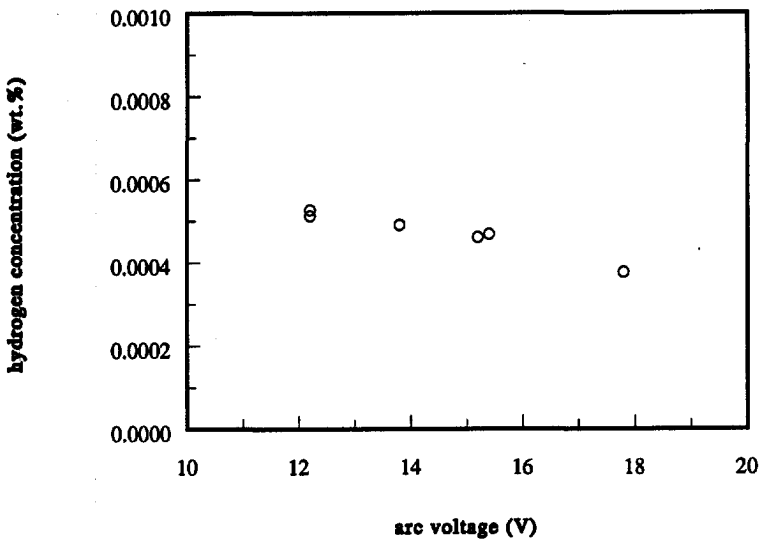

Fig. 4.11 Hydrogen concentration (saturation value) in the sample as a function of arc voltage.

4.3.5 Influence of sample weight on hydrogen absorption

The standard weight of the samples used in the experiments described above was 0.9 g. To determine the influence of the sample weight on the hydrogen absorption, a series of experiments was carried out with samples of different weight (between 0.25 and 2.7 g), the other experimental conditions being those listed in Table 4.2. In Fig. 4.12 the measured hydrogen concentration is plotted as a function of sample weight.

It appears that the hydrogen concentration decreases with increasing sample weight until the sample reaches a weight of about 1.5 gram. Above this weight the hydrogen concentration in the sample remains virtually constant. A similar relationship between hydrogen content and sample weight was found by Salter [4.4]. An explanation for the observed behaviour will be given in section 4.7.4.

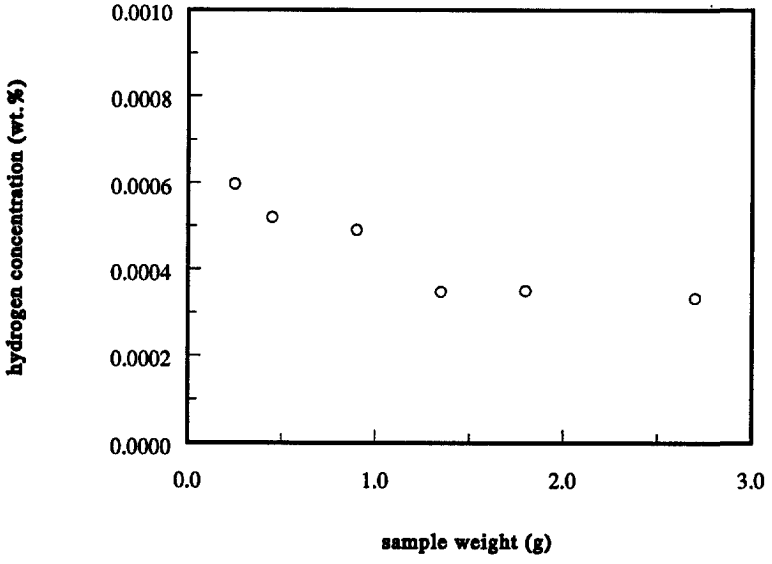

Fig. 4.12 Hydrogen concentration (saturation value) in the sample as a function of sample weight.

4.3.6 *Hydrogen absorption measurements on mild steel and stainless steel*

In order to evaluate the influence of alloying elements on the hydrogen absorption, some experiments were carried out on mild steel Fe 360 and austenitic stainless steel AISI 321. The chemical compositions of these steels are given in Table 4.1.
The experiments were carried out as a function of arc time in an argon-5% hydrogen atmosphere, the other experimental conditions being those listed in Table 4.2. The results of the experiments are presented in Fig. 4.13. In this figure the hydrogen concentration in the sample is plotted as a function of arc time for the two steels, together with the data for pure iron.

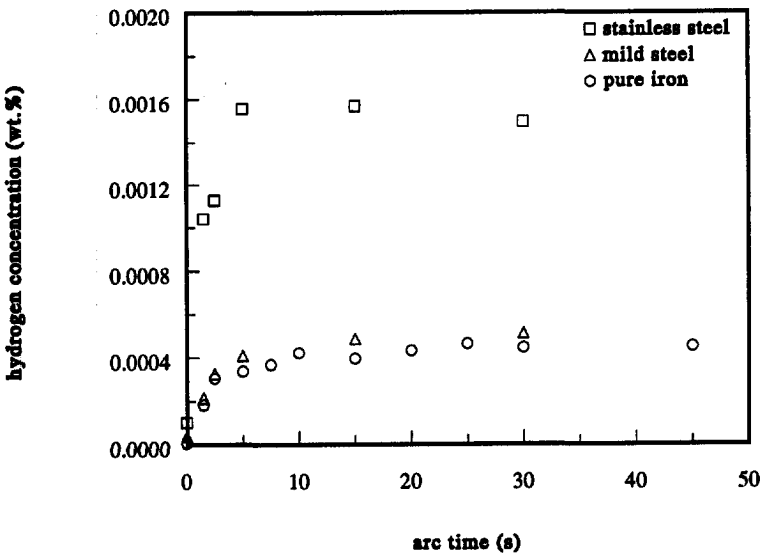

Fig. 4.13 Hydrogen concentration (saturation value) in the sample as a function of arc time for three different materials.

The results depicted in Fig. 4.13 show that the absorption curve of mild steel scarcely differs from that of pure iron. This is not surprising, since the concentration of alloying elements and impurities in mild steel is relatively small.
The absorption curve of stainless steel on the other hand differs significantly from that of pure iron. This difference can be attributed to the presence of alloying elements in stainless

steel in relatively high concentrations. These elements (in particular chromium) not only increase the solubility of hydrogen in liquid iron (see Fig. 2.5), but also reduce the diffusion rate of hydrogen in solid iron [4.6]. Both effects result in a higher value of the hydrogen content in the sample after solidification and cooling.

4.4 Determination of the initial hydrogen concentration

It must be realized that the amount of hydrogen measured in the experiments described above is not equal to the amount present in the liquid metal at the moment the arc is extinguished. In fact, it is very likely that a relatively large part of the hydrogen originally present in the material will be lost between the moment of extinction of the arc and the moment the sample is analyzed. This is due to the fact that the hydrogen measurement takes place after cooling of the sample, which takes a certain period of time, and that part of the hydrogen will leave the sample during this cooling period.
It is evident that the amount of hydrogen which leaves the sample during cooling is dependent on the diffusion coefficient of hydrogen in solid iron, which in turn is dependent on the temperature. The amount of hydrogen which will be lost can be relatively large, due to the high diffusion rate of hydrogen in iron, especially at the high temperature of the weld metal just after extinction of the arc [4.7].
From a theoretical point of view, the initial hydrogen concentration (i.e. the hydrogen concentration of the sample at the moment the arc is extinguished) is much more important than the measured hydrogen concentration, which is strongly dependent on the cooling conditions of the sample. In fact, it is the initial hydrogen concentration, rather than the measured hydrogen concentration, on which modelling of the absorption mechanism should be based.

Attempts were made to determine the initial hydrogen concentration in pure iron samples from the measured hydrogen concentration (saturation value) in two ways:

- by extrapolation to zero cooling time of measured values obtained with different cooling rates;
- by calculation from the measured values using a finite element program.

Both approaches will be briefly described below.

4.4.1 Influence of cooling time

To demonstrate the effect of the cooling rate on the measured hydrogen concentration, a series of experiments was carried out with different cooling rates, the other process conditions being the standard welding conditions given in Table 4.2.
The cooling rate of the sample was varied by changing the composition of the cooling gas mixture from pure argon to pure helium. Because of the higher thermal conductivity of helium compared to that of argon, the cooling rate increases with increasing helium percentage in the shielding gas mixture. Values of the thermal conductivity of argon and helium at different temperatures are listed in Table 4.3.

Table 4.3 Thermal conductivity (10^{-6} J s^{-1} cm^{-1} $°C^{-1}$) of argon and helium [4.8].

element	T = - 240°C	T = 4.4°C	T = 26.7°C	T = 48.9°C
argon	-	168.0	178.4	190.5
helium	353.3	1434.7	1509.9	1575.7

In the experiments which are described below, the cooling time is defined as the time interval between the moment of extinction of the arc and the moment the sample reaches a temperature of 300°C. The temperature of 300°C is chosen because this is the minimum detection limit of the pyrometer used.

In Fig. 4.14 the measured hydrogen concentration in the sample is plotted as a function of the cooling time. The figure clearly shows that during cooling a considerable fraction of the absorbed hydrogen disappears from the sample. This fraction increases with increasing cooling time. For instance, a variation in cooling time from 4 seconds using pure helium as cooling gas to 10 seconds using pure argon as cooling gas results in a decrease from about 0.00050 to about 0.00022 wt.% hydrogen in the sample.

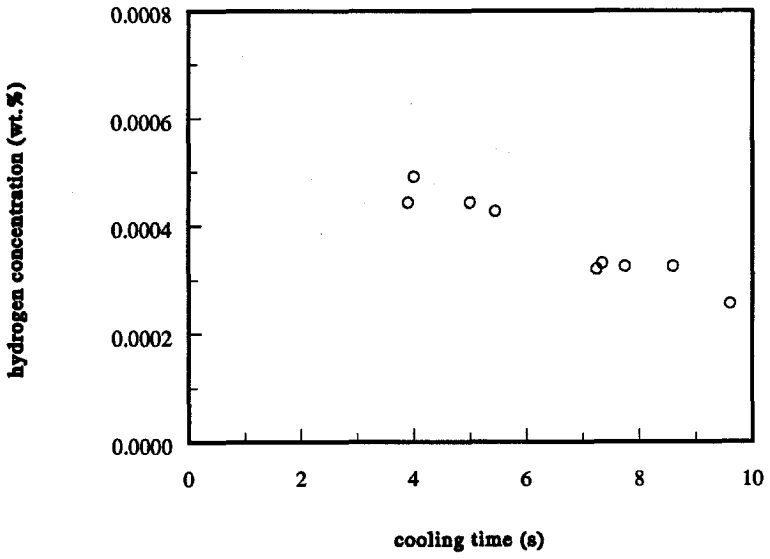

Fig. 4.14 Hydrogen concentration in the sample as a function of cooling time.

The minimum cooling time attainable when using the cooling procedure described above was found to be slightly less than 4 seconds. Attempts were made to further reduce the cooling time by using helium cooled to -196°C by means of liquid nitrogen. However, it was found that this had scarcely any effect on the cooling rate of the sample.
This finding is primarily due to the fact that the thermal conductivity of helium decreases rapidly with decreasing temperature, especially in the temperature range below room temperature (see Table 4.3).

In principle, the value of the initial hydrogen concentration in the sample can be obtained by extrapolation of the measured values of the hydrogen concentration to zero cooling time. However, the value thus obtained is far from reliable, due to the lack of data at small cooling times (below a cooling time of 4 seconds), as becomes evident when considering the data presented in Fig. 4.14.
In view of this, attempts were made to determine the initial hydrogen concentration by means of calculation.

4.4.2 Calculation of the initial hydrogen concentration

Calculation of the initial hydrogen concentration in the sample was carried out numerically with the help of a personal computer, using the measured hydrogen concentration and the cooling history of the sample as monitored by the optical pyrometer.
Basis of the calculation is the diffusion of hydrogen through the sample to the surface, where it can escape to the surrounding. The diffusion is governed by Fick's First and Second Laws of diffusion [4.9]:

$$J = -D\frac{dc}{dx} \tag{4.1}$$

and

$$\frac{\partial c}{\partial t} = D\left(\frac{\partial^2 c}{\partial x^2}\right) \tag{4.2}$$

in which J = flux, defined as the number of atoms of one species crossing unit area per unit time,
dc/dx = concentration gradient in direction x,
c = concentration,
t = time,
D = diffusion coefficient.

In order to be able to carry out these calculations, a number of assumptions were made. These assumptions are formulated below.

- The sample has a perfectly spherical shape. This assumption does not differ much from reality. Under the experimental conditions used, the true shape of the samples was found to deviate not more than 5% from that of a sphere.
- The calculations refer to the total amount of hydrogen in the sample. Trapping of hydrogen in the material (residual hydrogen) becomes a real possibility only at temperatures below 350°C [4.10]. This means that during most of the cooling time all hydrogen in the sample is able to diffuse through the iron.

- No bubble formation occurs during the heating and cooling process, as was observed under the present experimental conditions.
- At the moment of extinction of the arc the hydrogen is evenly distributed over the sample (no concentration gradient).
- The hydrogen can leave the sample through the entire surface. This is actually not the case for the area where the sample is in contact with the copper table, but this area is relatively small. Apart from this area the sample is in direct contact with the surrounding shielding gas atmosphere.
- All hydrogen reaching the surface will immediately recombine and disappear into the surrounding gas atmosphere.
- The temperature of the sample surface, which is measured with the pyrometer, is equal to the temperature at any location within the sample.
- Both the temperature dependence of the diffusion coefficient and the changes in diffusion coefficient due to phase transformations (from liquid to delta-ferrite, from delta-ferrite to austenite and from austenite to alpha-ferrite) are taken into account. The values of the diffusion coefficient used in the calculations are taken from the curve depicted in Fig. 4.15 (see Table 2.1).

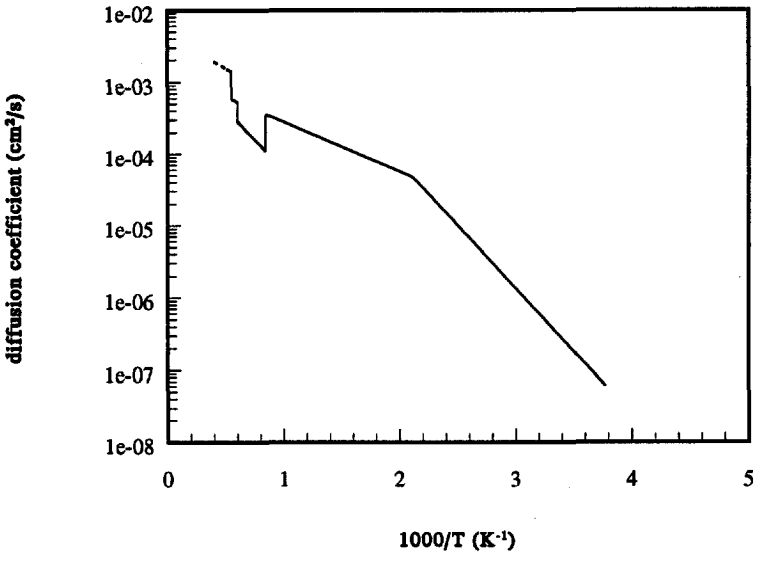

Fig. 4.15 The diffusion coefficient of hydrogen in pure iron as a function of temperature.

Based on Fick's Laws of diffusion and using the assumptions formulated above, a finite element program was developed for calculation of the initial hydrogen concentration in the sample. In this approach the sample is divided in small concentric segments, and the change in hydrogen concentration with time is calculated for each of the segments in distinct time steps. Because the sample is assumed to have a spherical shape the situation can be described by the approximate equations [4.11]:

$$\frac{1}{R^2}\frac{\partial}{\partial R}\left(R^2\frac{\partial c}{\partial R}\right) = \frac{1}{i(\delta R)^2}[(i+1)c_{i+1,j} - 2ic_{i,j} + (i-1)c_{i-1,j}] \quad \text{for } i \neq 0,$$

and

$$\frac{1}{R^2}\frac{\partial}{\partial R}\left(R^2\frac{\partial c}{\partial R}\right) = \frac{6}{(\delta R)^2}(c_{1,j} - c_{0,j}) \quad \text{for } i=0. \tag{4.3}$$

in which δR = segment size,
i = rank number of the segment,
j = rank number of the time step,
R = distance from the centre of the sample,
c = concentration.

The time step and the segment size are limited by the diffusion coefficient. The calculation is computationally straightforward, but has a stability restriction which can be expressed by the equation:

$$\frac{2D}{(\delta R)^2}\delta t \leq \frac{1}{2} \tag{4.4}$$

in which D = diffusion coefficient,
δR = segment size,
δt = length of the time step.

Using Eq. (4.4) a time step of 0.0001 seconds and a segment size of 0.01 mm was chosen.

4.4.3 Justification of the calculation approach

To verify the validity of the calculation approach as described in the previous section, calculations were carried out of the initial hydrogen concentration for different cooling times using the experimental results given in Fig. 4.14 as input data.
The results of these calculations are summarized in Fig. 4.16. In this figure both the measured and the initial hydrogen concentration in the sample are given as a function of cooling time.
From Fig. 4.16 it becomes clear that a significant part of the hydrogen absorbed in the sample is lost during cooling. The magnitude of the hydrogen loss depends on the cooling conditions. For example, in the case of cooling with helium (cooling time about 4 s) the hydrogen loss is about 45% of the amount originally present in the sample, whereas in the case of cooling with argon (cooling time about 9.5 s) the hydrogen loss amounts to about 70%. These observations are consistent with the experimental findings of Howden and Milner [4.7].

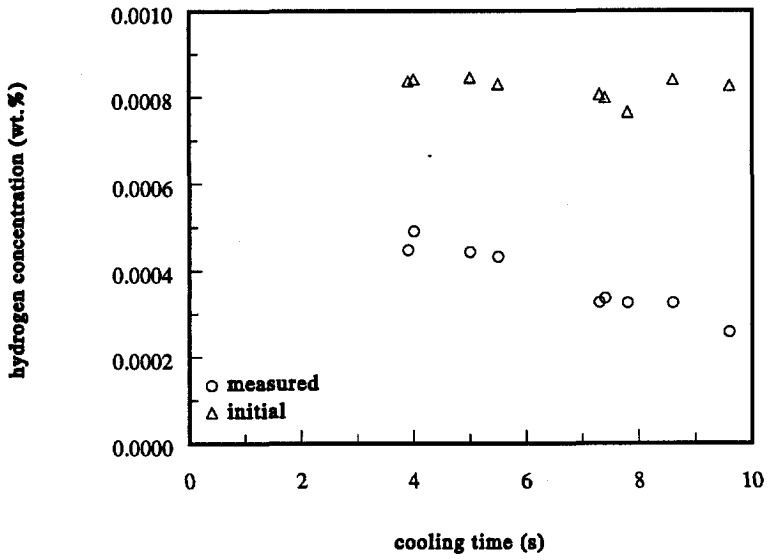

Fig. 4.16 Measured and initial hydrogen concentration in the sample as a function of cooling time.

It is important to note that the initial hydrogen concentration as calculated from the experimental results obtained with different cooling rates, is virtually independent of the cooling time. This should be expected, as the experiments were carried out using identical process parameters. The finding that the calculated initial hydrogen concentration in the sample is independent of the cooling time is a strong indication that the calculation procedure used is reliable.

To explore the possibilities of the calculation approach, the initial hydrogen concentration in the sample was calculated for all measured hydrogen values obtained under various process conditions (hydrogen partial pressure, arc current, arc length and sample weight) using the cooling history.

In Fig. 4.17 the ratio of the measured and the initial hydrogen concentration in the sample for a number of different welding conditions and a constant sample weight is plotted as a function of cooling time. The figure clearly shows that, although there is considerable scatter, a distinct relationship exists between this ratio and the cooling time. This implies that it is possible to determine the initial hydrogen concentration from the measured value for each set of experimental conditions when the cooling history is known.

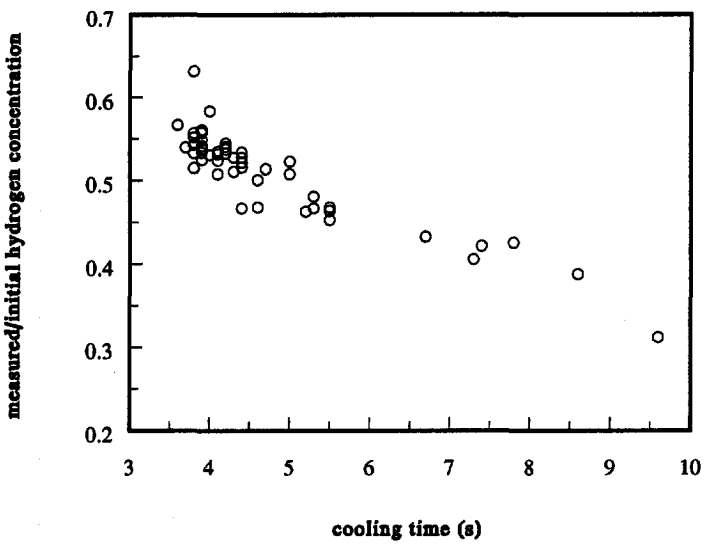

Fig. 4.17 Ratio of the measured hydrogen concentration and the calculated initial hydrogen concentration in the sample as a function of cooling time.

4.4.4 Calculation of the hydrogen concentration profile in the sample during cooling

In order to obtain insight in the hydrogen distribution within the sample during cooling of the sample after extinction of the arc, hydrogen concentration profiles in the sample were calculated for different periods of time after arc extinction. The results are presented in Fig. 4.18. In this figure the calculated hydrogen concentration in the sample is plotted against the distance from the centre of the sample for different periods of time after arc extinction. The hydrogen concentration at the moment the arc is extinguished is taken as 100%. The process conditions used for the calculations were the standard conditions listed in Table 4.2.
The curves in the figure give the hydrogen concentration in the sample after different cooling times: from right to left after 0.25, 0.75, 1.50, 2.50 and 3.75 seconds of cooling, respectively. The measured surface temperatures corresponding with these cooling times are 1560, 1440, 1160, 785 and 315°C, respectively. Immediately after the start of the cooling the hydrogen concentration near the surface of the sample drops rapidly, becoming zero at the surface itself. As expected, the concentration gradient in the vicinity of the surface decreases with increasing cooling time.

In Fig. 4.19 the calculated hydrogen content of the sample is plotted as a function of the cooling time. Again the hydrogen content of the sample at the moment the arc is extinguished is taken to be 100%. The values of the hydrogen content corresponding with the five cooling times used in Fig. 4.18 are 79, 72, 68, 65 and 62%, respectively.
The figure shows that in the first tenths of a second after extinction of the arc a large part of the hydrogen leaves the sample. In fact, the first quarter of the total amount of hydrogen present in the sample disappears in about four tenths of a second.
The strong decrease in hydrogen loss with cooling time is due to the fact that most hydrogen near the surface leaves the sample immediately after extinction of the arc, while the diffusion of the hydrogen in the interior decreases rapidly.

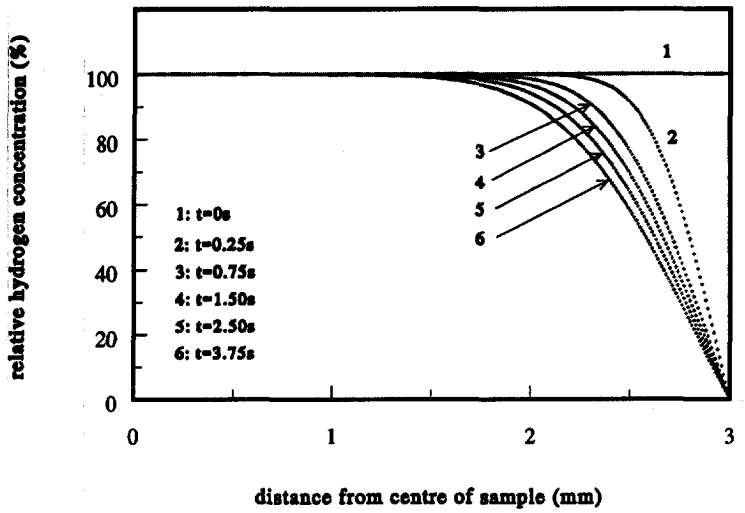

Fig. 4.18 Relative hydrogen concentration in the sample for different periods of times after arc extinction as a function of the distance from the center of the sample.

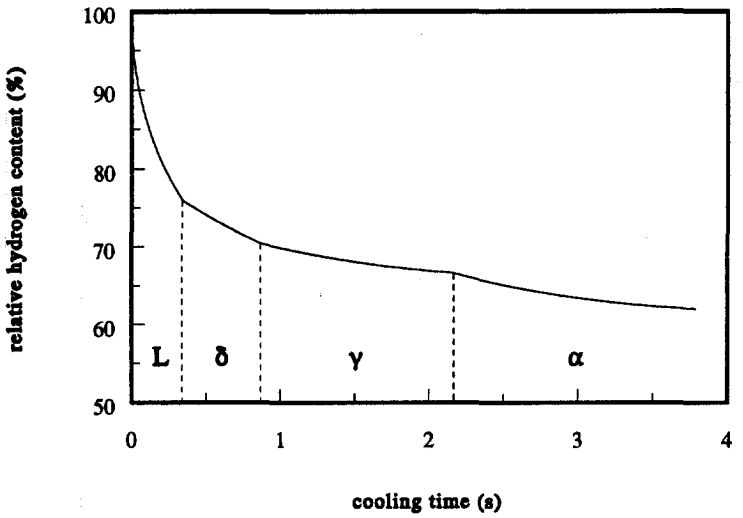

Fig. 4.19 Relative hydrogen content of the sample as a function of the cooling time.

4.5 Modelling of the hydrogen absorption process

In this section a model will be presented of hydrogen absorption under stationary arc conditions. This model is similar to the model recently proposed for nitrogen absorption under stationary arc conditions [4.1,4.2]. Basis of the model is the assumption that the hydrogen concentration in the melt at any moment is the result of two mutually independent processes: inflow of hydrogen and outflow of hydrogen (see Fig. 4.20).

- Inflow of hydrogen takes place exclusively through the interface between the arc and the liquid metal, the inflow rate being determined by the arc conditions (notably the partial pressure of the hydrogen in the arc and the temperature of the arc). In Fig. 4.20 this hydrogen flow is depicted by the large arrows.
- Outflow of hydrogen takes place through the entire outer surface of the liquid metal (including that part of the surface which is covered by the arc), the outflow rate being proportional to the hydrogen concentration in the liquid metal. In Fig. 4.20 this hydrogen flow is depicted by the small arrows.

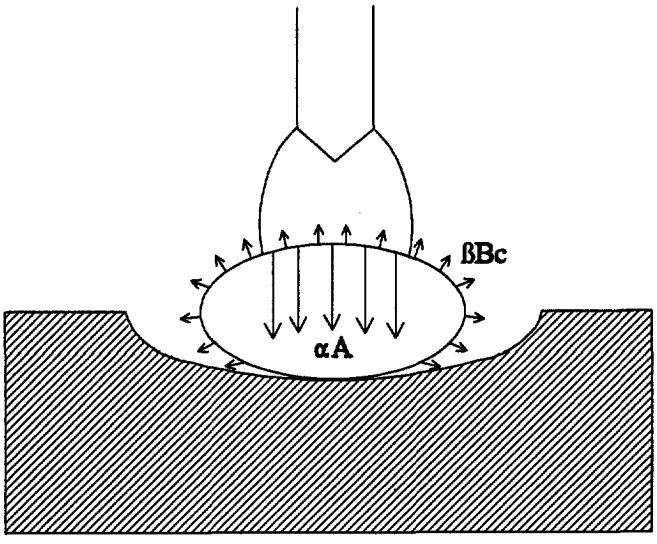

Fig. 4.20 Schematic representation of the absorption process.

On this basis the time dependent change in the hydrogen concentration in the sample can be described by the equation:

$$\frac{dH}{dt} = W\frac{dc}{dt} = \alpha A - \beta Bc \qquad (4.5)$$

in which H = amount of hydrogen present in the liquid metal,
t = time,
W = sample weight,
c = hydrogen concentration in the liquid metal,
α = absorption coefficient (amount of hydrogen entering the liquid metal per unit area per unit time),
A = interface area between arc and liquid metal,
ß = desorption coefficient (a proportionality factor depending on the temperature of the liquid metal),
B = interface area between liquid metal and surrounding gas phase.

The solution of differential equation (4.5) can be written as:

$$c(t) = \frac{\alpha A}{\beta B}\left[1 - \exp\left(\frac{-\beta B}{W}t\right)\right] \qquad (4.6)$$

When t is large (long arc time) the exponential term will become negligibly small, and an equilibrium situation (saturation) will arise. Saturation occurs when the amount of hydrogen entering the liquid metal per unit time equals the amount of hydrogen leaving the liquid metal per unit time.
Under these conditions the equation can be written in the form:

$$c_s = \frac{\alpha A}{\beta B} \qquad (4.7)$$

in which c_s = equilibrium concentration.

With the help of Eqs. (4.5), (4.6) and (4.7) it is possible to predict the hydrogen concentration in the sample for any given situation. However, this requires knowledge of the quantities A, B, α and ß. Values of A and B can be obtained experimentally, values of α and ß can be determined using one of the two methods described in the next section.

It should be kept in mind that the hydrogen concentration referred to in the model described in the foregoing, is the initial hydrogen concentration (as obtained using the calculations described in section 4.4.2) rather than the measured hydrogen concentration, which strongly depends on the cooling conditions.

4.6 Determination of the absorption coefficient and the desorption coefficient

4.6.1 Determination of the absorption coefficient and the desorption coefficient using the time dependence of the hydrogen absorption

A possible way of determining α and ß is based on fitting the experimentally obtained time dependent data with Eqs. (4.6) and (4.7).
In practice, the most convenient approach is to insert the experimental data in Eq. (4.8), which is a combination of Eqs. (4.6) and (4.7):

$$c(t) = c_s \left[1 - \exp\left(\frac{-\beta B}{W} t\right)\right] \qquad (4.8)$$

in which c = concentration,
c_s = equilibrium concentration,
ß = desorption coefficient (a proportionality factor depending on the temperature of the liquid metal),
B = interface area between liquid metal and surrounding gas phase,
W = sample weight,
t = time.

This approach results in a value of ß.
By combining Eqs. (4.6) and (4.7) a similar relationship between c(t) and α can be obtained, from which a value of α can be extracted.

As an example, the values of the absorption coefficient and the desorption coefficient were determined for an experiment carried out with a hydrogen content in the shielding gas of 10 vol.% (see Fig. 4.21).
For the saturation value of the hydrogen concentration, c_s, the average of the initial values of the hydrogen concentration obtained in experiments lasting longer than one minute were taken, whereas for the calculation of the value of α and ß only the concentration values which differ considerably from the equilibrium concentration were used.
The values of the absorption coefficient and the desorption coefficient thus obtained are given in Table 4.4.
With this method values of α and ß can be determined with an accuracy of about 10%.

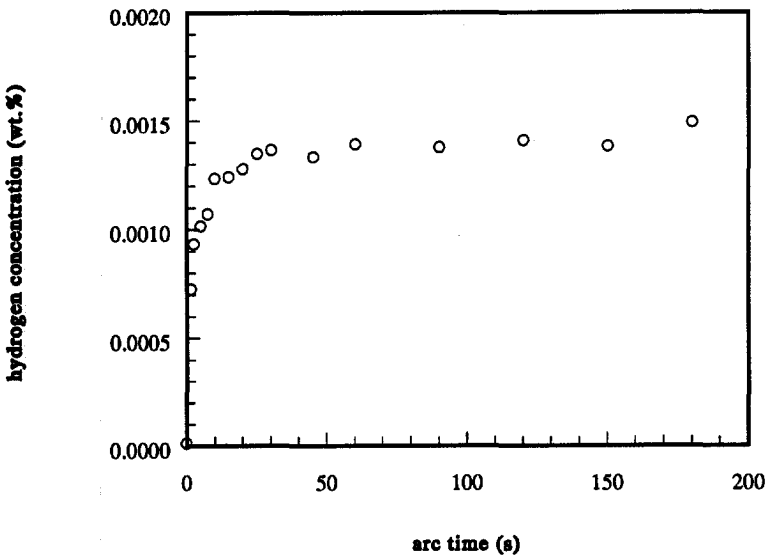

Fig. 4.21 Initial hydrogen concentration in the sample as a function of arc time for argon shielding gas mixed with 10 vol.% hydrogen.

Table 4.4 Values of the absorption coefficient and the desorption coefficient obtained with two different methods.

method	α (g/sm^2)	ß (g/sm^2)
time dependence of the absorption	35	$3.0x10^3$
degassing of the sample	32	$2.6x10^3$

4.6.2 Determination of the absorption coefficient and the desorption coefficient by means of degassing

Another way of determining α and ß is based on additional experiments in which the absorption of hydrogen is eliminated. This can be realised in the following way. Immediately after the sample is loaded with hydrogen under normal experimental conditions, the shielding gas composition is changed to a pure argon atmosphere and the arc is re-ignited directly after the cooling of the sample is completed. During the second arc period absorption does not take place and only desorption occurs.

Consequently, the absorption term can be left out of Eq. (4.8). Integration of the modified equation leads to:

$$\beta = \frac{-W \cdot \ln(c)}{Bt} \tag{4.9}$$

in which ß = desorption coefficient (a proportionality factor depending on the temperature of the liquid metal),
W = sample weight,
c = concentration,
B = interface area between liquid metal and surrounding gas phase,
t = time.

By measuring the concentration as a function of time, the value of ß can be obtained. From the value of ß the value of α can be calculated using Eq. (4.7).

To test the method described above, degassing experiments were carried out after hydrogen loading in an argon-10 vol.% hydrogen atmosphere, the other experimental conditions being the standard conditions listed in Table 4.2.
The results of these experiments are presented in Fig. 4.22. In this figure the logarithm of the initial hydrogen concentration is plotted as a function of the degassing time. From the slope of the straight line drawn through the experimental points the desorption coefficient can be calculated using Eq. (4.9). From the value of the desorption coefficient and the value of the equilibrium concentration the absorption coefficient can be determined with the help of Eq. (4.7). The values thus obtained are presented in Table 4.4.
With this method α can be determined with an accuracy of about 25% and ß with an accuracy of about 20%.

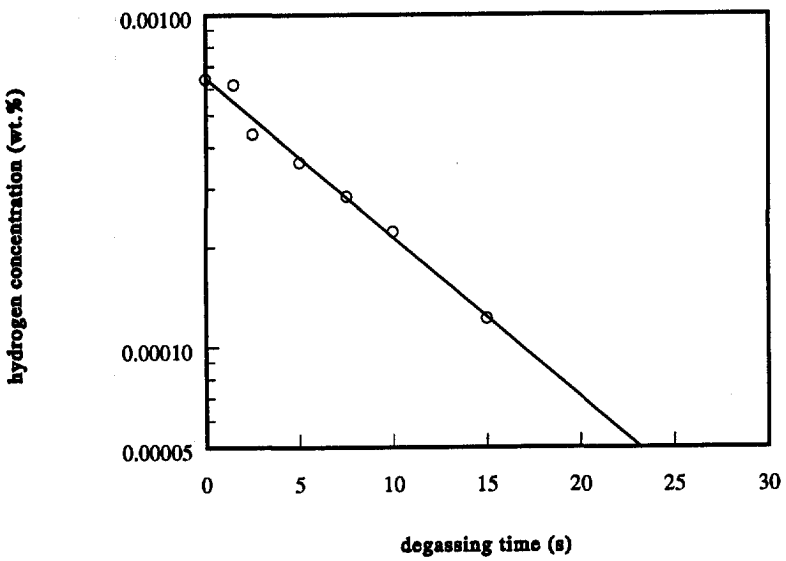

Fig. 4.22 Logarithm of the initial hydrogen concentration in the sample as a function of the degassing time in a pure argon atmosphere.

When considering the data listed in Table 4.4 it can be concluded that the results of the two methods described above are in reasonable agreement.
In the present work the first method, based on the time dependence of the hydrogen absorption (described in section 4.6.1) was used to determine α and ß.

4.7 Application of the model

In the previous section a model was developed which describes the hydrogen absorption in a small button-like sample during arc welding under stationary arc conditions. The main parameters in this model are the absorption coefficient and the desorption coefficient.
In order to test the feasibility of this model, values of α and ß were determined for the different experimental situations described in section 4.3. For the determination of α and ß the initial values of the hydrogen concentration were used, which were calculated from the measured values following the procedure outlined in section 4.4.2. The value of A was obtained from photographic images of the arc, whereas for the value of B the total surface area of the sample was taken.

4.7.1 Hydrogen partial pressure

In section 4.3.2 attention was given to experiments carried out to determine the influence of the hydrogen percentage in the shielding gas on the hydrogen absorbed by the liquid metal. The results of these experiments are shown in Fig. 4.23. In this figure the measured values together with the initial values of the hydrogen concentration in the sample are plotted as a function of the hydrogen percentage in the shielding gas.

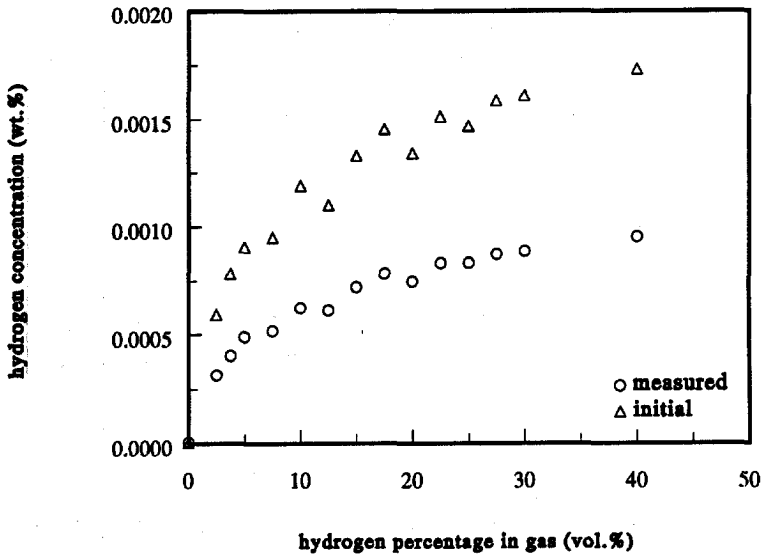

Fig. 4.23 Measured and initial hydrogen concentration in the sample as a function of the hydrogen percentage in the shielding gas.

As can be seen, the measured curve and the initial curve are similar in shape, which is reflected by the fact that the fraction of the hydrogen which remains behind in the material is about constant (between 50 and 55% of the amount originally present) independent of the shielding gas composition.
The figure shows that both the measured and the initial hydrogen concentration increase with addition of hydrogen to the shielding gas and that the rate of increase decreases with increasing hydrogen in the shielding gas. The results observed are similar to those obtained by Uda [4.12], Chew and Willgoss [4.13] and Tsuboi et al. [4.3].

The values of the absorption coefficient and the desorption coefficient were determined for different values of the hydrogen percentage in the shielding gas (2.5, 5, 10 and 20 vol.%) using the procedure outlined in section 4.6.1. The absorption curves corresponding with these hydrogen percentages are given in Fig. 4.4 to Fig. 4.7.
In Table 4.4 the results of the calculations are given. Both the absorption coefficient and the desorption coefficient increase with hydrogen percentage in the shielding gas, the increase of α being more pronounced than that of ß.
The increase of α is directly related to the fact that with increasing hydrogen content in

the shielding gas the probability that a hydrogen molecule is adsorbed at the surface of the liquid metal (the first step of the absorption process) increases. The slight increase of ß is attributed to the increase of the temperature of the weld pool with increasing hydrogen content in the shielding gas. Other investigators also observed an increase in desorption with increasing weld pool temperature [4.5].

Table 4.4 Values of c_s, A, B, α and ß for different shielding gas compositions.

H_2 (vol.%)	c_s (wt.%)	A (m^2)	B (m^2)	α (g/sm^2)	ß (g/sm^2)
2.5	$6.0x10^{-4}$	$8x10^{-6}$	$1.1x10^{-4}$	23	$2.8x10^{3}$
5	$9.9x10^{-4}$	$10x10^{-6}$	$1.1x10^{-4}$	28	$2.6x10^{3}$
10	$13.6x10^{-4}$	$12x10^{-6}$	$1.1x10^{-4}$	38	$3.0x10^{3}$
20	$15.7x10^{-4}$	$14x10^{-6}$	$1.1x10^{-4}$	46	$3.8x10^{3}$

At this point a comment should be made about the influence of the arc on the solubility of hydrogen in iron. The solubility of hydrogen in iron under non-arc equilibrium conditions is given by Sieverts' Law [4.14]:

$$[H] = K\sqrt{p_{H_2}} \tag{4.10}$$

in which [H] = hydrogen concentration in the metal,
K = solubility coefficient,
p_{H2} = hydrogen partial pressure.

The solubility coefficient, which characterizes the solubility of hydrogen in a material, is defined as:

$$K = K_0 \cdot \exp\left(\frac{-\Delta H}{RT}\right) \tag{4.11}$$

in which K = solubility coefficient,
K_0 = solubility constant,
ΔH = change in enthalpy,
R = gas constant,
T = absolute temperature.

It is interesting to check whether and if so to what extend the experimental data as obtained in the present work obey Sieverts' Law.
In Fig. 4.24 values of the initial hydrogen concentration in the sample are plotted as a function of the square root of the hydrogen percentage in the shielding gas. As shown by Eq. (4.10), Sieverts' Law predicts a linear relationship between the hydrogen concentration in the sample and the square root of the hydrogen percentage in the shielding gas. The figure shows that this is only the case for small values of the hydrogen percentage in the shielding gas (below about 20 vol.%). At larger values the experimental points deviate increasingly from the straight line. These results are consistent with those obtained by Uda [4.12].

The deviation from Sieverts' Law at high values of the hydrogen percentage in the shielding gas is attributed to evaporation of the liquid metal as observed during the experiments, which results in a decrease of the effective hydrogen partial pressure. Evaporation is believed to occur in particular at the arc-liquid interface and increases with increasing hydrogen in the shielding gas due to contraction of the arc (see section 3.3.1). From the slope of the straight line drawn in Fig. 4.24 the value of K can be obtained, using Eq. (4.11). By inserting this value together with an appropriate value of ΔH [4.5] in Eq. (4.11), the temperature of the liquid metal and the arc plasma in the vicinity of the arc-metal interface can be estimated. This yields a temperature of about 2100 K, which seems a reasonable value.

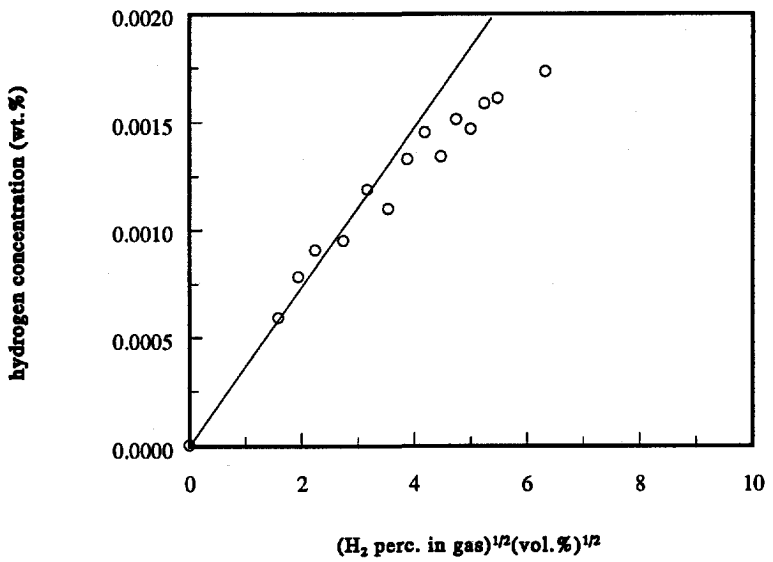

Fig. 4.24 Initial hydrogen concentration in the sample as a function of the square root of the hydrogen percentage in the shielding gas.

4.7.2 Arc current

In Fig. 4.25 both the measured and the initial hydrogen concentration in the sample, as obtained by experiments and calculations (see section 4.3.3 and section 4.6.1) are plotted as a function of arc current

The figure shows that the initial hydrogen concentration increases continuously with increasing arc current, whereas the measured concentration seems to reach a saturation level. The observed difference in shape between the two curves is caused by the increase in temperature of the sample (increase in cooling time) with increasing arc current, resulting in a smaller fraction of the initial hydrogen content remaining behind in the sample.

Values of the absorption coefficient and the desorption coefficient were determined for three different arc currents (100, 200 and 300 A). The results are listed in Table 4.5, which shows a slight increase in α and a strong increase in ß with increasing arc current.

The increase in ß is attributed to the increase of the weld pool temperature with increasing arc current, as confirmed by pyrometric measurements.

Table 4.5 Values of c_s, A, B, α and ß for different values of the arc current.

arc current (A)	c_s (wt.%)	A (m^2)	B (m^2)	α (g/sm^2)	ß (g/sm^2)
100	9.9×10^{-4}	10×10^{-6}	1.1×10^{-4}	28	2.6×10^{3}
200	10.2×10^{-4}	24×10^{-6}	1.1×10^{-4}	31	6.7×10^{3}
300	13.5×10^{-4}	39×10^{-6}	1.1×10^{-4}	34	9.1×10^{3}

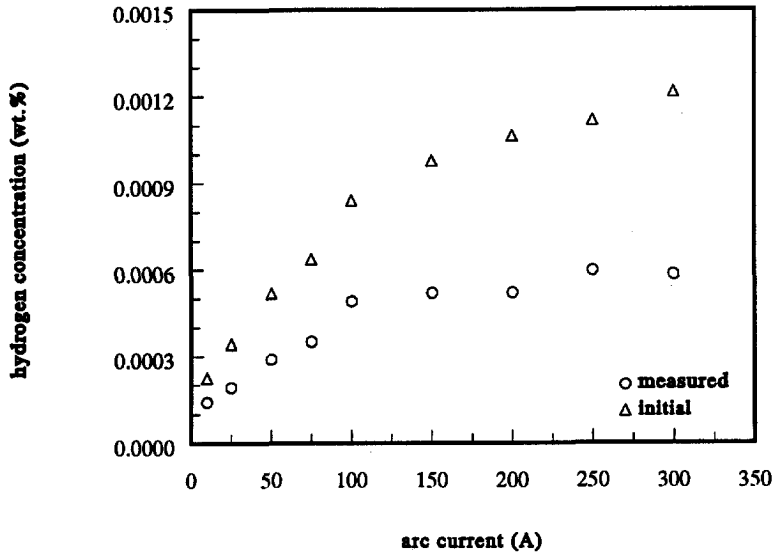

Fig. 4.25 Measured and initial hydrogen concentration in the sample as a function of arc current.

4.7.3 Arc length

The influence of the arc length on the hydrogen absorption is demonstrated in Fig. 4.26. In this figure the measured hydrogen concentration (see section 4.3.4) and the initial hydrogen concentration (see section 4.6.1) are plotted as a function of the arc length for arc length values in the range of 1.5 to 7.5 mm.
The figure shows that both the measured hydrogen concentration and the initial hydrogen concentration decrease slowly with increasing arc length. The observed behaviour is in agreement with the results of other work [4.4,4.15].

Values of α and β were calculated for arc length values of 1.5, 3 and 6 mm. The results are given in Table 4.6.
It appears that with increasing arc length α remains virtually constant, whereas β increases. The increase of β is due to the increase of the weld pool temperature with increasing arc length.

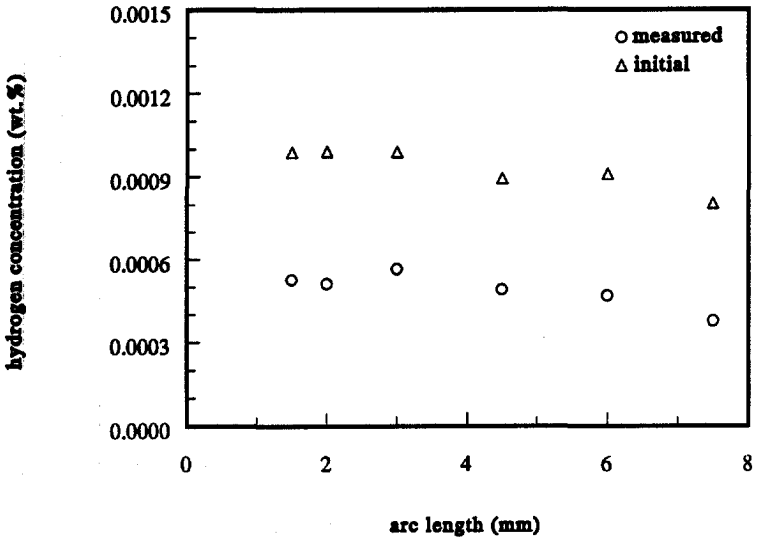

Fig. 4.26 Measured and initial hydrogen concentration in the sample as a function of arc length.

Table 4.6 Values of c_s, A, B, α and ß for different values of the arc length.

arc length (mm)	c_s (wt.%)	A (m^2)	B (m^2)	α (g/sm^2)	ß (g/sm^2)
1.5	9.9×10^{-4}	7×10^{-6}	1.1×10^{-4}	28	1.8×10^{3}
3	9.9×10^{-4}	10×10^{-6}	1.1×10^{-4}	28	2.6×10^{3}
6	9.1×10^{-4}	12×10^{-6}	1.1×10^{-4}	25	3.0×10^{3}

4.7.4 Sample weight

In Fig. 4.27 the measured hydrogen concentration (see section 4.3.5) and the initial hydrogen concentration (see section 4.6.1), are plotted as a function of sample weight. The figure shows that both the measured and the initial hydrogen concentration decrease with increasing sample weight, until the sample reaches a weight of about 1 gram. Above this weight the hydrogen concentration seems to remain constant. A similar relationship between hydrogen concentration and sample weight was observed by Salter [4.4].

Values of α and ß were calculated for three different sample weight values (0.9, 1.8 and 2.7 g). The results of these calculations are given in Table 4.7.
The table shows that both α and ß are only slightly affected by sample weight in the range used. This is not surprising in view of the fact that the arc temperature is expected not to change with sample weight, whereas the weld pool temperature is observed to remain virtually constant.

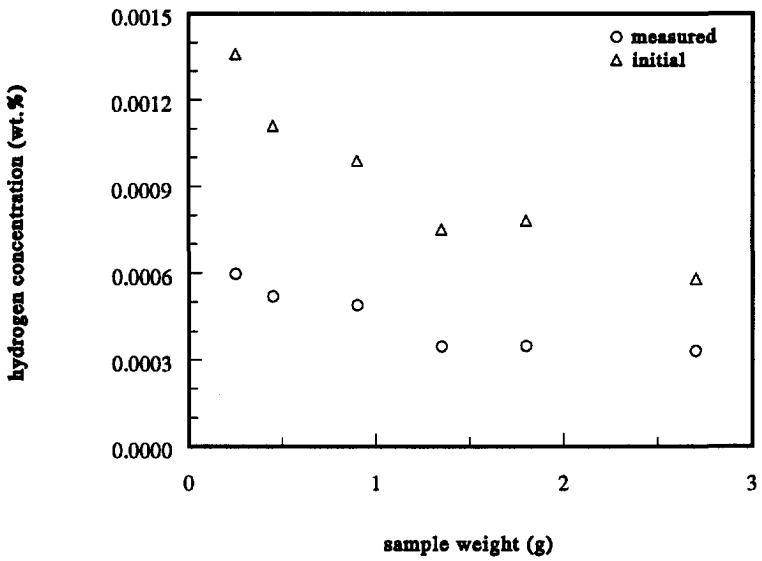

Fig. 4.27 Measured and initial hydrogen concentration in the sample as a function of the sample weight.

Table 4.7 Values of c_s, A, B, α and ß for different sample weights.

sample weight (g)	c_s (wt.%)	A (m^2)	B (m^2)	α (g/sm^2)	ß (g/sm^2)
0.9	9.9×10^{-4}	10×10^{-6}	1.1×10^{-4}	28	2.6×10^{3}
1.8	7.8×10^{-4}	15×10^{-6}	1.8×10^{-4}	23	2.6×10^{3}
2.7	5.8×10^{-4}	15×10^{-6}	2.3×10^{-4}	25	2.9×10^{3}

4.8 Conclusions

In this chapter the results are presented of experiments in which small samples of iron and steel were welded in hydrogen containing atmospheres under stationary arc conditions. These experiments were aimed at obtaining information about the hydrogen absorption process and lead to the following conclusions.

- The measured hydrogen concentration in the sample increases with arc time and reaches a saturation concentration within a relatively short time.
- This saturation concentration depends on the various process parameters: it is virtually independent of arc length, increases with hydrogen percentage in the shielding gas and with arc current and decreases with sample weight.
- A large part of the hydrogen absorbed during welding leaves the sample during cooling. The initial hydrogen concentration in the sample can be calculated with the help of a finite element program.
- Hydrogen absorption can be described by a model based on two mutually independent processes: inflow and outflow.
  Inflow of hydrogen takes place exclusively through the interface between the arc and the liquid metal, the inflow rate being determined by the arc conditions (notably the partial pressure of the hydrogen in the arc and the temperature of the arc).
  Outflow of hydrogen takes place through the entire outer surface of the liquid metal (including that part of the surface which is covered by the arc), the outflow rate being proportional to the hydrogen concentration in the liquid metal.
- The absorption coefficient and the desorption coefficient can be determined for various process conditions.
  The absorption coefficient increases with hydrogen percentage in the shielding gas, while the desorption coefficient increases with hydrogen percentage in the shielding gas, arc current and arc length.
- Hydrogen absorption under stationary arc conditions obeys Sieverts' Law.

References

4.1 G. den Ouden and O. Griebling, "Nitrogen absorption during arc welding", in Proceedings of the 2nd International Conference on Recent Trends in Welding Science and Technology, Gatlinburg (1989), 431-435.

4.2 J.W. Hooijmans and G. den Ouden, "The influence of oxygen on nitrogen absorption during arc melting of iron", Welding Journal (Welding Research Supplement) 71 (1992), 377s-380s.

4.3 J. Tsuboi, S. Nakano and K. Sato, "Behavior of hydrogen in arc welding (Report 1) - Hydrogen absorption in tungsten arc melting -", Transactions of the Japan Welding Society 5 (1974), 103-108.

4.4 G.R. Salter, "Hydrogen absorption in arc welding", British Welding Journal 10 (1963), 316-325.

4.5 J.F. Elliott, M. Gleiser and V. Ramakrishna, "Thermochemistry for steelmaking, Volume II", Reading, Massachusetts, Addison-Wesley (1963).

4.6 J.O.M. Bockris, M.A. Genshaw and M. Fullenwider, "The electro-permeation of hydrogen into metals", Electrochimica Acta 15 (1970), 47-60.

4.7 D.G. Howden and D.R. Milner, "Hydrogen absorption in arc melting", British Welding Journal 10 (1963), 304-316.

4.8 Metals Handbook, 9th edition, volume 6, ASM, Metals Park (1983).

4.9 P.G. Shewmon, Diffusion in solids, McGraw-Hill (1963), 1-19.

4.10 H.H. Johnson, "Hydrogen in iron", Metallurgical Transactions B, 19B (1988), 691-707.

4.11 J. Cranck, The mathematics of diffusion, Oxford, Clarendon (1975).

4.12 M. Uda, "A new process for preparation of ultrafine metal particles", Transactions National Research Institute for Metals 24 (1982), 218-225.

4.13 B. Chew and R.A. Willgoss, "Weld metal hydrogen absorption during TIG-welding with argon-hydrogen gas shields", in Proceedings of the International Conference on Weld Pool Chemistry and Metallurgy, London (1980), 155-165.

4.14 A. Sieverts, "Die Löslichkeit von Wasserstoff in Kupfer, Eisen und Nickel", Zeitschrift für Physikalische Chemie 77 (1911), 591-613.

4.15 I.I. Pirch, A.A. Erokhin and A.I. Pugin, "Relationships governing the absorption of hydrogen by liquid metals in arc heating", Welding Production 27 (1980), 8-11.

CHAPTER 5

Hydrogen absorption during arc welding

5.1 Introduction

In the previous chapter attention was given to hydrogen absorption during arc heating and melting of small button-like samples under stationary arc conditions.
Experiments carried out under these conditions are not of direct practical use, but have the advantage that they yield basic information about the mechanism of hydrogen absorption, which can be used when studying hydrogen absorption under arc welding conditions with a travelling arc.

The present chapter deals with hydrogen absorption during GTA welding. In GTA welding the arc moves with a constant speed (travel speed) with respect to the workpiece to be welded. This situation differs from the stationary situation described in the previous chapter in two respects:

- continuous melting (at the front side of the weld pool) and solidification (at the back side of the weld pool) occurs;
- the hydrogen absorbed by the liquid metal in the weld pool can leave not only through the surface to the gaseous surrounding, but also through the fusion boundary to the solid base metal adjacent to the weld pool.

Both phenomena play an important role and complicate the absorption mechanism as will be shown below.

The structure of this chapter is as follows.
Firstly, a description is given of the materials and equipment used and the experimental procedure followed. After this the results are presented of experiments carried out with pure iron aimed at determining the influence of the different process parameters on the hydrogen absorption. This is realized by varying each process parameter seperately, whereas the other parameters are kept constant. The welding parameters which are varied include shielding gas composition, arc current, arc length and travel speed. Also the results are presented of experiments carried out with mild steel and stainless steel. This is

followed by the presentation of the attempts (experiments and calculations) which were made to determine the initial hydrogen concentration in the weld pool. Finally, a model is developed which is used to explain the results obtained in the experiments with varying process parameters, and with which hydrogen levels in welds obtained under practical conditions can be predicted.

5.2 Experimental conditions

5.2.1 Materials

The experiments were carried out with three materials: technical pure iron (Armco), mild steel (Fe 360) and austenitic stainless steel (AISI 321), with emphasis on pure iron. The chemical compositions of the materials are given in Table 5.1.

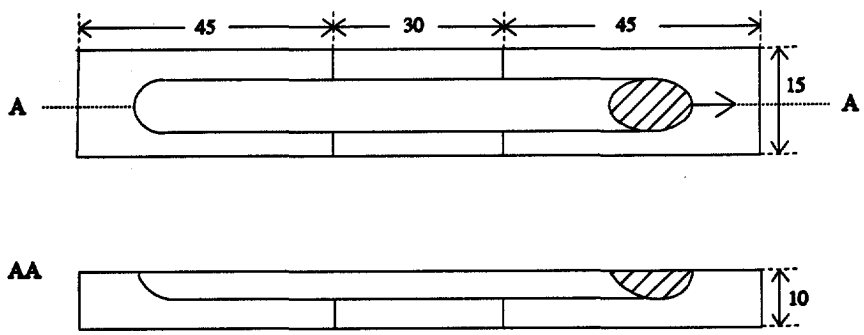

Fig. 5.1 Dimensions (mm) of the test pieces used in the experiments with travelling arc.

The shape of the workpiece was chosen to be identical to that described in the IIW procedure [5.1]. It consists of three parts, as shown in Fig. 5.1. The middle piece (test piece) has the dimensions 30 x 15 x 10 mm, the other two pieces have the dimensions 45 x 15 x 10 mm. The starting piece is used to ignite the arc on and to start the welding run. The end piece is used to terminate the welding run and to extinguish the arc. The test piece is used for the determination of the amount of hydrogen, absorbed during welding.

Table 5.1 The chemical compositions (wt.%) of the materials used.

element	pure iron Armco	mild steel Fe 360	stainless steel AISI 321
Cr	0.0179	0.015	21.1
Ni	0.013	0.02	14.3
Mo	0.005	-	2.31
C	0.026	0.47	0.029
P	0.0047	0.019	0.034
S	0.005	0.031	0.013
Si	0.0379	0.23	0.923
Al	0.0398	-	0.0855
Ti	0.00107	-	0.00071
Mn	0.031	0.67	1.60
O	0.002	1.01	0.016
N	0.001	0.004	0.002
H	0.000009	0.000022	0.000064

5.2.2 *Equipment*

The experiments were carried out under travelling arc conditions, using the equipment described in the IIW procedure [5.1]. The total setup is given in Fig. 5.2. Central part of the equipment is a copper block (see Fig. 5.3), on which the pieces to be welded were fixed with the use of two wedges. This is done to obtain an optimal heat flow away from the test piece. Above the copper block a thoria-doped tungsten electrode, having a diameter of 3.2 mm, is placed. This electrode can be moved in vertical direction to make it possible to vary the arc length. The copper block was put on a construction which could be moved with variable speed in a horizontal direction under the electrode.
The shielding gas was forced to flow along the electrode through a normal gas cup (diameter 8 mm) towards the weld. The arc welding experiments were performed in mixtures of argon (purity 99.998%) and hydrogen (purity 99.998%). These mixtures were obtained by mixing the two gases in a chamber consisting of a number of parallel plates in which small holes were drilled. The two gases to be used were brought into the chamber and were completely mixed due to the turbulent flow in the chamber.
The flow rate of all component gases was adjusted and measured using flow controllers. The flow rate of the complete mixture was adjusted to 10 l/minute. Each flow controller has an accuracy of about 1%.

Arc welding was carried out using a DC power source (ESAB DTA300). This welding machine is provided with high frequency ignition facilities, with which the arc was ignited. Arc voltage and arc current were measured continuously with a shunt and a welding monitor. Both were continuously registered by means of an x-t recorder.
The influence of the different process parameters on the hydrogen absorption was determined by varying each process parameter seperately, while the others were kept constant. The standard conditions used are listed in Table 5.2.

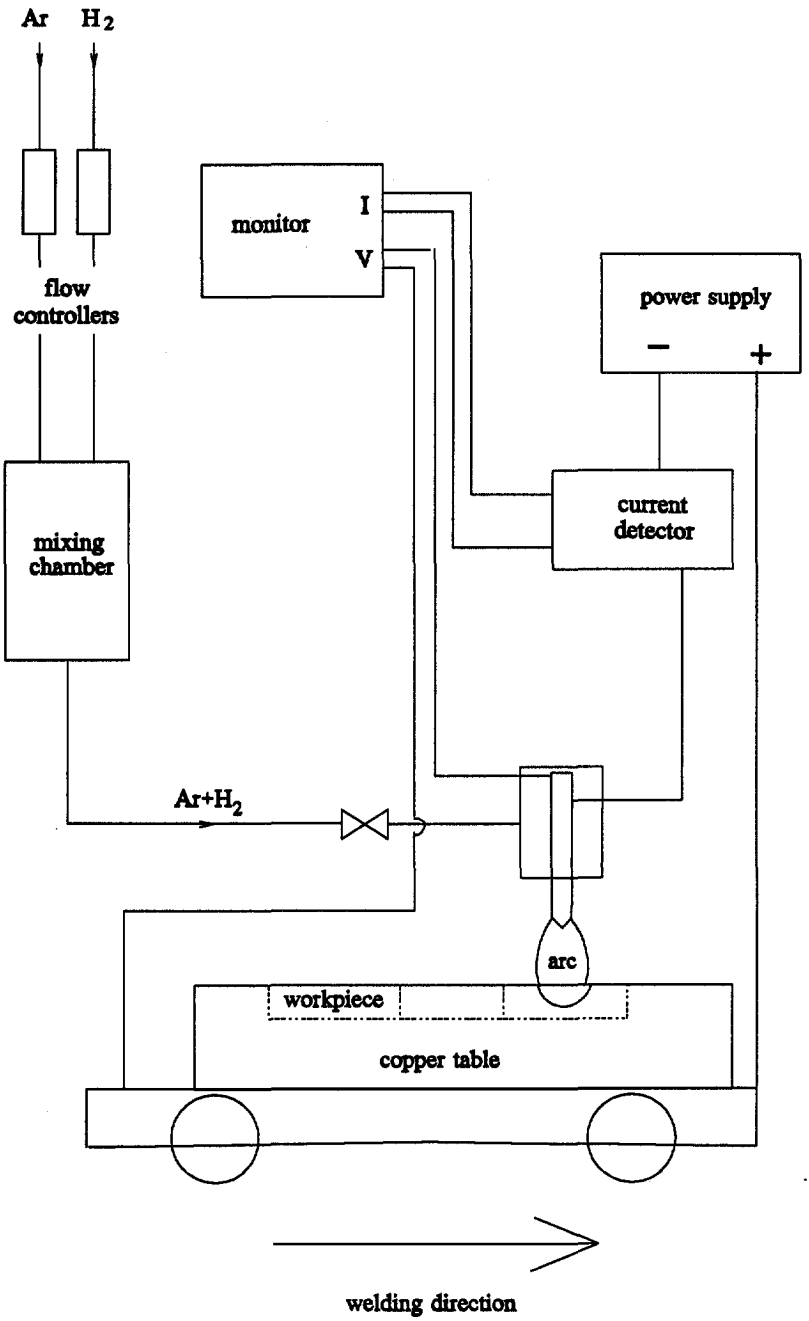

Fig. 5.2 Schematic presentation of the setup used in the experiments with travelling arc.

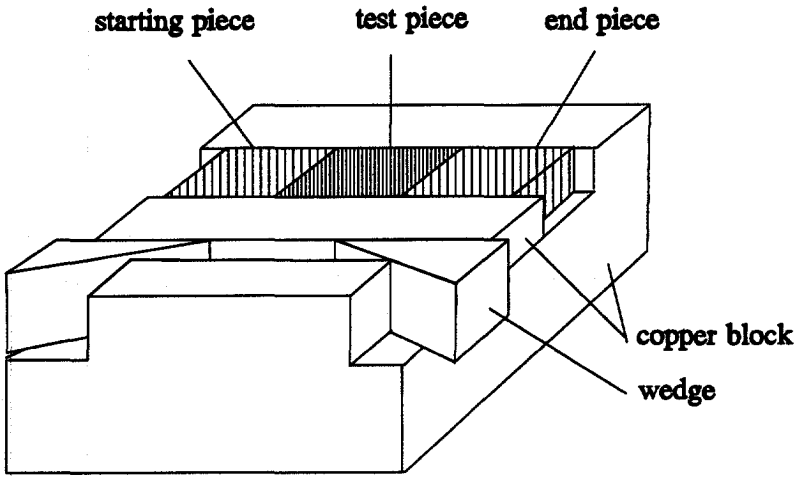

Fig. 5.3 Central part of the setup used in experiments with travelling arc (not on scale).

Table 5.2 Standard arc welding conditions.

arc current	100 A
arc voltage	13.5 V
arc length	3 mm
test piece size	30 x 15 x 10 mm
polarity	electrode negative
electrode diameter	3.2 mm
electrode top angle	60°
shielding gas composition	95% argon- 5% hydrogen
shielding gas flow rate	10 l/minute
travel speed	3.1 mm/s

5.2.3 *Experimental procedure*

In each experiment the IIW procedure was followed [5.1].
Before each experiment the copper block and the test pieces were thoroughly cleaned. The test pieces were then fixed on the copper block using two wedges. Between the copper block and the test pieces annealed copper foil was placed to facilitate the contact.
The gas with the desired ratio was allowed to flow towards the starting piece for approximately one minute, in order to remove any trace of unwanted gases from the gas tubes. After this the arc was ignited with the use of high frequency facilities and the welding run was started.
When the arc was extinguished, the workpiece (the three pieces welded together) was taken from the copper block as quickly as possible and put into water, after which it was placed into liquid nitrogen where it was kept until analysis. The time between the moment the arc left the test piece and the moment the workpiece was put in the water was about 17 seconds.

5.2.4 *Gas analysis*

To determine the amount of diffusable hydrogen in the test piece after welding the method proposed by IIW [5.1] was used. Firstly, the workpiece was taken out of the liquid nitrogen. Due to the low temperature, the material is very brittle, so the starting piece and the end piece could be separated from the test piece, which was then placed in acetone, to be warmed up to room temperature. This was done to prevent ice from covering the surface of the sample. The acetone was subsequently removed from the surface with a gas flow of cold air.
After this the test piece was put in a eudiometer filled with mercury. With a magnet the test piece was transported to the closed arm of the eudiometer. As a result of the lower density of the test piece compared to the density of the mercury, the test piece will rise to the highest possible position (see Fig. 5.4). The whole operation from taking the sample out of the liquid nitrogen to starting the measurement was performed in about 25 seconds. The time the test piece remained under mercury was 72 hours. After this time the amount of gas, which had left the sample, was measured. This was done by measuring the height of the gas column in the closed arm of the eudiometer.

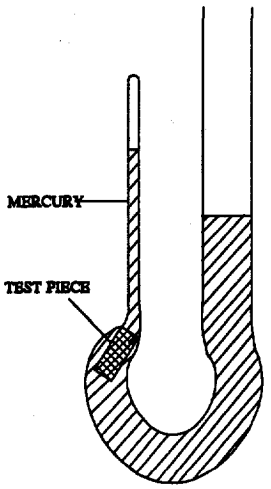

Fig. 5.4 Eudiometer used for the hydrogen measurement of welded test pieces.

5.2.5 Determination of weld geometry

The welds obtained were transversely sectioned at various locations. After grinding and polishing the cross sections up till 3 μm, they were etched with Kalling (5 g $CuCl_2$ in 100 ml ethyl alcohol and 100 ml hydrochloric acid). Kalling, which etches the grain boundaries, is used because of its capability to reveal the weld shape.
The cross section area of the weld was measured with the use of a Leica CBA 8000 image analyzing computer.

The weight of the molten metal in the test piece, used for calculating the hydrogen concentration in the weld metal, was obtained by multiplying the cross section area of the weld with the test piece length.

5.3 Hydrogen absorption measurements

In this section the results are presented of experiments dealing with the influence of various process parameters on the hydrogen absorption. Attention is focused on the influence of hydrogen partial pressure, arc current, arc length and travel speed. Also the results of measurements on two types of steel are presented and discussed.
It should be noted that the absorbed hydrogen is expressed in terms of the hydrogen concentration in the weld metal, i.e. the total weight of diffusible hydrogen in the test piece after welding (measured by means of the IIW method described in section 5.2.4), divided by the weight of the weld metal.

5.3.1 Influence of hydrogen percentage in the shielding gas on hydrogen absorption

The influence of the hydrogen percentage in the shielding gas on the hydrogen absorption was determined by carrying out experiments with different amounts of hydrogen in the argon based shielding gas (between 0 and 25 vol.%). In Fig. 5.5 the hydrogen concentration is plotted as a function of the hydrogen percentage in the shielding gas.
The figure shows that the hydrogen concentration in the weld metal increases with increasing hydrogen percentage in the shielding gas. An identical increase of the hydrogen concentration with increasing hydrogen content in the shielding gas was observed by White [5.2].
It was also observed that with increasing hydrogen percentage in the shielding gas the volume of the weld pool (transverse cross section of the weld) increases, which is consistent with the results presented in section 3.4.1. Consequently, the total amount of hydrogen in the test piece increases more strongly with increasing hydrogen percentage in the shielding gas than suggested by Fig. 5.5. The total amount of hydrogen is important in relation with the danger of hydrogen cracking (see section 2.6.2).

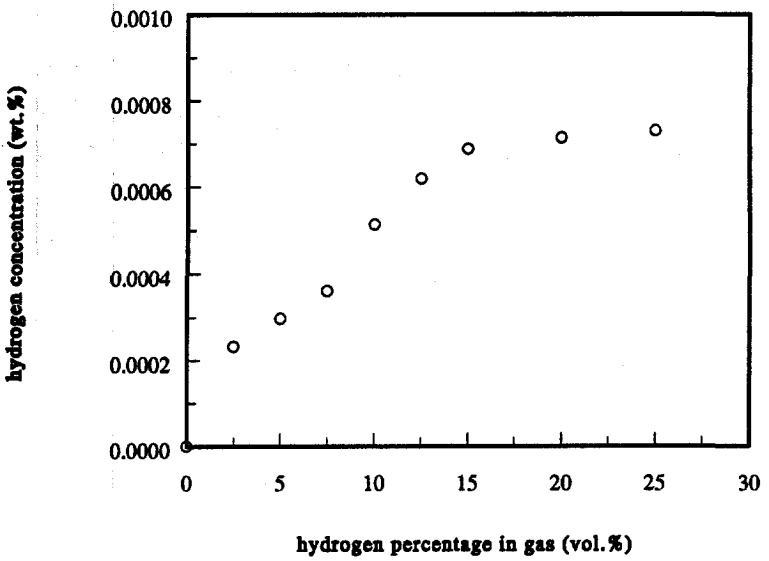

Fig. 5.5 Hydrogen concentration in the weld metal as a function of the hydrogen percentage in the shielding gas.

5.3.2 Influence of arc current on hydrogen absorption

In order to determine the influence of arc current on the hydrogen absorption, experiments were carried out for different values of arc current between 25 and 300 A. The results of these experiments are given in Fig. 5.6, in which the hydrogen concentration in the weld metal is plotted as a function of the arc current.

The figure shows that initially the hydrogen concentration increases strongly with increasing arc current. Above a value of about 125 A only a small increase in the hydrogen concentration is observed. A similar relationship for the hydrogen concentration with arc current was reported by Frolov [5.3] and Howden [5.4].

It was found that with increasing arc current also the volume of the weld pool (transverse cross section of the weld) increases. This is to be expected as the heat input is directly (linearly) related to the arc current.

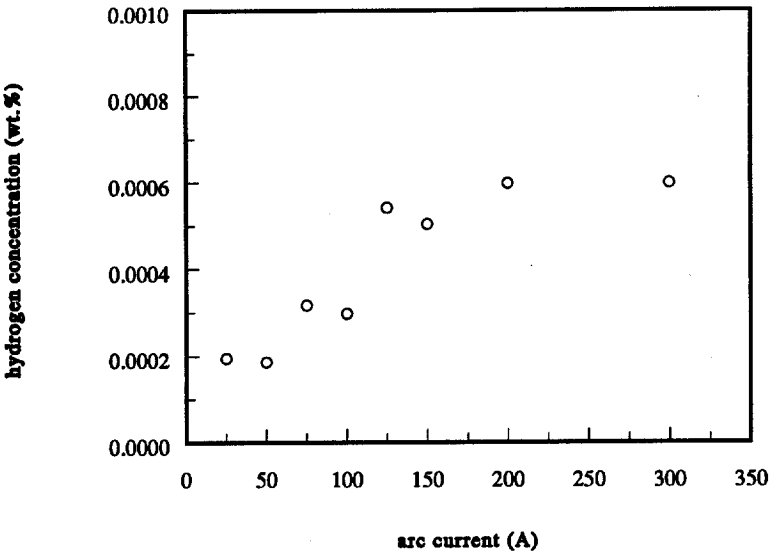

Fig. 5.6 Hydrogen concentration in the weld metal as a function of arc current.

5.3.3 Influence of arc length on hydrogen absorption

The influence of the arc length on the hydrogen absorption is demonstrated in Fig. 5.7. In this figure the hydrogen concentration in the weld metal is plotted as a function of the arc length, for arc length values between 1.5 and 6 mm.

The figure shows that the influence of the arc length on the hydrogen concentration in the weld metal, in the range of the arc length values used, is negligibly small. A similar conclusion can be drawn for the influence of the arc voltage, as arc length is linearly related to arc voltage (see section 4.3.4). Similar results were obtained by Howden [5.4]. With increasing arc length (arc voltage) the weld pool was found to increase in size, which is caused by the increase in heat input in the weld.

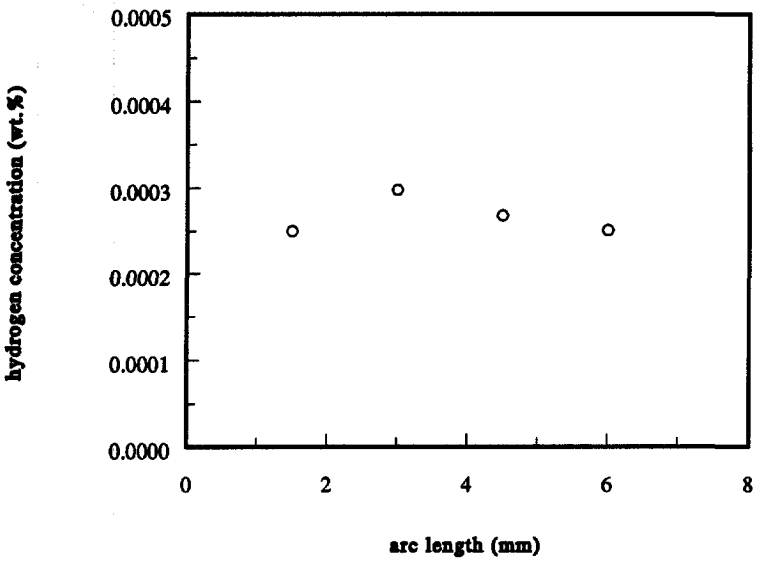

Fig. 5.7 Hydrogen concentration in the weld metal as a function of arc length.

5.3.4 Influence of travel speed on hydrogen absorption

The experiments described above were carried out with a travel speed of 3.1 mm/s. In order to determine the influence of the travel speed on the hydrogen absorption, a series of experiments was carried out with different travel speeds in the range of 2.5 to 18 mm/s. The results of these experiments are given in Fig. 5.8.

The figure shows that with increasing travel speed the hydrogen concentration in the weld metal decreases from about 0.00030 wt.% at a travel speed of 2.5 mm/s to less than about 0.00005 wt.% at a travel speed of 18 mm/s.

As expected, the weld pool volume (transverse cross section of the weld) decreases with increasing travel speed, due to the fact that with increasing travel speed the heat input in the material decreases.

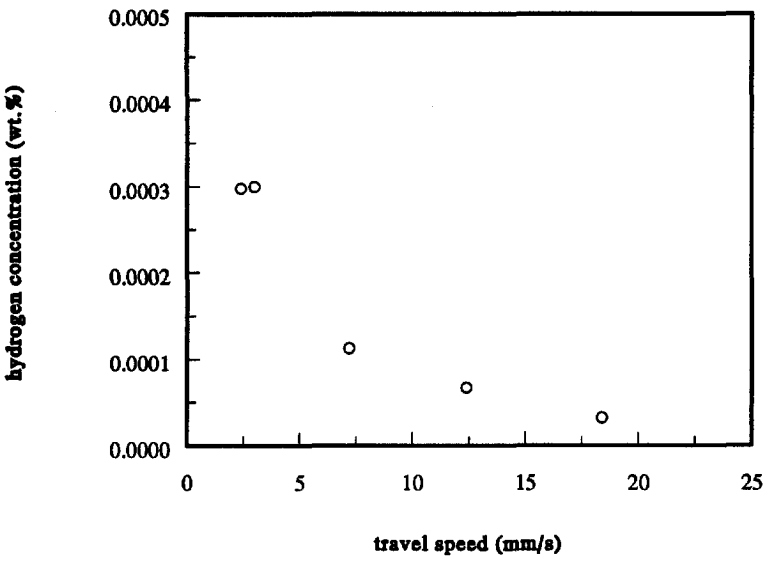

Fig. 5.8 Hydrogen concentration in the weld metal as a function of travel speed.

5.3.5 Influence of heat input on hydrogen absorption

The heat input is an important parameter in practical welding. In section 2.4.1 the heat has been defined as the quantity of energy introduced in the weld per unit length, which can be expressed by:

$$H_i = \frac{f_1 VI}{v} \tag{5.1}$$

in which H_i = heat input,

f_1 = heat transfer efficiency, the heat transferred to the workpiece per unit time divided by the power of the heat source,

V = arc voltage,

I = arc current,

v = travel speed of the heat source.

In Fig. 5.9 the influence of the heat input on the hydrogen absorption is demonstrated. For the heat input the values obtained in the experiments with different arc current and different travel speed are used. For f_1 a value of 0.7 is used [5.6].
The figure shows that the hydrogen concentration in the weld increases with increasing heat input.

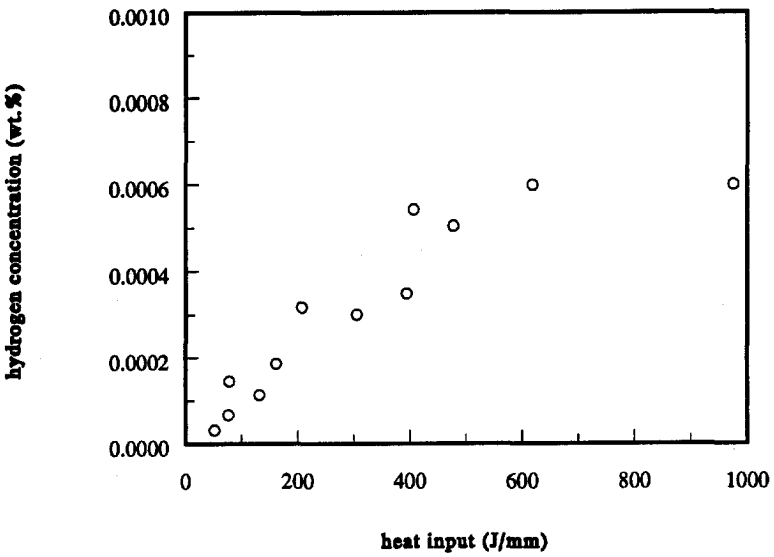

Fig. 5.9 Hydrogen concentration in the weld metal as a function of heat input.

5.3.6 Hydrogen absorption measurements on mild steel and stainless steel

In addition to the experiments carried out with pure iron, also some experiments were carried out with mild steel Fe 360 and stainless steel AISI 321. The chemical compositions of these steels are given in Table 5.1.
In Fig. 5.10 the hydrogen concentration in the weld metal is plotted as a function of the hydrogen percentage in the shielding gas for pure iron, mild steel and stainless steel. For all three materials the hydrogen concentration in the weld metal increases with increasing hydrogen in the shielding gas. Furthermore, it can be seen that more hydrogen is absorbed in stainless steel than in mild steel and pure iron. This is presumably due to the higher solubility of hydrogen in stainless steel.

The observed hydrogen absorption in stainless steel is considerably smaller than in the case of welding under stationary arc conditions (see Fig. 4.13). This is due to the fact that under travelling arc conditions only the diffusible hydrogen is measured, whereas in the case of stationary arc conditions the total amount of hydrogen, the sum of the diffusible and residual hydrogen, is determined.

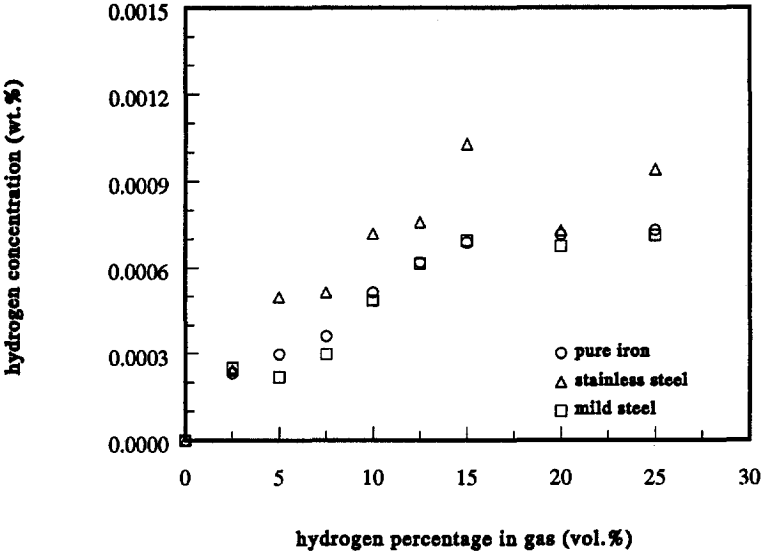

Fig. 5.10 Hydrogen concentration in pure iron, mild steel and stainless steel weld metal as a function of the hydrogen percentage in the shielding gas.

5.4 Determination of the initial hydrogen concentration

As already pointed out in the previous chapter, the amount of hydrogen measured is not equal to the amount present in the liquid metal at the moment welding is finished. In fact, a relatively large part of the hydrogen originally present in the weld will be lost between the moment the liquid metal solidifies and the moment the test piece is analyzed. In the case of welding under travelling arc conditions the hydrogen can not only escape through the surface to the surrounding (the only escape possibility in the case of the stationary experiments dealt with in Chapter 4), but also through the fusion boundary to the solid metal adjacent to the weld pool.

It is evident that the amount of hydrogen which leaves the test piece is dependent on the

diffusion coefficient, which in turn is dependent on the temperature, and on the weld shape. The amount which will be lost can be relatively large, due to the high diffusion rate of hydrogen in iron, especially at high temperature [5.5].
As stated before, the initial hydrogen concentration (i.e. the hydrogen concentration in the liquid weld metal) is a much more important quantity than the measured hydrogen concentration. In fact, it is the initial hydrogen concentration, rather than the measured hydrogen concentration, on which explanations and modelling should be based.

In view of this, attempts were made to obtain the initial hydrogen concentration from the measured hydrogen concentration. Two approaches were followed:

- an experimental approach (extrapolation of measured values to zero test piece size and to zero cooling time);
- calculation from the measured values using a finite element method.

5.4.1 Experimental estimation of the initial hydrogen concentration

Hydrogen redistribution in the material
As mentioned above, part of the hydrogen absorbed in the weld metal during the welding process escapes in the course of time to the solid metal adjacent to the weld pool. This will lead to a gradual redistribution of the hydrogen in the test piece. In order to estimate the effect of this redistribution, an experiment was carried out using the test plate configuration shown in Fig. 5.11.
The test plate is composed of 15 pieces (5 rows of 3 pieces), partly separated from each other by a shallow groove (2 mm) at the bottom side. The pieces have the same dimensions as those used in the standard experiments.
The test plate was placed on the copper block. A welding run was made over the central pieces of the test plate, using the standard process conditions given in Table 5.2. Immediately after welding the plate was put into water and subsequently stored in liquid nitrogen. Due to the cooling to -196°C the plate becomes brittle and could easily be broken into separate pieces.
The hydrogen concentration in each piece (the amount of hydrogen divided by the weight of the piece) was measured using the IIW mercury method described in section 5.2.4. The results are given in Table 5.3. The values given show that almost all hydrogen remains in the central pieces and that only a very small part of the hydrogen diffuses from the central pieces to the adjacent side pieces.

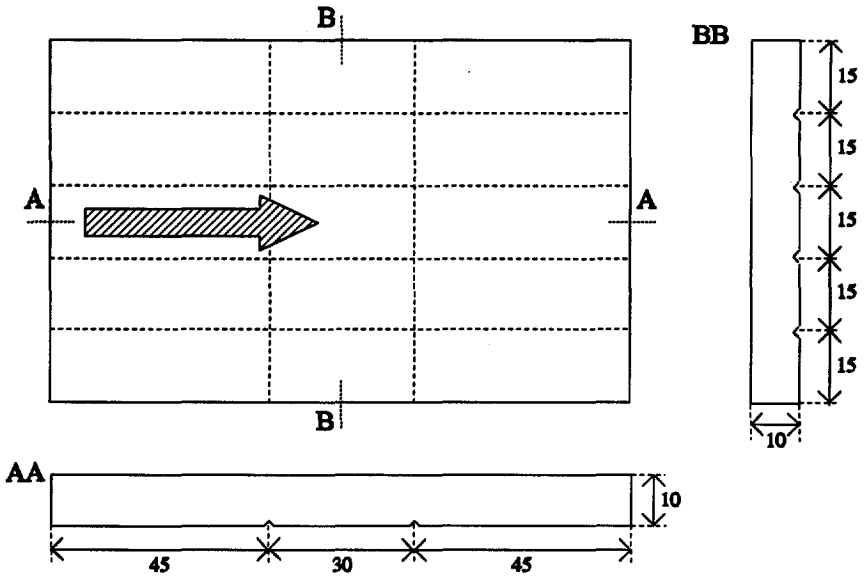

Fig. 5.11 Test plate configuration (mm) used to estimate the hydrogen redistribution after welding. The direction of welding is indicated by the arrow.

Table 5.3 The hydrogen concentration (wt.%) in the different parts of the test plate.

0.000002	0.000003	0.000002
0.000002	0.000002	0.000003
0.000021	0.000033	0.000025
0.000004	0.000004	0.000002
0.000000	0.000004	0.000001

Influence of test piece size

During welding of the test piece, hydrogen in the solidified weld metal starts to diffuse to the surroundings. The amount of hydrogen leaving the weld metal in this way depends on the size of the test piece. An indication of the hydrogen concentration in the liquid weld metal (the initial hydrogen concentration) can be obtained by extrapolation of the hydrogen concentration values obtained for different test piece sizes.

Welding experiments were carried out with test pieces of different size (length in welding direction) using the standard process parameters listed in Table 5.2. After each experiment the test piece was put into water as quickly as possible, i.e. within about 17 seconds. The hydrogen concentration in each test piece was measured using the IIW mercury method (see section 5.2.4).

The results are given in Fig. 5.12, from which it can be seen that the hydrogen concentration decreases with test piece size. Extrapolation of the experimental data to zero test piece size yields a value of about 0.0004 wt.% for the hydrogen concentration in the weld metal. However, it must be realized that this value does not include the hydrogen which leaves the test piece between the moment the welding is completed and the moment the test piece is put into water.

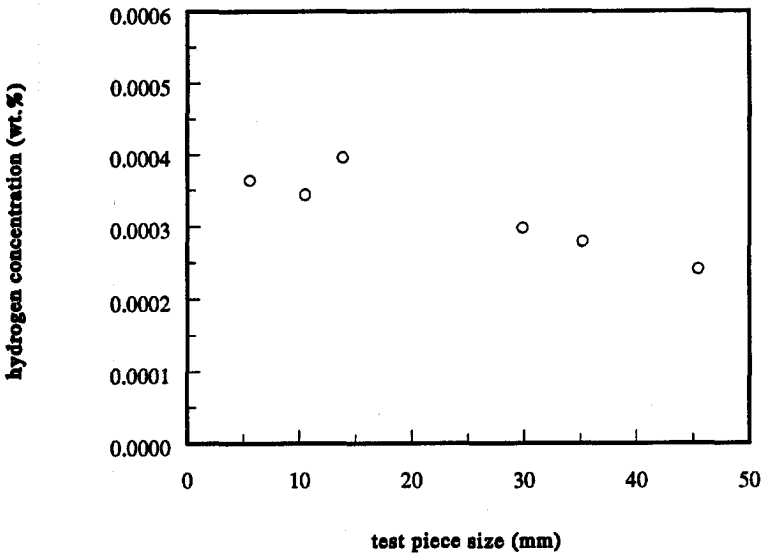

Fig. 5.12 Hydrogen concentration in the weld metal as a function of test piece size.

Influence of cooling time

Experiments were performed, in which the hydrogen concentration in the weld metal was measured as a function of cooling time (the time between the moment the arc leaves the test piece and the moment the workpiece is put in water). Extrapolation of the obtained values to zero cooling time gives information about the hydrogen concentration in the weld metal during welding.

In Fig. 5.13 the hydrogen concentration in the weld metal is plotted as a function of cooling time for two different test piece sizes (10 and 30 mm).

The results obtained show that reduction of the cooling time leads to a higher hydrogen concentration in the weld metal. This was expected, as with shorter cooling time less hydrogen will diffuse out of the test piece. During the first seconds of cooling a large part of the hydrogen leaves the sample. Unfortunately, extrapolation to zero cooling time is unreliable due to the lack of results obtained at short cooling times.

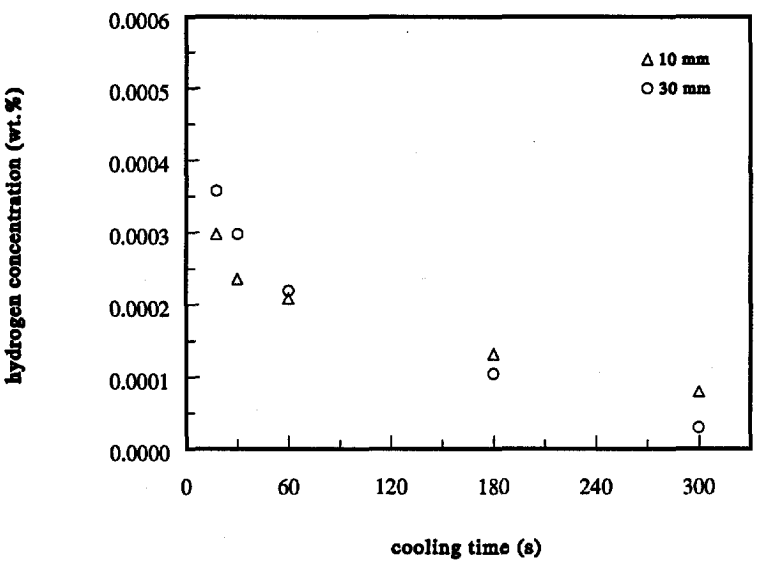

Fig. 5.13 Hydrogen concentration in the weld metal for two test piece sizes as a function of cooling time.

Theoretically speaking, a combination of the extrapolations to zero test piece size and to zero cooling time should yield the hydrogen concentration in the weld pool during welding (initial hydrogen concentration).
However, this approach does not lead to accurate results, especially due to the lack of data at short cooling times. In view of this, no further attempts were made to continue the experimental approach. Instead, attention was focussed on determining the initial hydrogen concentration by means of calculation.

5.4.2 Calculations of the initial hydrogen concentration

Calculation of the initial hydrogen concentration in the weld metal was carried out numerically with the help of a finite element program using the measured amount of hydrogen in the test piece as input data. The principle of this calculation method was described in section 4.4.2 and the method was successfully applied for arc welding under stationary (non-travelling) arc conditions. Basis of the calculation is the diffusion of hydrogen through the material, governed by Fick's First and Second Law of diffusion (see Eqs. (4.1) and (4.2)).
Application of the calculation method in the case of welding under travelling arc conditions is more difficult due to the non stationary process conditions.

In order to be able to carry out the calculations, a number of assumptions must be made. These assumptions are formulated below.

- The escape of hydrogen from the test piece during the moment the liquid metal solidifies and the moment the test piece is put into water is regarded as a two-dimensional diffusion problem. This can be justified by the fact that the travel speed of the arc is much greater than the rate of the hydrogen diffusion.
  Thus, the test piece can be considered as a series of slices in each of which the hydrogen diffuses only in a plane normal to the welding direction. The hydrogen concentration in the total test piece was taken to be the average of the hydrogen concentrations in the different slices of the material.
- The area of the transverse cross section of the weld has the form of a perfect half ellipse. The elliptical shape of the weld is in good agreement with the true shape observed during welding under practical conditions.

- The diffusion coefficient of hydrogen in the material is constant ($1 \cdot 10^{-4}$ mm^2/s) during the entire cooling period. This assumption can be justified with the help of Fig. 5.14 and Fig. 5.15.

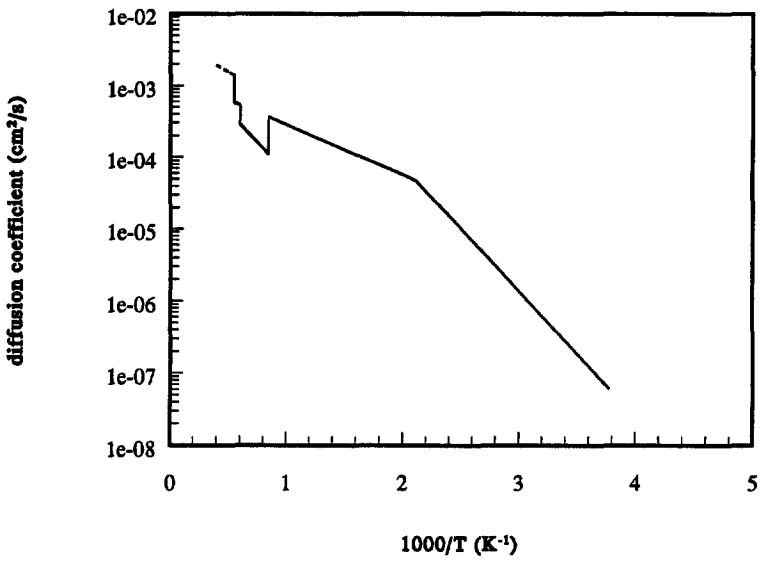

Fig. 5.14 Diffusion coefficient of hydrogen in pure iron as a function of temperature.

In Fig. 5.14 the diffusion coefficient of hydrogen in pure iron is given as a function of temperature, whereas in Fig. 5.15 the hydrogen left in the test piece (percentage of the hydrogen originally present) is plotted as a function of the diffusion coefficient.

It is evident that more accurate results would be obtained when temperature dependent values of the diffusion coefficient would be used in the calculations. Unfortunately, however, insufficient knowledge is available about the change of the temperature profile in the material during the cooling period [5.6,5.7].

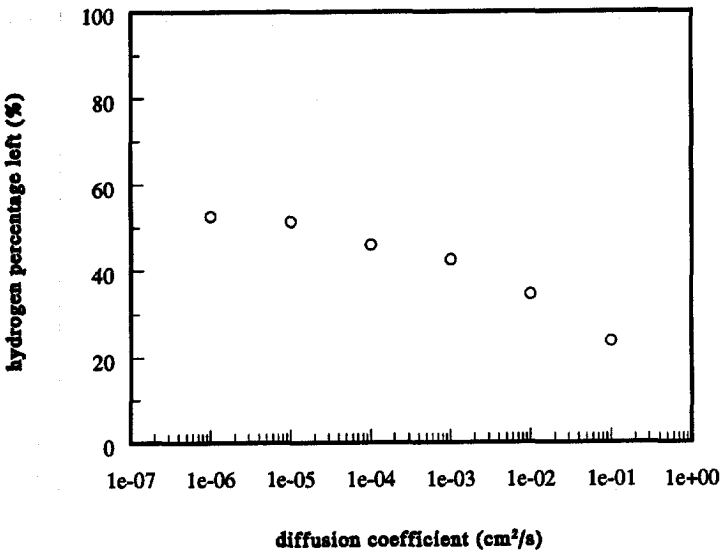

Fig. 5.15 Hydrogen left in the material (percentage of the hydrogen originally present) after cooling of the test piece as a function of the diffusion coefficient.

- No bubble formation occurs during the entire welding process.
- At the moment the weld solidifies, the hydrogen is evenly distributed over the weld (no concentration gradient), while in the surrounding material of the same slice no hydrogen is present.
- The hydrogen which reaches the surface of the test piece in atomic form will immediately recombine and disappear into the surrounding atmosphere.

Using the assumptions formulated above a finite element calculation program was developed [5.8]. In this approach the sample is divided in small slices (see Fig. 5.16).

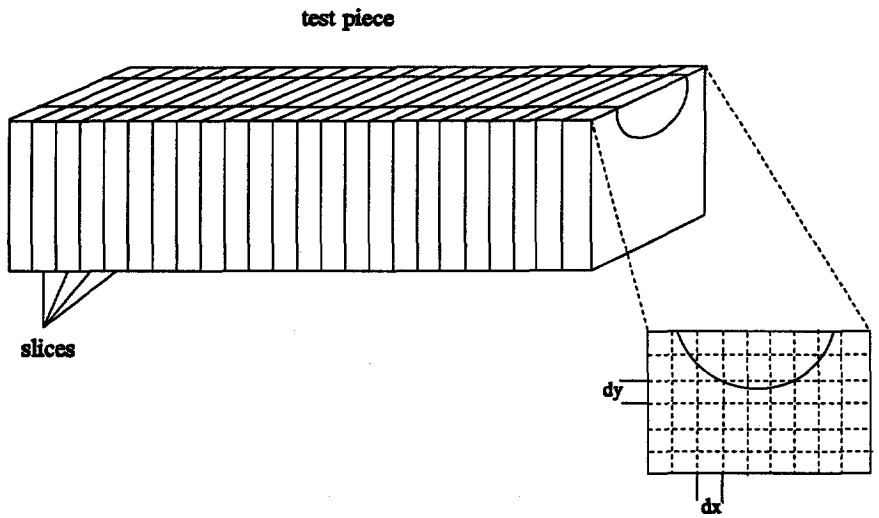

Fig. 5.16 Division in slices and segments of the test piece used for the numerical calculations of the initial hydrogen concentration.

The change in hydrogen concentration with time is calculated for each of the segments in distinct time steps. The used equation can be written as:

$$\frac{c_{i,j,n+1} - c_{i,j,n}}{\delta t} = \frac{D}{(\delta x)^2}\left(c_{i-1,j,n} - 2c_{i,j,n} + c_{i+1,j,n}\right) + \frac{D}{(\delta y)^2}\left(c_{i-1,j,n} - 2c_{i,j,n} + c_{i+1,j,n}\right) \qquad (5.2)$$

in which c = concentration,
δt = length of the time step,
D = diffusion coefficient,
δx = segment size in the x-direction,
δy = segment size in the y-direction,
i = rank number of the segment in the x-direction,
j = rank number of the segment in the y-direction,
n = rank number of the time step.

The time step and the segment size are limited by the diffusion coefficient. This method is computationally straightforward, but has a stability restriction which can be expressed by the equation:

$$D\left(\frac{1}{(\delta x)^2}+\frac{1}{(\delta y)^2}\right)\delta t \leq \frac{1}{2} \tag{5.3}$$

5.4.3 Justification of the calculation approach

To verify the validity of the calculation approach as described in the previous section, calculations were carried out of the initial hydrogen concentration for different values of the test piece size and for different values of the cooling time, using the experimental results given in Fig. 5.12 and Fig. 5.13 as input data.

In Fig. 5.17 the measured and the initial hydrogen concentration are plotted as a function of cooling time for a test piece of 30 mm. The measured hydrogen concentration decreases with increasing cooling time, whereas the initial hydrogen concentration remains virtually constant at a value of about 0.0007 wt.%.

In Fig. 5.18 the measured and the initial hydrogen concentration are plotted as a function of test piece size. The measured concentration decreases slightly with increasing test piece size, whereas again the initial hydrogen concentration remains constant at a value of about 0.00075 wt.%.

The fact that the calculated initial hydrogen concentration is practically independent both of the cooling time and the test piece size confirms the validity of the calculation method used.

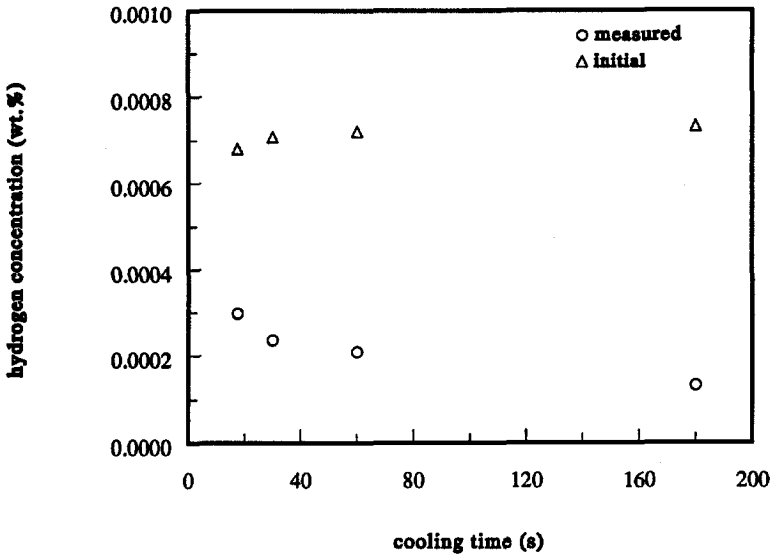

Fig. 5.17 Measured and initial hydrogen concentration in the weld pool using a test pieces size of 30 mm as a function of cooling time.

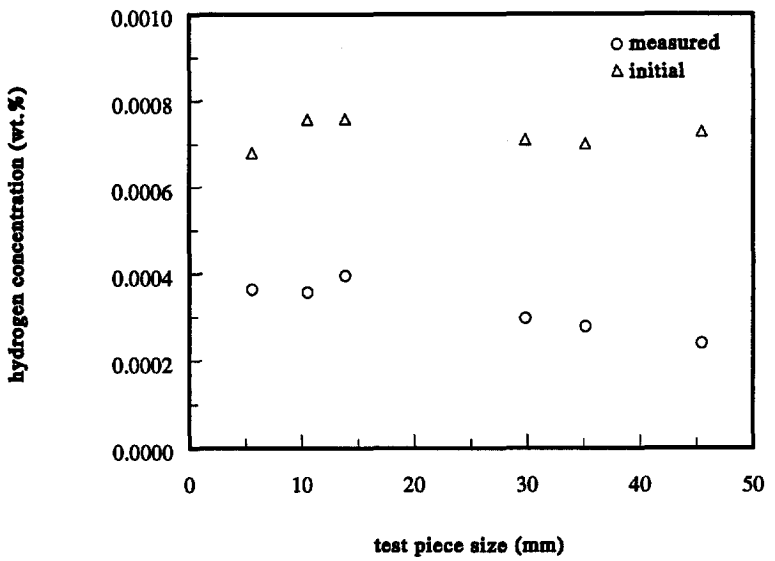

Fig. 5.18 Measured and initial hydrogen concentration in the weld pool as a function of test piece size.

5.4.4 *Calculation of the hydrogen concentration profile in the test piece during cooling*

In order to obtain insight in the hydrogen distribution within the test piece as a function of cooling time, hydrogen concentration profiles in the test piece were calculated for different moments after the onset of cooling. Some of the results obtained are presented in Fig. 5.19. In this figure the profiles at four different moments (10, 20, 40 and 60 seconds after the onset of cooling) are plotted in the form of iso-concentration lines, which connect points of identical hydrogen concentration. The initial hydrogen concentration in the weld pool is taken as 100% and the fusion boundary is presented by a thick line.
The figure shows that in a very short time after the onset of cooling most hydrogen in the vicinity of the weld pool surface has left the test piece, and the hydrogen concentration is maximal near the bottom of the weld pool. With increasing time available for diffusion, the hydrogen will gradually be further dispersed through the test piece. This is also illustrated in Fig. 5.22, in which the hydrogen left in the test piece (percentage of the hydrogen originally present) is plotted as a function of the cooling time.

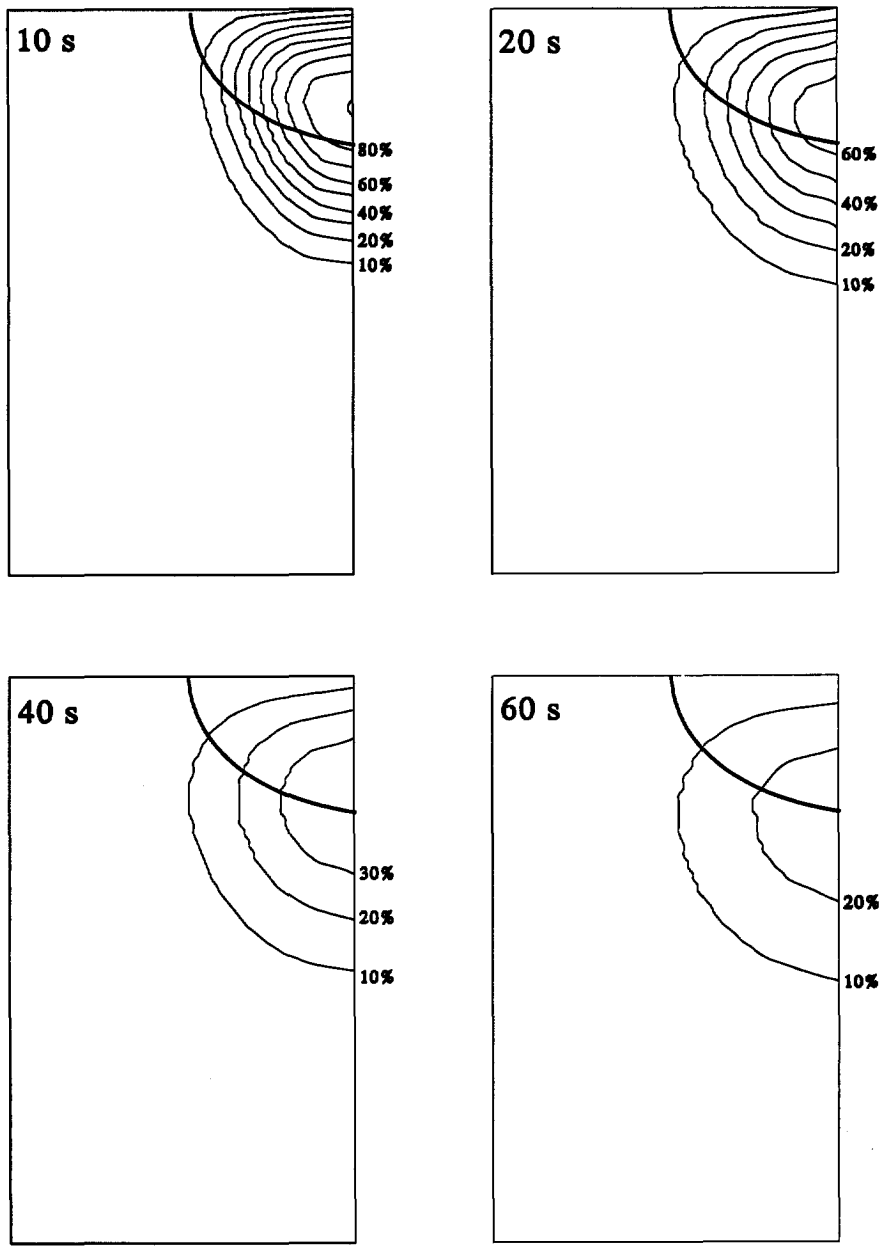

Fig. 5.21 Profiles of the hydrogen concentration in the test piece at different moments after the onset of cooling. The initial hydrogen concentration is taken as 100%. The fusion boundary is represented by a thick line.

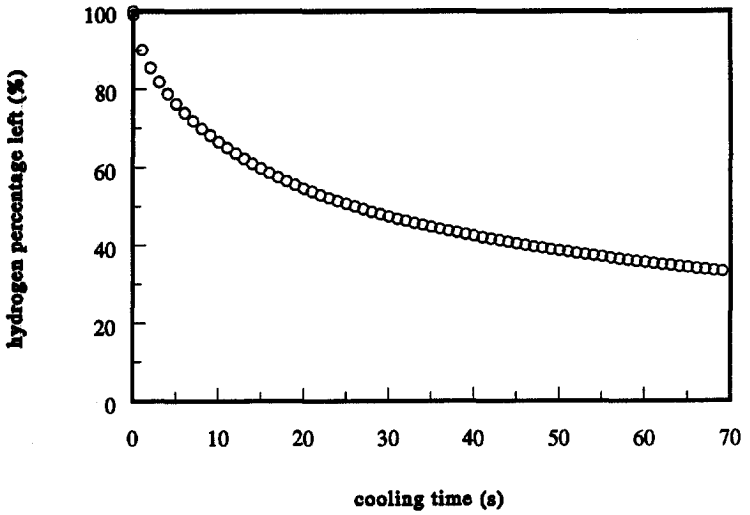

Fig. 5.22 Hydrogen left in the test piece (percentage of the hydrogen originally present) plotted as a function of the cooling time.

5.5 Influence of hydrogen percentage in the shielding gas on initial hydrogen concentration

In section 5.3.1 experiments were described which were carried out to determine the influence of the hydrogen percentage in the shielding gas on the hydrogen absorption by the liquid metal. The results of these experiments are shown in Fig. 5.23. In this figure the measured values together with the initial values of the hydrogen concentration in the weld pool are plotted as a function of the hydrogen percentage in the shielding gas.

The figure demonstrates that the measured hydrogen concentration increases initially with increasing hydrogen percentage in the shielding gas and reaches a saturation value above about 15 vol.% hydrogen, whereas the initial hydrogen concentration increases without reaching a saturation value.

The difference in shape of both curves can be attributed to the increase in ratio between the free surface and the volume of the weld with increasing hydrogen percentage in the shielding gas (see section 5.4.4).

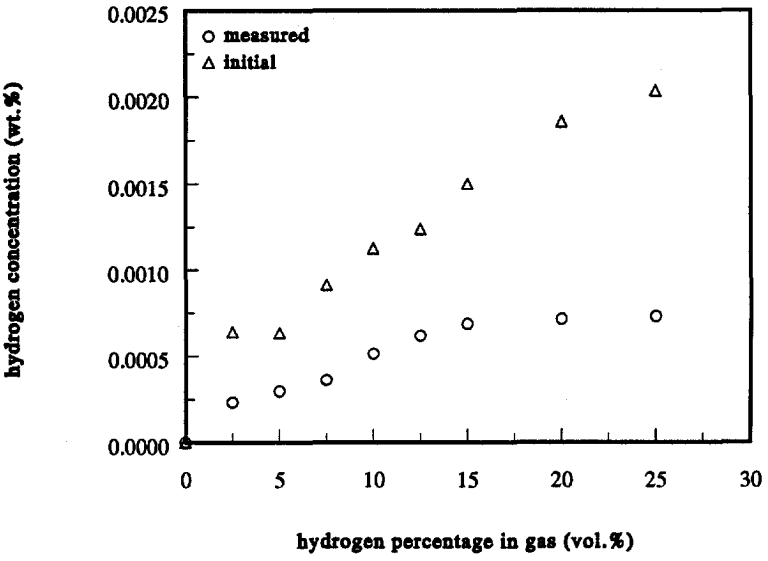

Fig. 5.23 Measured and initial hydrogen concentration in the weld as a function of the hydrogen percentage in the shielding gas.

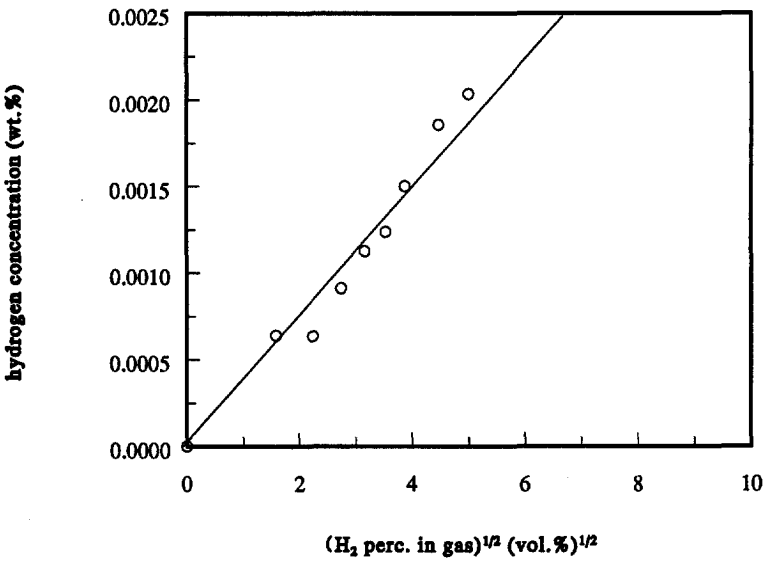

Fig. 5.24 Initial hydrogen concentration in the weld pool as a function of the square root of the hydrogen percentage in the shielding gas.

In Fig. 5.24 the initial hydrogen concentration in the weld pool is plotted as a function of the square root of the hydrogen percentage in the shielding gas. The figure shows that, as in the case of stationary arc welding (see section 4.7.1), Sieverts' Law is also obeyed under travelling arc conditions.

5.6 Modelling of the hydrogen absorption process

Arc welding of a material in a hydrogen containing atmosphere under travelling arc conditions can be modelled in a similar way as for arc welding under stationary arc conditions (see section 4.5). Basis of the model is the assumption that the hydrogen concentration in the weld pool is the result of two mutually independent processes: inflow of hydrogen and outflow of hydrogen (see Fig. 5.25).

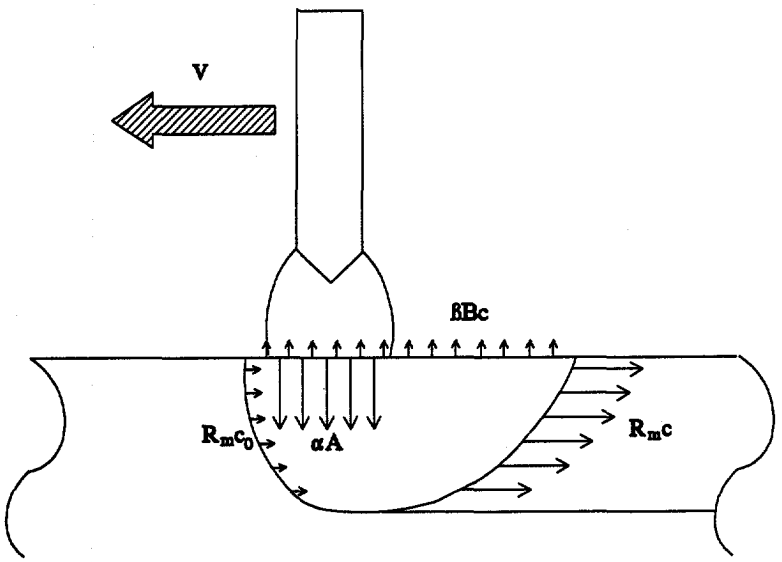

Fig. 5.25 Schematic representation of the absorption process.

- Inflow of hydrogen takes place through the interface between the arc and the liquid metal, the inflow rate being determined by the arc conditions (notably the partial pressure of the hydrogen in the arc and the temperature of the arc). A second source is the hydrogen which enters the weld pool due to melting of the material in front of the weld pool. However, the amount of hydrogen entering the weld pool in this way is relatively small, due to the very low solubility of hydrogen in iron at room temperature.
- Outflow of hydrogen takes place through the entire surface of the liquid metal (including that part of the surface which is covered by the arc), the outflow rate being proportional to the hydrogen concentration in the liquid metal. Because the diffusion coefficient of hydrogen in iron at high temperature is quite high, not only the outer surface of the weld pool must be taken into account, but also the fusion boundary where molten metal is in contact with the solid metal. In addition to the hydrogen leaving the weld pool through the outer surface and the fusion boundary, hydrogen also leaves the weld pool by solidification of the liquid metal in which it is dissolved.

On this basis, the time dependent change of the hydrogen concentration in the liquid weld metal can be described by the equation:

$$\frac{dH}{dt} = W\frac{dc}{dt} = \alpha A - \beta Bc + R_m c_0 - \eta R_m c \qquad (5.4)$$

in which H = amount of hydrogen present in the liquid metal,
t = time,
W = weight of the liquid metal in the weld pool,
c = hydrogen concentration in the liquid metal,
α = absorption coefficient (amount of hydrogen entering the liquid metal per unit area per unit time),
A = interface area between arc and liquid metal,
β = desorption coefficient (a proportionality factor depending on the temperature of the liquid metal),
B = interface area between liquid metal and surrounding gas atmosphere,
R_m = melting rate (amount of metal which melts per unit time), being equal to the solidification rate (amount of metal which solidifies per unit time),
c_0 = original hydrogen concentration in the material,
η = constant representing the fraction of the hydrogen which is frozen in during solidification.

The hydrogen entering the weld pool consists of two parts: the hydrogen absorbed under the arc, represented by the term αA, and the hydrogen which enters the weld pool due to the melting of the material, represented by the term $R_m c_0$.
The hydrogen leaving the weld pool also consists of two parts: the hydrogen disappearing from the weld pool due to solidification, represented by the term $\eta R_m c$, and the hydrogen leaving the material through the upper surface of the weld, represented by the term βBc. Actually, Eq. (5.4) should also contain a term representing the hydrogen leaving the weld pool by diffusion through the fusion boundary to the solid base material. However, this term is negligibly small with respect to the term βBc and for this reason has been omitted.

The solution of differential Eq. (5.4) can now be written as:

$$c(t) = \frac{\alpha A + R_m c_0}{\beta B + \eta R_m} \left[1 - \exp\left(\frac{-(\beta B + \eta R_m)}{W} t\right)\right] \tag{5.5}$$

After sufficiently long time an equilibrium situation is achieved and the hydrogen concentration reaches a saturation value, c_s, which can be expressed as:

$$c_s = \frac{\alpha A + R_m c_0}{\beta B + \eta R_m} \tag{5.6}$$

By substitution of:

$$R_m = vs\rho \tag{5.7}$$

in which R_m = melting rate (amount of metal which melts per unit time), being equal to the solidification rate (amount of metal which solidifies per unit time),

v = travel speed,

s = surface area of the weld cross section,

ρ = density of the material.

and taking η=1 (no hydrogen bubble formation occurs during solidification) and c_0=0 (c_0 is smaller than 0.00001 wt.%), one finally obtains the equation:

$$c_s = \frac{\alpha A}{\beta B + vs\rho} \tag{5.8}$$

With the help of Eq. (5.8) it is possible to predict the hydrogen concentration in the liquid metal for any given situation. However, to make this possible the quantities A, B, α, ß, v and s should be known. Values of A, B, v and s can be measured directly, whereas values of α and ß can be obtained from the results of the stationary arc welding experiments described in section 4.7.

5.7 Evaluation of the feasibility of the model

In the previous section a model was developed which describes the absorption of hydrogen in the liquid weld metal during welding under travelling arc conditions.
Basic feature of the model is that under equilibrium conditions the inflow of hydrogen into the liquid metal equals the outflow of hydrogen from the liquid metal.
The essential parameters of the model are the absorption coefficient α, the desorption coefficient ß, the interface area between the arc and the liquid metal A, the interface area between the liquid metal and the surrounding atmosphere B, the surface area of the weld cross section s and the travel speed v.

In order to test the feasibility of this model, values of the saturation concentration c_s were determined for each of the following process parameters (the other parameters having the standard values listed in Table 5.2):

- hydrogen percentage in the shielding gas (5, 10 and 20 vol.%),
- arc current (100, 200 and 300 A),
- arc length (1.5, 3 and 6 mm) and
- travel speed (3, 7 and 18 mm/s).

The results are presented in Tables 5.4-5.7. In these tables values of the various model parameters and of c_s (model) and c_s (initial) are listed.
The tables show that good agreement exists between the values of c_s (model) and c_s (initial) for all cases examined. This implies that the model is valid for a relatively wide range of experimental conditions and that it can be used to predict the initial hydrogen level in welds produced under realistic welding conditions.

Table 5.4 Values of various model parameters and of c_s (model) and c_s (initial) for different shielding gas compositions.

H_2 (vol.%)	α (g/sm^2)	ß (g/sm^2)	αA (g/s)	ßB (g/s)	vsρ (g/s)	c_s model (wt.%)	c_s initial (wt.%)
5	28	$2.6x10^3$	$2.9x10^{-4}$	0.11	0.36	$6.2x10^{-4}$	$6.4x10^{-4}$
10	38	$3.0x10^3$	$8.7x10^{-4}$	0.19	0.48	$13.0x10^{-4}$	$11.3x10^{-4}$
20	46	$3.8x10^3$	$13.7x10^{-4}$	0.31	0.57	$15.6x10^{-4}$	$18.6x10^{-4}$

Table 5.5 Values of various model parameters and of c_s (model) and c_s (initial) for different arc currents.

I (A)	α (g/sm^2)	ß (g/sm^2)	αA (g/s)	ßB (g/s)	vsρ (g/s)	c_s model (wt.%)	c_s initial (wt.%)
100	28	$2.6x10^3$	$2.9x10^{-4}$	0.11	0.36	$6.2x10^{-4}$	$6.4x10^{-4}$
200	31	$6.7x10^3$	$9.4x10^{-4}$	0.38	0.48	$10.9x10^{-4}$	$10.9x10^{-4}$
300	34	$9.1x10^3$	$15.5x10^{-4}$	0.66	0.61	$12.2x10^{-4}$	$14.8x10^{-4}$

Table 5.6 Values of various model parameters and of c_s (model) and c_s (initial) for different arc lengths.

l (mm)	α (g/sm^2)	ß (g/sm^2)	αA (g/s)	ßB (g/s)	vsρ (g/s)	c_s model (wt.%)	c_s initial (wt.%)
1.5	28	$1.8x10^3$	$2.2x10^{-4}$	0.05	0.29	$6.5x10^{-4}$	$7.6x10^{-4}$
3	28	$2.6x10^3$	$2.9x10^{-4}$	0.11	0.36	$6.2x10^{-4}$	$6.4x10^{-4}$
6	25	$3.0x10^3$	$3.6x10^{-4}$	0.18	0.46	$5.6x10^{-4}$	$6.5x10^{-4}$

Table 5.7 Values of various model parameters and of c_s (model) and c_s (initial) for different travel speeds.

v (mm/s)	α (g/sm^2)	ß (g/sm^2)	αA (g/s)	ßB (g/s)	vsρ (g/s)	c_s model (wt.%)	c_s initial (wt.%)
3	28	$2.6x10^3$	$2.9x10^{-4}$	0.11	0.36	$6.2x10^{-4}$	$6.4x10^{-4}$
7	28	$2.6x10^3$	$1.5x10^{-4}$	0.05	0.60	$2.3x10^{-4}$	$3.7x10^{-4}$
18	28	$2.6x10^3$	$0.9x10^{-4}$	0.03	0.64	$1.3x10^{-4}$	$1.6x10^{-4}$

5.8 Conclusions

In this chapter the results are presented of experiments dealing with the hydrogen absorption during welding of iron and steel under travelling arc conditions.
The results obtained lead to the following conclusions.

- The hydrogen concentration depends on the process parameters: it increases with hydrogen percentage in the shielding gas, arc current and heat input, decreases with travel speed and is independent of arc length.
- A large part of the hydrogen leaves the test piece during cooling. The initial hydrogen concentration in the weld pool can be calculated with the help of a finite element program.
- Hydrogen absorption under travelling arc conditions obeys Sieverts' Law.
- The absorption process during travelling arc welding can be described in terms of a model similar to the model developed for hydrogen absorption during stationary arc welding. The model is valid for a relatively wide range of experimental conditions and can be used to predict the initial hydrogen level in welds produced under realistic welding circumstances.

References

5.1 International Institute for Welding, Document II-1155-91 (1991).

5.2 D.R. White, "In process measurements of hydrogen in welding", Construction Engineering Research Labatory, CERL-TM-M-86/15 (1986).

5.3 V.V. Frolov and V.Y. Suvorin, "Behaviour of hydrogen in a welding arc discharge", Welding Production 15 (1968), 5-10.

5.4 D.G. Howden, "Behavior of hydrogen in arc weld pools", in Proceedings of the International Conference on weld pool chemistry and metallurgy, London (1980), 205-215.

5.5 E.W. Johnson and M.L. Hill, "The diffusivity of hydrogen in alpha iron", Transactions of the Metallurgical Society AIME 218 (1960), 1104-1112.

5.6 G. den Ouden, Lastechnologie, Delft, Delftse Uitgevers Maatschappij (1987), 85-89.

5.7 Welding Handbook, 7th edition, volume 1: "Fundamentals of welding", Miami, Florida, American Welding Society (1976).

5.8 J. Crank, The mathematics of diffusion, Oxford, Claredon (1975).

Summary

In this thesis the results are presented of a study dealing with the absorption of hydrogen in iron and steel during gas tungsten arc welding. Generally speaking, hydrogen has a detrimental effect on the mechanical properties of iron and steel (pore formation and hydrogen-induced cracking) and, hence, fundamental insight in the absorption process is of vital importance.

After a general introduction and a discussion of the behaviour of hydrogen in metals and of the arc welding process, attention is directed to the influence of hydrogen addition to the argon shielding gas on the welding arc and the weld pool geometry. This is relevant because both the arc and the weld pool geometry are related to the amount of hydrogen absorbed.
It appears that the optical appearance of the arc changes with addition of hydrogen to the shielding gas, the most important change being contraction of the arc. This effect is the result of the changes in the temperature and the temperature distribution in the arc. Furthermore, the contact area between the arc and the liquid metal increases with hydrogen percentage in the shielding gas.
The arc voltage increases with hydrogen partial pressure. This increase in arc voltage can be attributed to an increase in electrical field strength, due to the higher thermal conductivity of hydrogen compared to that of argon.
The addition of hydrogen to the shielding gas results in a larger heat input in the weld pool and in an increase in the melting efficiency. In the case of pure iron this leads to an increase in both the weld width and the weld depth. In the case of mild steel and stainless steel the extra heat input leads primarily to an increase in weld depth. The difference between the weld pool shapes of stainless steel, mild steel and pure iron can be attributed to the fluid flow in the weld pool. With stainless steel and mild steel this flow is directed inward, resulting in a deep narrow weld, while with pure iron fluid flow is of minor importance.
Above a critical hydrogen level in the shielding gas, pore formation starts to occur in the weld pool. This critical hydrogen level depends on material composition and welding conditions.

In order to obtain information about the hydrogen absorption process, experiments were carried out under stationary arc welding conditions. Small samples of iron and steel were

completely molten using a gas tungsten arc in a hydrogen containing argon shielding gas under different process conditions.

It was found that the hydrogen saturation concentration in the sample is reached within a relatively short time. This saturation concentration increases with hydrogen percentage in the shielding gas and with arc current, decreases with sample weight and is virtually independent of arc length.

Due to the high diffusion rate of hydrogen in iron a large part of the hydrogen initially present will leave the sample during cooling. The initial hydrogen concentration in the sample was calculated with the help of a finite element program.

A model was developed which describes the absorption process. According to this model, the hydrogen concentration in the sample is the result of two mutually independent processes: inflow and outflow. Inflow of hydrogen takes place exclusively through the interface between the arc and the liquid metal, the inflow rate being determined by the arc conditions (notably the partial pressure of the hydrogen in the arc and the temperature of the arc). Outflow of hydrogen takes place through the entire outer surface of the liquid metal (including that part of the surface which is covered by the arc), the outflow rate being proportional to the hydrogen concentration in the liquid metal.

The absorption coefficient and the desorption coefficient were determined for various process conditions. The absorption coefficient increases with hydrogen percentage in the shielding gas. The desorption coefficient increases with hydrogen percentage in the shielding gas, with arc current and with arc length.

Furthermore, it was found that hydrogen absorption during arc welding obeys Sieverts' Law.

Hydrogen absorption was also studied under more realistic circumstances by performing GTA welding experiments under travelling arc conditions.

The obtained results show that the hydrogen concentration is independent of arc length, increases with hydrogen partial pressure and with arc current, and decreases with travel speed.

A large part of the hydrogen leaves the test piece during cooling. The initial hydrogen concentration in the weld pool was calculated with the help of a finite element program.

The model developed for stationary arc welding was extended to welding under travelling arc conditions.

The model is valid for a relatively wide range of experimental conditions and can be used to predict the initial hydrogen level in welds produced under realistic welding circumstances.

Samenvatting

Opname van waterstof in ijzer en staal tijdens booglassen

Dit proefschrift beschrijft de resultaten van een onderzoek naar de opname van waterstof in ijzer en staal tijdens booglassen. Inzicht in het opnameproces is van groot belang, omdat waterstof aanleiding kan geven tot verslechtering van de mechanische eigenschappen van ijzer en staal (porievorming en waterstofscheuren).

Na een algemene inleiding worden achtereenvolgens het gedrag van waterstof in metalen en de belangrijkste kenmerken van het booglasproces besproken. Vervolgens wordt aandacht geschonken aan de invloed van de toevoeging van waterstof aan het argon beschermgas op de eigenschappen van de boog en de vorm van het lasbad. Zowel de boog als de lasbadvorm spelen een belangrijke rol bij de waterstofopname.
Het blijkt dat het zichtbare gedeelte van de boog verandert wanneer waterstof aan het beschermgas wordt toegevoegd. Het opvallendste effect is het samentrekken van de boog, hetgeen waarschijnlijk wordt veroorzaakt door veranderingen in temperatuur en temperatuurverdeling. Voorts blijkt dat de grootte van het grensvlak tussen de boog en het vloeibare metaal groter wordt met toenemend waterstofgehalte in het beschermgas.
Met het waterstofgehalte in het beschermgas neemt ook de boogspanning toe. Dit effect kan worden toegeschreven aan de verhoging van de elektrische veldsterkte als gevolg van de grotere thermische geleidbaarheid van waterstof in vergelijking met argon.
De toevoeging van waterstof aan het beschermgas resulteert in een grotere warmte-inbreng in het lasbad en in een hoger smeltrendement. De grotere warmte-inbreng heeft bij zuiver ijzer een toename van zowel de lasbadbreedte als de lasbaddiepte tot gevolg. Bij ongelegeerd staal en roestvast staal neemt voornamelijk de lasbaddiepte toe. Het verschil in lasbadvorm tussen ongelegeerd staal en roestvast staal enerzijds en zuiver ijzer anderzijds wordt waarschijnlijk veroorzaakt door het optreden van vloeistofstromingen in het lasbad. Bij ongelegeerd staal en roestvast staal is de stroming naar het centrum van het lasbad gericht, resulterend in een smal diep lasbad, terwijl bij zuiver ijzer nauwelijks stromingen in het lasbad aanwezig zijn.
Bij een bepaald waterstofgehalte in het beschermgas kan porievorming in de las optreden. Het waterstofgehalte waarboven porievorming optreedt is afhankelijk van zowel de chemische samenstelling van het materiaal als de procesparameters.

Om inzicht in het opnamemechanisme van waterstof te krijgen werden experimenten uitgevoerd met een stilstaande boog. In een waterstofhoudende argonatmosfeer werden kleine preparaten van ijzer en staal volledig gesmolten met behulp van een boog, onder verschillende procesomstandigheden.
Het blijkt dat de hoeveelheid opgenomen waterstof toeneemt met de tijd en dat in korte tijd verzadiging wordt bereikt. De hoogte van de verzadigingsconcentratie neemt toe met het waterstofgehalte in het beschermgas en met de stroomsterkte, neemt af met het gewicht van het proefstuk en is onafhankelijk van de booglengte.
Door de hoge diffusiesnelheid van waterstof in ijzer zal een gedeelte van de waterstof dat tijdens het booglassen in het materiaal opgenomen is, bij het afkoelen van het preparaat weer ontsnappen. De oorspronkelijke hoeveelheid waterstof in het proefstuk is berekend met behulp van een eindige-elementen programma.
Het blijkt dat het opnameproces beschreven kan worden met een model, waarin twee onafhankelijke mechanismen een rol spelen: absorptie en desorptie. Absorptie van waterstof vindt alleen daar plaats waar de boog in contact is met het vloeibare metaal. De grootte van de absorptie wordt bepaald door de omstandigheden in de boog (vooral door het waterstofgehalte en de temperatuur). Desorptie van waterstof vindt plaats over het gehele oppervlak van het vloeibare metaal (inclusief het gedeelte waar de boog aangrijpt). De grootte van de desorptie hangt af van de waterstofconcentratie in het materiaal.
Voor verschillende procesomstandigheden zijn de absorptiecoefficient en de desorptie-coefficient bepaald. De absorptiecoefficient neemt toe met het waterstofgehalte in het beschermgas, terwijl de desorptiecoefficient toeneemt met het waterstofgehalte in het beschermgas, met de lasstroom en met de booglengte.
Tevens blijkt de waterstofopname tijdens het lassen te voldoen aan de Wet van Sieverts.

Ook bij het lassen onder praktijkomstandigheden is de opname van waterstof bestudeerd. Hiertoe werden lasexperimenten uitgevoerd met een lopende boog.
Het waterstofgehalte in de las blijkt onafhankelijk te zijn van de booglengte, toe te nemen met het waterstofgehalte in het beschermgas en met de lasstroom en af te nemen met de voortloopsnelheid.
Een groot gedeelte van de waterstof dat opgenomen is tijdens het booglassen verlaat het proefstuk weer bij het afkoelen. Met een eindige-elementen programma is de oorspronkelijke hoeveelheid waterstof in het lasbad berekend.
Op basis van de verkregen resultaten werd een model ontwikkeld waarmee de opname van waterstof bij het lassen met voortlopende boog beschreven kan worden. Met het model kunnen waterstofgehaltes in het lasbad onder praktijkomstandigheden worden voorspeld.

Dankwoord

Omdat zeer velen meegeholpen hebben aan de tot stand koming van dit proefschrift, wil ik hier graag iedereen bedanken die dit werk mogelijk hebben gemaakt. Ik doel hierbij op de hulp die ik bij het werk zelf heb gekregen. Echter ook de prettige sfeer in het Laboratorium voor Materiaalkunde heeft dit proefschrift mogelijk gemaakt.

Mijn promotor Gert den Ouden wil ik speciaal bedanken. Hij is met zijn positieve instelling een voortdurende bron van inspiratie geweest.
Met zijn afstudeerwerk heeft Raph Pieters meegeholpen aan de tot stand koming van hoofdstuk 3. Hij heeft mijn beeld van afstudeerders in gunstige zin beinvloed.
Alle leden van de sectie Lastechnologie & NDO hebben meegewerkt aan mijn plezierige tijd in de groep in het bijzonder en in Delft in het algemeen.
Van deze sectie waren de technici voor het bouwen van de apparatuur onontbeerlijk: Gijs Kerkhof, Willem Brabander en Frans Bosman.
Bij de waterstofanalyses heeft Ton Klijnhout, ondanks vele verhuizingen, zeer veel hulp geboden, terwijl Ton de Haan bereid was een plekje voor mijn kwikmeetapparatuur af te staan.
Een aantal mensen hebben me binnen en buiten het gebouw begeleid met zinnige en onzinnige opmerkingen: Ton Aendenroomer, Wouter Bruins, Marcel Hermans, Xiao You Hong, Jan-Paul Krugers, Jaap Meijer, Ma Tao, Anneke van Veen, Hindrik de Vries en Johan Zijp.
Tot slot wil ik mijn ouders bedanken voor hun steun en geduld.